AD-A146 827 NONLINEAR OPTICAL STUDIES OF RYDBERG ATOMS USING DEGENERATE FOUR-WAVE MIXING(U) HUGHES RESEARCH LABS MALIBU CA J F LAM ET AL. AUG 84 ARO-17432.13-PH 1/2

UNCLASSIFIED DAAG29-81-C-0008 F/G 20/6 NL

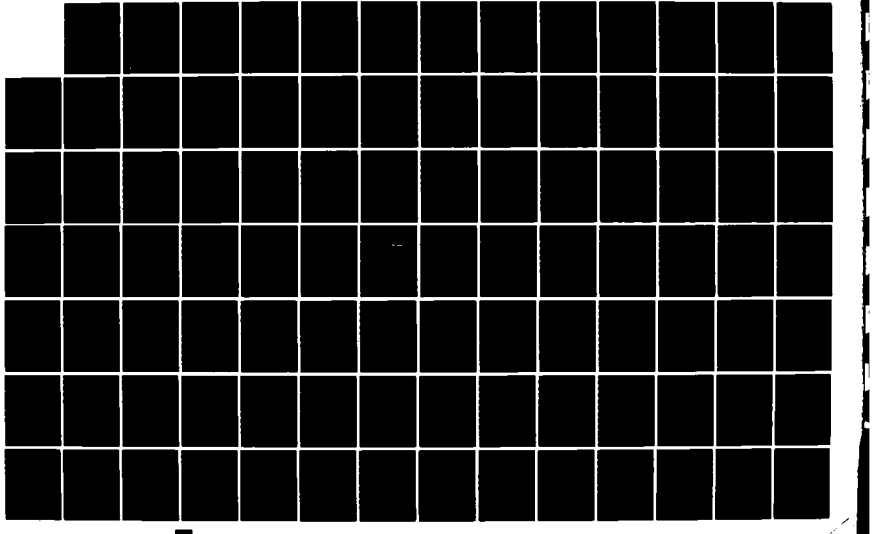

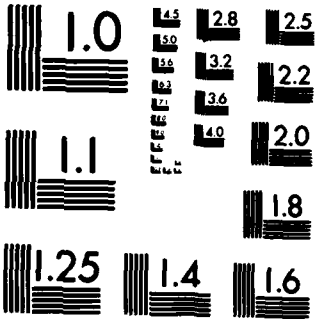

ARO 17432.13-PH

NONLINEAR OPTICAL STUDIES OF RYDBERG ATOMS USING DEGENERATE FOUR–WAVE MIXING

J.F. Lam, R.A. McFarlane, and D.G. Steel

Hughes Research Laboratories
3011 Malibu Canyon Road
Malibu, CA 90265

August 1984

DAAG29–81–C–0008
Final Report
March 1981 through August 1984

U.S. ARMY RESEARCH OFFICE
Post Office Box 12211
Research Triangle Park, NC 27709

UNCLASSIFIED

SECURITY CLASSIFICATION OF THIS PAGE

REPORT DOCUMENTATION PAGE

1a. REPORT SECURITY CLASSIFICATION	1b. RESTRICTIVE MARKINGS
2a. SECURITY CLASSIFICATION AUTHORITY	3. DISTRIBUTION/AVAILABILITY OF REPORT: Approved for public release; distribution unlimited.
2b. DECLASSIFICATION/DOWNGRADING SCHEDULE	
4. PERFORMING ORGANIZATION REPORT NUMBER(S)	5. MONITORING ORGANIZATION REPORT NUMBER(S)
6a. NAME OF PERFORMING ORGANIZATION: Hughes Research Laboratories; 6b. OFFICE SYMBOL (If applicable)	7a. NAME OF MONITORING ORGANIZATION
6c. ADDRESS (City, State and ZIP Code): 3011 Malibu Canyon Road, Malibu, CA 90265	7b. ADDRESS (City, State and ZIP Code)
8a. NAME OF FUNDING/SPONSORING ORGANIZATION: U.S. Army Research Office; 8b. OFFICE SYMBOL (If applicable)	9. PROCUREMENT INSTRUMENT IDENTIFICATION NUMBER: DAAG29-81-C-0008
8c. ADDRESS (City, State and ZIP Code): Post Office Box 12211, Research Triangle Park, NC 27709	10. SOURCE OF FUNDING NOS. — PROGRAM ELEMENT NO. / PROJECT NO. / TASK NO. / WORK UNIT NO.
11. TITLE (Include Security Classification): Nonlinear Optical Studies of Rydberg Atoms Using Degenerate Four-Wave Mixing	
12. PERSONAL AUTHOR(S): J.F. Lam, R.A. McFarlane, D.G. Steel	
13a. TYPE OF REPORT: Final Report; 13b. TIME COVERED: FROM 3/81 TO 6/84; 14. DATE OF REPORT (Yr., Mo., Day): August 1984; 15. PAGE COUNT: 133	
16. SUPPLEMENTARY NOTATION: The views, opinions, and/or findings contained in this report are those of the author(s) and should not be construed as an official Dept. of the Army position, policy, or decision, unless so designated by other documentation.	
17. COSATI CODES — FIELD / GROUP / SUB. GR.	18. SUBJECT TERMS (Continue on reverse if necessary and identify by block number)

19. ABSTRACT (Continue on reverse if necessary and identify by block number)

The spectral behavior of the third order nonlinear optical response of atomic sodium was studied. As a result, new kinds of frequency domain spectroscopy techniques were developed: nearly degenerate four-wave mixing, polarization nearly degenerate four-wave mixing, frequency domain three-state spectroscopy, and nonlinear Hanle effect in degenerate four-wave mixing. These techniques have provided new information on several areas of collision physics including: dephasing collisions (spectral broadening and frequency shift), velocity changing collisions, state changing collisions, and spin-flip collisions.

20. DISTRIBUTION/AVAILABILITY OF ABSTRACT: UNCLASSIFIED/UNLIMITED ☒ SAME AS RPT. ☐ DTIC USERS ☐	21. ABSTRACT SECURITY CLASSIFICATION: UNCLASSIFIED
22a. NAME OF RESPONSIBLE INDIVIDUAL: R.A. McFarlane	22b. TELEPHONE NUMBER (Include Area Code): (213) 456-6411; 22c. OFFICE SYMBOL

DD FORM 1473, 83 APR EDITION OF 1 JAN 73 IS OBSOLETE.

UNCLASSIFIED

SECURITY CLASSIFICATION OF THIS PAGE

PROBLEM STATEMENT

The technical objective of this program has been to evaluate the third order optical nonlinearity of Rydberg atoms, and to quantify the effect of rare gas collisions on the spectral response. The initial approach has been to use degenerate four-wave mixing (DFWM). However, we determined that alternative spectroscopy techniques developed on this program could provide improved sensitivity and measurement ability. Furthermore, we found that the current understanding of collision effects was inadequate to explain collision effects on Rydberg states, on the intermediate states or on the ground state. Hence, the problem was generalized to achieve an understanding of the total four-wave resonant nonlinear response of both two and three-level systems in the presence of dephasing collisions (both spectral broadening and frequency shift), velocity changing collisions, and spin-flip or m-mixing collisions. Our interpretation includes the effects of degeneracies and optical pumping.

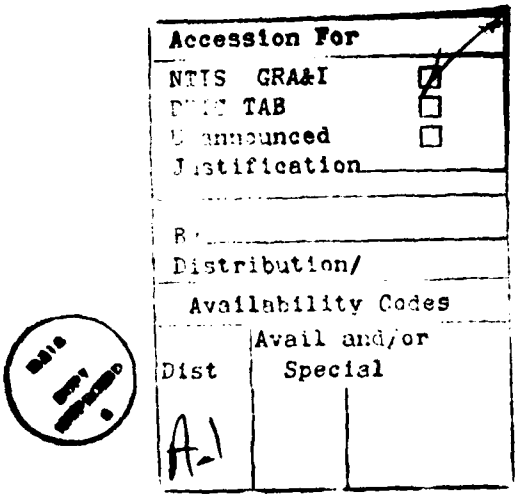

SUMMARY OF RESULTS

On this technical program, four new frequency domain nonlinear laser spectroscopy techniques were developed, each one providing new capability to study the effects of atomic collisions. We have quantified the role of collision effects on hyperfine optical pumping. This is critical for an accurate interpretation of cw frequency domain nonlinear optical spectroscopy experiments. The key results are briefly summarized below and discussed in detail in reprints included as appendices.

1. Zeeman Coherence in DFWM. We demonstrated for the first time the ability to experimentally isolate the effects of Zeeman coherence using DFWM. This provided new understanding of the polarization properties of phase conjugate mirrors.

2. Nearly Degenerate Four-Wave Mixing (NDFWM). Using two cw stabilized tunable dye lasers, we demonstrated the multiresonant behavior of NDFWM. NDFWM provides the ability to simultaneously measure the transverse relaxation rate, as well as the longitudinal relaxation rate in the frequency domain. Prior to this work, the longitudinal relaxation rate had always been measured in the time domain. In this work, we provided the first clear demonstration using nonlinear laser spectroscopy that the collision trajectory for sodium atoms in the 3p state is significantly different than the collision trajectory for sodium atoms in the 3s state. We showed the evolution of a closed quantum mechanical system into an open system. The behavior was observed as a collisional narrowing of the first or T_1 resonance in NDFWM.

3. Collisional Enhancement of DFWM. Using DFWM we showed that transitions that are normally weak in cw nonlinear laser spectroscopy due to hyperfine optical pumping are enhanced due to velocity changing collisions. To model the experimental results, a theory was developed to explain the data and provide the first estimate of the velocity changing collision cross section between sodium and two rare gases.

4. State Changing Collision Effects in Nonlinear Laser Spectroscopy. Using DFWM, we found that transitions that are not hyperfine optically pumped because of dipole selection rules become optically pumped due to state changing collisions. As a result we find that normally strong transitions become very weak in the presence of buffer gas collisions at pressures as low as 50 mTorr.

5. Polarization Nearly Degenerate Four-Wave Mixing (PNDFWM). Combining the results of Zeeman coherence DFWM and NDFWM, we found that collisional narrowing could also be observed due to spin-flip collisions. This technique provides a new way to measure spin-flip cross-sections in the frequency domain.

6. Measurement of the Collision Induced Frequency Shift and Spectral Broadening of 3s-ns Rydberg Transitions. Another spectroscopy technique designated frequency domain three-state spectroscopy (FDTS) provided nearly state specific collision cross-section information for Rydberg states. The experiments provided the first simultaneous measurements of the frequency shift parameter and the pressure broadening cross-section of the 3s-ns superposition Rydberg state. Both collision effects must be measured in order to confirm the validity of collision models.

7. Nonlinear Hanle Effect in DFWM. Using our ability to isolate Zeeman coherence in DFWM, we have demonstrated a nonlinear Hanle type behavior. The experiment showed the strong dependence of the Zeeman coherence signal on the applied magnetic field. The results indicate that the Hanle effect may be useful for studies where fluorescence signals are hard to observe, such as in rotational-vibration molecular spectroscopy.

8. Theory of four-wave mixing in two- and three-level systems, including collision effects and degeneracy of the energy levels. We have developed a general theory of DFWM and NDFWM using the density operator equations. This theory is valid for any value of laser detuning from resonance, but is restricted to the weak signal limit. The theory includes the effects of collisions with foreign gas perturbers, degeneracy of the energy levels and the effects of atomic motion. It predicts the subnatural linewidths in NDFWM and the behavior of DFWM signal as a function of buffer gas pressure. Two models were constructed to explain the behavior of the resonance at $\delta = 0$. The first model uses the dressed atom picture and is based on the conservation of energy. The second is

based on quantum mechanical amplitudes and describes the effect of quantum interference on the signal. Both models yield the same conclusion: the subnatural linewidth at $\delta = 0$ arises from evolution to an open system in the presence of collisions.

PARTICIPATING SCIENTIFIC PERSONNEL

Dr. Ross A. McFarlane, Principal Investigator

Dr. Juan F. Lam

Dr. Duncan G. Steel

PUBLICATIONS AND PRESENTATIONS

1. D.G. Steel, J.F. Lam, and R.A. McFarlane, "Atomic coherence effects in resonant four-wave mixing spectroscopy of sodium," presented at the Fifth International Conference on Laser Spectroscopy, Jasper, Alberta, 29 June to 3 July 1981. Proceedings - Laser Spectroscopy V - Editors: A.R.W. McKellar, T. Oka, B.P. Stoicheff (Springer-Verlag, New York, 1981).

2. J.F. Lam, "Doppler-free laser spectroscopy via degenerate four-wave mixing," Optical Engineering 21, 219 (1982).

3. D.G. Steel, R.A. McFarlane, and J.F. Lam, "Pressure induced effects on cw degenerate and nearly degenerate four-wave mixing," presented at the Twelfth International Quantum Electronics Conference, Munich, W. Germany, June 1982.

4. J.F. Lam, D.G. Steel, and R.A. McFarlane, "Collision studies of highly excited atomic states using a new cw four-wave mixing spectroscopy technique," presented at the Twelfth International Quantum Electronics Conference, Munich, W. Germany, June 1982.

5. D.G. Steel, J.F. Lam, and R.A. McFarlane, "High-resolution spectroscopy and collision studies of high-lying atomic states using four-wave mixing," Phys. Rev. A 26, 1146 (1982).

6. J.F. Lam and R.L. Abrams, "Theory of noninear optical coherences in resonant degenerate four-wave mixing," Phys. Rev. A. 26, 1539 (1982).

7. J.F. Lam, D.G. Steel, and R.A. McFarlane, "Collisionally induced narrowing of the longitudinal relaxation linewidth in nearly degenerate four-wave mixing," Phys. Rev. Lett. 49, 1628 (1982).

8. D.G. Steel and R.A. McFarlane, "Enhancement of four-wave mixing signals due to velocity-changing collisions," Phys. Rev. A. 27, 1217 (1983).

9. D.G. Steel and R.A. McFarlane, "Collisional destruction of four-wave-mixing signals in sodium in the presence of low-pressure buffer gas," Phys. Rev. A. 27, 1687 (1983).

10. J.F. Lam, D.G. Steel, and R.A. McFarlane, "Spectral narrowing and related effects of collision dynamics in resonant degenerate four-wave-mixing," presented at the Sixth International Conference on Laser Spectroscopy, Interlaken, Switzerland, June 1983 and in Proceedings - Laser Spectroscopy VI - Editors: H.P. Weber and M. Luthy (Springer-Verlag, New York, 1983).

11. J.F. Lam, D.G. Steel, and R.A. McFarlane, "Collision effects on Zeeman coherences using nearly degenerate four-wave mixing," presented at the Thirteenth International Quantum Electronics Conference, Anaheim, CA, June 1984.

12. D.G. Steel and R.A. McFarlane, "High resolution spectroscopy and collision studies of Rydberg states by frequency domain three state spectroscopy (FDTS)." Submitted for publication.

13. P.R. Berman, G. Khitrova, and J.F. Lam, "Interpretation of pump-probe and four-wave mixing line shapes." Submitted for publication.

14. J.F. Lam, D.G. Steel, and R.A. McFarlane, "Observation of collision-induced subnatural Zeeman coherence linewidths in the Doppler limit." Submitted for publication.

APPENDICES

Presented at Fifth International Conference
on Laser Spectroscopy
Jasper, Alberta. June 29 - July 3, 1981

ATOMIC COHERENCE EFFECTS IN RESONANT FOUR-WAVE MIXING SPECTROSCOPY OF SODIUM

D.G. Steel, J.F. Lam, and R.A. McFarlane
Hughes Research Laboratories
3011 Malibu Canyon Road
Malibu, CA 90265

This paper presents preliminary experimental and theoretical results on two new aspects of sub-Doppler spectroscopy using resonant four-wave mixing and cw tunable dye lasers. The first technique uses degenerate four-wave mixing (DFWM) to study optically induced Zeeman coherences while the second technique uses nondegenerate FWM to study excited atomic states.

The starting point in the analysis of four-wave mixing processes is the quantum mechanical transport equation for the density operator ρ [1]. The perturbation calculation is carried out to include terms in the series expansion of ρ up to third order. In the calculations we assume counterpropagating pumps (E_f and E_b) and a nearly collinear probe (E_p). Phase-matching results in the signal (E_s) counterpropagating to E_p. The analysis assumes a Maxwellian velocity distribution yielding after velocity integration a third order polarization in terms of Plasma Dispersion functions.

For a two level system with degeneracies, we calculate the contribution to the DFWM signal arising from optically induced spatial modulation of atomic populations and atomic coherences (Zeeman coherence) between degenerate levels. Damping is included as a phenomenological decay from the two levels at rates γ_1 and γ_2. The frequency dependence of the signal (in the extreme Doppler limit and for small $\alpha_o\ell$) is given by $E_s = C\, E_f E_b E_p^*/(\gamma_{12}+i\Delta)$ where $\Delta=\omega-\omega_o$, $2\gamma_{12} = (\gamma_1+\gamma_2)$ is the linewidth, and $\alpha_o\ell$ is the absorption length product. The Doppler-free property of the signal arises because only the v=0 velocity group can interact simultaneously with all four waves.

When all four beams are copolarized, the dipole selection rules imply that all four waves interact with the same transition ($\Delta m=0, \pm1$) resulting in a population dependent interaction. However, with the appropriate choice of pump and probe field polarizations, the presence of magnetic degeneracies allows the possibility of generating optically induced Zeeman coherences between degenerate states. Consider the choice of electric field polarization vectors given by $\hat{e}_f = \hat{\varepsilon}_+$, $\hat{e}_b = \hat{\varepsilon}_-$ and $\hat{e}_p = \hat{\varepsilon}_-$. The action of the forward pump E_f and input probe E_p, generates a spatial modulation of the Zeeman coherence between states $|\alpha J_\alpha M_\alpha\rangle$ and $|\alpha J_\alpha M_\alpha+2\rangle$, which are connected to a common state $|\beta J_\beta M_\alpha+1\rangle$. The four-wave mixing signal is generated via a scattering of the backward pump field E_b from the spatial interference, and it has an electric field polarization given by $\hat{\varepsilon}_+$. Physically, the Zeeman coherence induced by E_f and E_p can be viewed as an electric quadrupole. The Zeeman coherence is susceptible to depolarizing collisions in contrast to the population which experiences velocity changing collisions.

In the case $\hat{e}_f = \hat{e}_b = \hat{x}$ and $\hat{e}_p = \hat{y}$, the DFWM signal is polarized in the y-direction. The strength of the signal arising from both ground and

ARO Contract: DAAG29-81-C-0008

excited state coherences depends on the respective life-times. The relative strengths are given by I_g and I_e and $C \propto (I_g+I_e)$. As an example for this polarization case, $I_g = (8\gamma_D)^{-1} \sum_{M_2} |\langle J_2M_2|\mu|J_1M_2-1\rangle|^2|\langle J2M2|\mu|J1M2+1\rangle|^2 -$

$(16\gamma_1)^{-1} \sum_{M_2} [|\langle J_2M_2|\mu|J_1M_2+1\rangle|^4 + |\langle J_2M_2|\mu|J_1M_2-1\rangle|^4 -$

$|\langle J_2M_2|\mu|J_1M_2+1\rangle|^2|\langle J_2M_2+2|\mu|J_1M_2+1\rangle|^2 - |\langle J_2M_2|\mu|J_1M_2-1\rangle|^2|\langle J_2M_2-2|\mu|J_1M_2-1\rangle|^2]$

The first term is proportional to $\gamma_D^{-1} = (\gamma_1+\gamma_{ph})^{-1}$ while the second term is proportional to γ_1^{-1}. γ_{ph} is determined by depolarization collisions. In general $I_e \neq I_g \neq 0$ but in the case $J=1 \rightarrow J=0$ if $\gamma_{ph}=0$ then $I_g=I_e=0$ and no DFWM signal is expected. In the presence of depolarizing collisions, $\gamma_{ph}\neq 0$, and therefore $\gamma_D \neq \gamma_1$ leading to a DFWM signal even in this special case. Similar results are obtained by Bloch and Ducloy [2].

For the second technique of nondegenerate FWM spectroscopy via a non-degenerate 3-level cascade-up system, we consider as a general example the case for which the backward pump oscillates at Ω_1 (which is resonant with transition frequency ω_{21}) and the forward pump and input probe oscillate at frequency Ω_2 (which is resonant with transition frequency ω_{32}). We assume that the level energies in the cascade-up 3-level system are given by $E_3>E_2>E_1$. The physical contribution to the FWM signal arises from the generation of a 2-photon coherence between levels $|1\rangle$ and $|3\rangle$ via the simultaneous action of E_f and E_b. In collinear geometry the resonance condition that must be satisfied in order for all four waves to interact with the same velocity group is given by $\Omega_2 - \omega_{32} = -(k_2/k_1)(\Omega_1-\omega_{21})$. The signal E_s is proportional to

$$E_s \alpha E_f E_b E_p^* e^{i(k_1 z+\Omega_1 t)} \left[\gamma_{13} + \left(\frac{k_2}{k_1} - 1\right)\gamma_{12} - i\left(\Delta_{32} + \frac{k_2}{k_1}\Delta_{21}\right)\right]^{-1}$$

$$\left\{(ik_1u_o)^{-1} Z'\left(-\frac{\Delta_{21} + i\gamma_{12}}{k_i u_o}\right)\right.$$

$$\left. + \left(\frac{k_2}{k_1} - 1\right)\left[\gamma_{13} + \left(\frac{k_2}{k_1} - 1\right)\gamma_{12} - i\left(\Delta_{32} + \frac{k_2}{k_1}\Delta_{21}\right)\right]^{-1}\left[Z\left(\frac{\Delta_{21}+\Delta_{32}+i\,\gamma_{13}}{\left(\frac{k_2}{k_1}-1\right)k_1u_o}\right) - Z\left(-\frac{\Delta_{21}+i\gamma_{12}}{k_1u_o}\right)\right]\right\}$$

where $\Delta_{21} = \Omega_1 - \omega_{12}$, $\Delta_{32} = \Omega_2 - \omega_{32}$, $\gamma_{ij} = (1/2)(\gamma_i+\gamma_j)$ and Z is the plasma dispersion function. In the Doppler limit, the frequency response of E_s is a Lorentzian whose linewidth is given by the 2-photon linewidth γ_{13}. We are presently extending the theory to include the effects due to AC Stark shift [3].

The experimental studies of these effects were made in atomic sodium using a stabilized Coherent Inc. ring dye laser. Using an experimental configuration discussed earlier [1] we studied the optical field induced Zeeman coherence using counterpropagating pumps arranged to be linear and copolarized. With the probe beam linearly polarized and the axis of quantization assumed parallel to the pump electric field, the population dependent physics could then be isolated from the Zeeman coherence by setting the probe polarization either parallel or orthogonal to the pumps. Fig. 1a is a DFWM spectrum of the D_2 line (γ=0.5890 μm) with the pumps and probe copolarized showing the signal resulting from population physics. Due to hyperfine (hf) optical pumping, only two components appear: the $3^2S_{1/2}(F=1)$-$3^2P_{3/2}(F=3)$ transition and the $3^2S_{1/2}(F=1)$-$3^2P_{3/2}(F=0)$ transition. The latter transition shows a splitting due to saturation. The insets show spectra at pump intensities well below 6 mW/cm^2, the saturation intensity for the first transition. Rotating the probe polarization 90° we obtain the signal resulting from

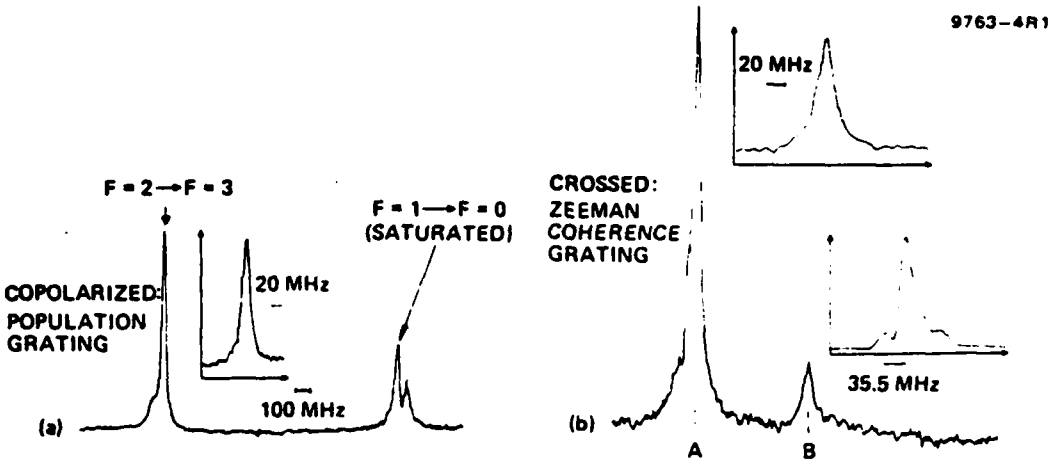

Fig.1 Frequency dependence of DFWM signal arising from population grating and Zeeman coherence

Zeeman coherence shown in Fig. 1b (arbitrary vertical scale). The low frequency transition (structure A) was observed as expected from the analysis and the high frequency transition was missing as predicted above. The central component (structure B) is a crossover resonance.

A more detailed analysis shows that the Zeeman signal should be reduced when upper or lower level coherence is removed. Due to the transit time and the finite laser linewidth, the ground state coherence is destroyed by application of a small magnetic field parallel to the pump electric field. Since the lower energy level splitting is of order 700 kHz/Gauss, we expect a significant signal reduction with a field of a few hundred milligauss. The effect of the sudden drop-off is shown in Fig.2a which is an oscillogram of the Zeeman signal versus field. Fig.2b shows the ordinary population signal dependence on magnetic field. The rise in both signals is presently not understood. Note at higher fields near 10 Gauss, corresponding to a line splitting on the order of the natural linewidth, both signals begin falling.

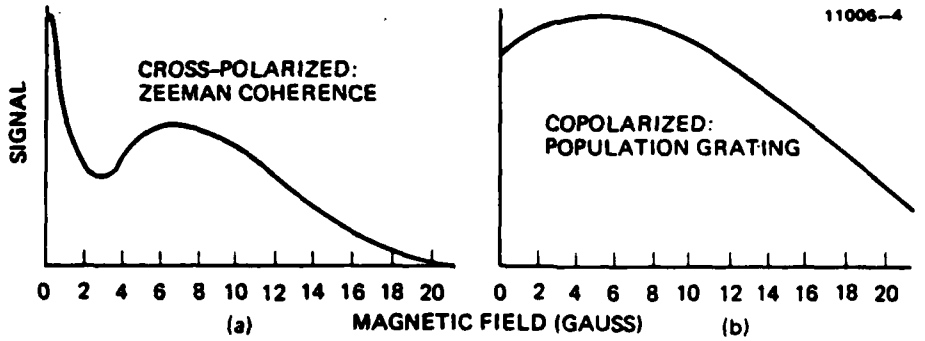

Fig.2 Dependence of DFWM signal on magnetic field

Demonstration of sub-Doppler nondegenerate four-wave mixing spectroscopy of excited states was achieved by coupling the $3^2S_{1/2}$-$3^2P_{3/2}$ transition to the $3^2P_{3/2}$-$4^2D_{5/2}$ and $3^2P_{3/2}$-$4^2D_{3/2}$ transitions. As an example of the potential usefulness of this coupling we show in Fig.3 an example of the resulting spectrum. Using two stabilized Coherent Inc. ring dye lasers, the forward pump and probe were tuned to the upper transition near 0.5688 μm while the backward pump was tuned to the lower transition at 0.5890 μm. A signal

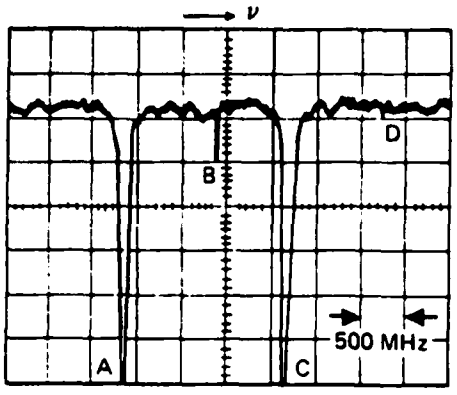

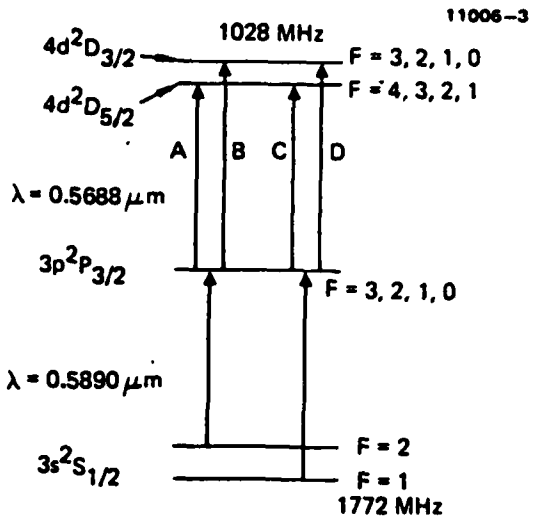

Fig.3 Frequency spectrum of optically induced two-photon coherence as observed by non-degenerate FWM. Level diagram shows observed transitions

was observed at 0.5890 μm as the 0.5688 μm laser was scanned. This interaction is perfectly phase matched for nearly collinear geometry. The four structures showing in Fig.3 are from the following transitions: A, $3^2S_{1/2}(F=2)-3^2P_{3/2}(F=3)-4^2D_{5/2}(F=4)$; B, $3^2{}_{1/2}(F=2)-3^2P_{3/2}(F=3)-4^2D_{3/2}(F=3)$; C, $3^2S_{1/2}(F=1)-3^2P_{3/2}(F=0)-4^2D_{5/2}(F=1)$; D, $3^2S_{1/2}(F=1)-3P_{3/2}(F=0)-4^2D_{3/2}(F=0)$. The other hf transitions were not observed because of optical pumping. The linewidth of the intense transitions was less than 10 MHz comparable to the expected two-photon linewidth.

It is a pleasure to acknowledge useful discussions of these results with Professor T.W. Hänsch of Stanford University. This work was supported in part by the Army Research Office under Contract No. DAAG29-81-C-0008.

References

1. J.F. Lam, D.G. Steel, R.A. McFarlane, and R.C. Lind, Appl. Phys. Lett. 38 June 15, 1981.
2. D. Bloch and M. Ducloy (private communication).
3. T.W. Hänsch and P. Toschek, Z. Physik 236, 213 (1970).

Doppler-free laser spectroscopy via degenerate four-wave mixing

Juan F. Lam
Hughes Research Laboratories
3011 Malibu Canyon Road
Malibu, California 90265

Abstract. The physics underlying the technique of degenerate four-wave mixing (DFWM) is presented. Its application to the measurement of energy decay and dephasing rates is considered in the regime of small absorption and coupling coefficients.

Keywords: optical phase conjugation; nonlinear laser spectroscopy, degenerate four-wave mixing; nonlinear optics; Doppler-free spectroscopy, single-photon transition, two-photon transition.

Optical Engineering 21(2), 219-223 (March/April 1982).

CONTENTS

I. INTRODUCTION

The invention of the laser has made a major impact in the field of spectroscopy since the unique properties of the laser radiation (quasi-monochromaticity, spatial coherence, and tunability) have provided the background for the appearance of the Doppler-free techniques in the studies of atomic and molecular spectra. In the years preceding the 1960s, the measurement of atomic and molecular linewidths was severely limited by the random motion of the atoms. However, the discovery of the Lamb dip[1] in 1963 brought to attention the possibility of directly measuring the natural or collision-broadened linewidths in a Doppler-broadened quantum system. Soon afterward, a series of novel schemes appeared that complemented the work of Lamb and co-workers. They are saturated absorption spectroscopy,[2] two-photon spectroscopy,[3] polarization spectroscopy,[4] and coherent transient spectroscopy,[5,6] to name a few.

Nonlinear phase conjugation came about in the study of aberration correction in optical systems by means of nonlinear optics.[7-9] It was shown that the processes of degenerate four-wave mixing (DFWM) as well as stimulated Brillouin scattering (SBS) provide means of generating phase-conjugated waves (see D. M. Pepper's paper, this issue of Optical Engineering for more detailed descriptions of these physical processes). The phenomenology was brought into definitive descriptions by using standard methods of nonlinear optics.[10-12] The potential of using DFWM as a spectroscopic tool did not come about until 1977 when the collision-induced coherence decay rate of the two-photon transition $3S \rightarrow 4D$ in sodium atoms perturbed by buffer gases was measured.[13] It was realized at that time that the resolution of the DFWM technique was not limited by the Doppler effect and gave a better signal-to-noise ratio. The elimination of the Doppler effect in the experiments was achieved by means of two-photon excitation of the atoms due to the nonlinear interaction of counterpropagating waves. And the better signal-to-noise ratio was obtained from the intrinsic property of DFWM, i.e., it generates a coherent phase-conjugate signal which can be temporally and or spatially separated from the input pulses.

The generalization of this work to one-photon resonant systems in the transient[14] and steady-state[15] regimes for the measurement of atomic and molecular parameters put DFWM in the proper place as an additional powerful tool of nonlinear laser spectroscopy. The objective of this article is to provide an overview of the physics behind the technique as well as to review briefly the accomplishments obtained so far in the pursuit of understanding of the basic interaction processes in gaseous systems. In an article of this nature, it is rather easy for the author to inadvertently overlook some of the work published in this rapidly growing field. The author would like to extend his apologies for such oversights.

The discussion is divided into two sections. The first section will treat the experimental situation for which one uses cw laser sources in the diagnostics of the atomic and molecular systems. The second section will deal with the case of pulsed excitation and time-delayed interaction processes. For sake of simplicity, we shall denote the former as steady-state DFWM and the latter as transient DFWM.

We shall restrict this discussion to the regime in which the intensity of the input fields is much smaller than the saturation intensity of the medium. Furthermore, in order to avoid problems arising from the medium length, we shall assume that both the absorption coefficient and coupling coefficient times the medium length be small compared to unity.

II. STEADY-STATE DFWM

We shall consider the physics of DFWM in two-level systems with nondegenerate states (Fig. 1), and nondegenerate three-level systems (Fig. 2). The interaction geometry is chosen such that the pump fields $\underline{E}_f$ and $\underline{E}_b$ are counterpropagating and the probe field $\underline{E}_p$ is nearly colinear with $\underline{E}_f$ (Fig. 3). The calculation of the spectral profile of the phase-conjugate field $\underline{E}_s$ is obtained by the perturbative solution of the quantum mechanical transport equation for the

Invited Paper PL-105 received Sep. 18, 1981, accepted for publication Sep. 28, 1981, received by Managing Editor Oct. 29, 1981.

density matrix ρ.

$$i\hbar(\gamma_\alpha + \vec{V}.\nabla)\rho_{\alpha\alpha} = \lambda_\alpha + [H.\rho]_{\alpha\alpha} \quad (1a)$$

$$i\hbar(\gamma_{\alpha\beta} + i(\omega-\omega_{\beta\alpha}) + \vec{V}.\nabla)\rho_{\alpha\beta} = [H.\rho]_{\alpha\beta} \; . \quad (1b)$$

where γ_α is the energy decay rate of level $|\alpha>$; λ_α is the incoherent pumping rate to level $|\alpha>$; $\gamma_{\alpha\beta}$ and $\omega_{\beta\alpha}$ are the dephasing rate and resonance frequency of transition $|\alpha> \rightarrow |\beta>$, respectively; $\vec{V}\cdot\nabla$ describes the effects of velocity and spatial hole burning; H is the Hamiltonian describing the electric dipole coupling to the radiation fields; $\rho_{\alpha\alpha}$ is a measure of the population in level $|\alpha>$; and $\rho_{\alpha\beta}$ is the measure of the coherent superposition of levels $|\alpha>$ and $|\beta>$. Due to their complexity, the details of the analysis will be omitted and only the results will be given (the reader is referred to the book entitled *Optical Phase Conjugation* edited by Robert Fisher, Academic Press (1982), for a more in-depth discussion). Furthermore, it is assumed that the input fields are in the same state of polarization.

A. Two-Level System

There exist two distinct physical contributions that can give rise to the phase-conjugate field $\vec{E}_s$. The first one arises from the spatial modulation of the population difference generated by the interference of the pump field $\vec{E}_f$ and probe field $\vec{E}_p$, and the subsequent coherent scattering of the pump field $\vec{E}_b$ off this spatial modulation. In the second one, it is the pump field $\vec{E}_b$ that creates an interference with the probe field $\vec{E}_p$. The phase-conjugate signal is obtained from the coherent scattering of the pump $\vec{E}_f$.

The generation of the spatial modulation and the phase-conjugate signals must necessarily involve the basic dynamics of resonance absorption and re-emission processes. The atoms or molecules must interact with the input and generated fields. Simple Doppler shift relations can be written to describe the nonlinear interaction processes, i.e.,

$$\omega - \omega_o - \vec{K}_n \cdot \vec{V} = 0 \quad (2a)$$

$$\omega - \omega_o - \vec{K}_p \cdot \vec{V} = 0 \quad (2b)$$

$$\omega - \omega_o + \vec{K}_p \cdot \vec{V} = 0 \; . \quad (2c)$$

where ω is the laser frequency, ω_o is the resonance frequency, K_n is the wave number of pump field $\vec{E}_n$, and $\vec{V}$ is the velocity of the atomic species.

The first two resonance conditions in Eq. (2) express the fact that the generation of the interference pattern involves absorption processes for one of the pump fields and the probe field. The last resonance condition is a statement of the coherent re-emission process. For nearly collinear geometry, Eq. (2) implies that only those atoms having $\vec{V} = 0$ along the wave propagation direction can interact effectively to generate a phase-conjugate signal. Hence the selection of the $\vec{V} = 0$ velocity group by the radiation fields leads to a Doppler-free interaction process. The spectrum of the phase-conjugate signal is given by a Lorentzian profile having a maximum at $\omega = \omega_o$ and a spectral width given by the natural linewidth of the quantum system.

The response of the medium is given by the polarization

$$\vec{P}(\vec{r},t) = \int_{-\infty}^{\infty} d^3V \, \rho_{12} \, \vec{\mu}_{21} + \text{c.c.} \; , \quad (3)$$

where $\vec{\mu}_{21}$ is the electric dipole moment. The integration takes into account the random motion of the atoms. One technique useful to evaluate Eq. (3) involves computing the density matrix ρ_{12} to third order in the field strengths using a Feynman-type diagrammatic approach. The various third-order perturbation schemes are depicted in Figs. (4) and (5), where p denotes population and c denotes optical coherences. A set of Feynman-type diagrams can then be drawn to visualize the effects of the radiation fields on the atoms. Figs. (4) and (5) show the various distinct quantum mechanical amplitudes that give rise to the polarization expression (3). Figure (4a) says that given an initial population difference, the effect of the pump field $\vec{E}_f$ is to generate a coherent superposition of lower and upper levels; i.e.,

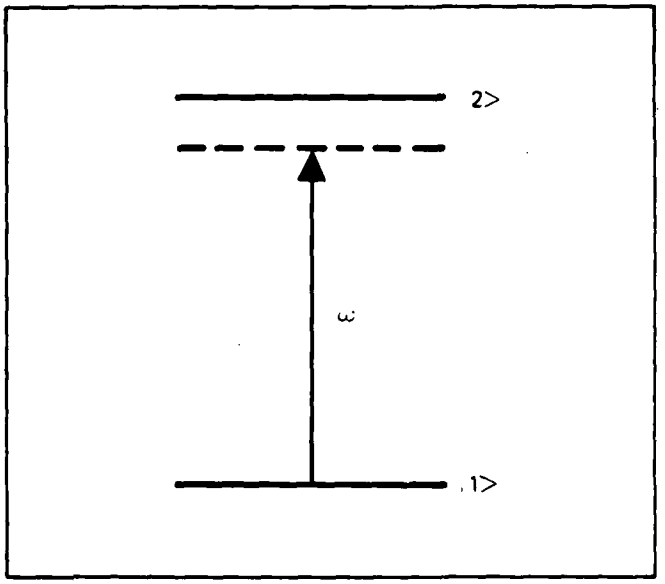

Fig. 1. Two-level system.

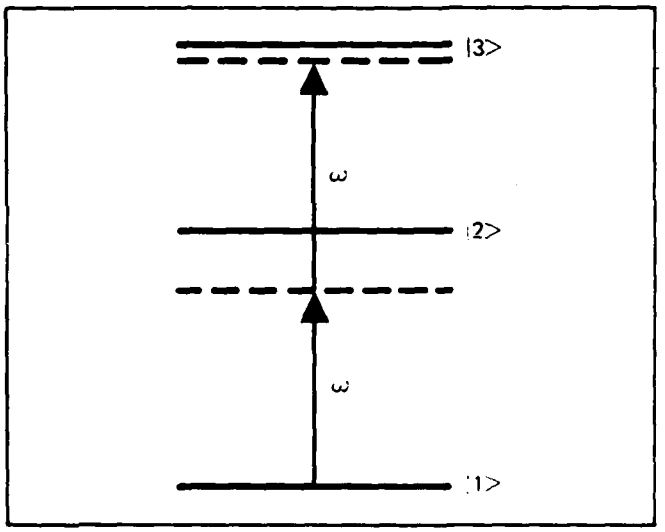

Fig. 2. Cascade-up three-level system.

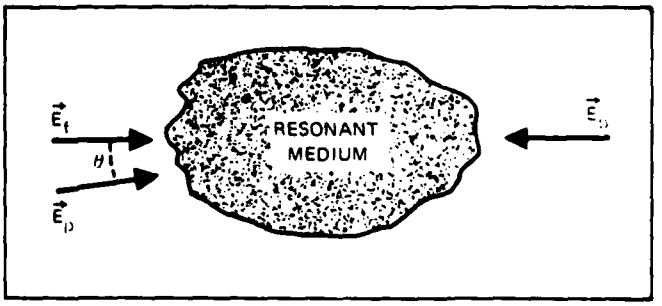

Fig. 3. The interaction geometry.

an optical coherence is produced. The action of the probe field produces changes in the population differences, i.e., a spatial modulation is created. Next, the pump field $\vec{E}_b$ generates an additional contribution to the optical coherence which is responsible for the polarization expression (3); i.e., it generates a phase-conjugate signal. A similar interpretation can be given to Figs. (4b) and (5).

A direct calculation of the sum of the diagrams or, equivalently, the quantum mechanical amplitudes, yields an expression for the polarization in terms of the plasma dispersion function. For the physical situation in which the natural linewidths, energy decay rates, and the laser detuning from resonance are much smaller then the Doppler width,[16] the nonlinear polarization becomes

$$P(\vec{r},t) = \frac{\text{constant}}{\gamma + i(\omega - \omega_0)} \xi_f \xi_b \xi_p^* e^{i(\omega t + \vec{K}_p \cdot \vec{r})} . \qquad (4)$$

where γ is the natural linewidth and the field envelope ϵ_n is defined to be $E(\vec{r},t) = \frac{1}{2}\xi(\vec{r})e^{i(\omega t - \vec{K}\cdot\vec{r})} + \text{c.c.}$ Expression (4) serves as a source in Maxwell's equation, and the resultant phase-conjugate signal is essentially proportional to the RHS of Eq. (4). Hence the spectrum of the phase-conjugate intensity is a Lorentzian and thus provides a powerful tool for determining the natural or collision broadened linewidths of any atomic or molecular system.

Experimental studies of the D_2 line of atomic sodium were carried out using the technique of DFWM.[17,18] The experimentally measured linewidth of the $3S_{1/2}(F=2)$ to $3P_{3/2}(F=3)$ transition was 20 MHz which is bigger than the well known value of 10 MHz. The discrepancy may be due to the stability of the Argon ion pumped cw dye laser system, residual Doppler shifts, and optical pumping. In another set of experiments, the spectra of gaseous SF_6 in the ν_3 mode was partially resolved using a CO_2 laser as a probe which was tuned around the P_{16} line.[19,20] At room temperature, the calculated Doppler width of gaseous SF_6 is 30 MHz. However, the spectral resolution of the experimental data was better than 5 MHz. This observation shows the Doppler-free nature of DFWM. A novel variation of the DFWM technique was developed to study the spectra of molecular iodine[21] and Argon discharges.[22] The essence of these approaches is to slightly detune the frequency of the probe field by an amount $+\delta$ away from the pump fields. From the law of conservation of energy, the phase-conjugate signal is slightly detuned from the pump field by an amount $-\delta$. Hence one can use the difference in frequency for heterodyne detection. For the I_2 study, the first measurement of the effects of quenching collisions on the ground state of the iodine molecules was made. It was found that the pressure broadening was roughly identical for both the ground and excited states, and the value of the pressure-broadened width was estimated to be 3.4—3.8 MHz torr. A typical experimental set-up that is used in the generation of phase-conjugate signal and studies of atomic or molecular spectra is shown in Fig. 6.

B. Three-Level System

The physical mechanism[23-25] giving rise to a phase-conjugate signal in a three-level system (see Fig. 2) is the generation of a two-photon coherence between the levels $|1\rangle$ and $|3\rangle$ by means of the counterpropagating pump fields; i.e., the action of the pump fields generates a coherent superposition of levels $|1\rangle$ and $|3\rangle$.[23] This excitation process has two interesting properties. First, unlike the spatial modulation mechanism of the one-photon transition, the two-photon coherence is spatially uniform and oscillates in time at twice the input frequency. Second, the resonance condition for the generation of the two-photon coherence is given by

$$2\omega - \Omega - (\vec{K}_f - \vec{K}_b)\cdot\vec{V} = 0 . \qquad (5)$$

where Ω is the transition frequency between levels $|3\rangle$ and $|1\rangle$. The counterpropagating nature of the pump fields implies that $\vec{K}_f + \vec{K}_b = 0$. Hence, the interaction process is Doppler-free, and all the atoms in the sample participate in the generation of the two-photon coherence.

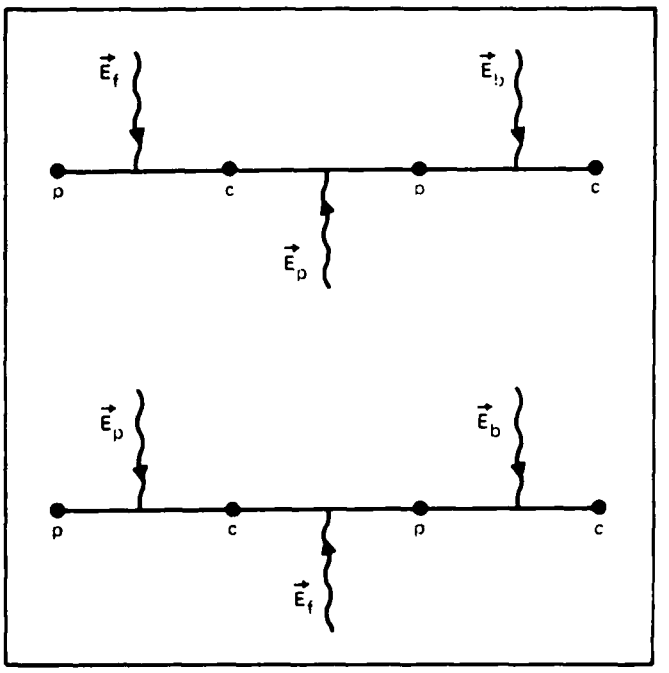

Fig. 4. Physical diagrams leading to the calculation of the third-order response in the case of the interference generated by the forward pump and probe.

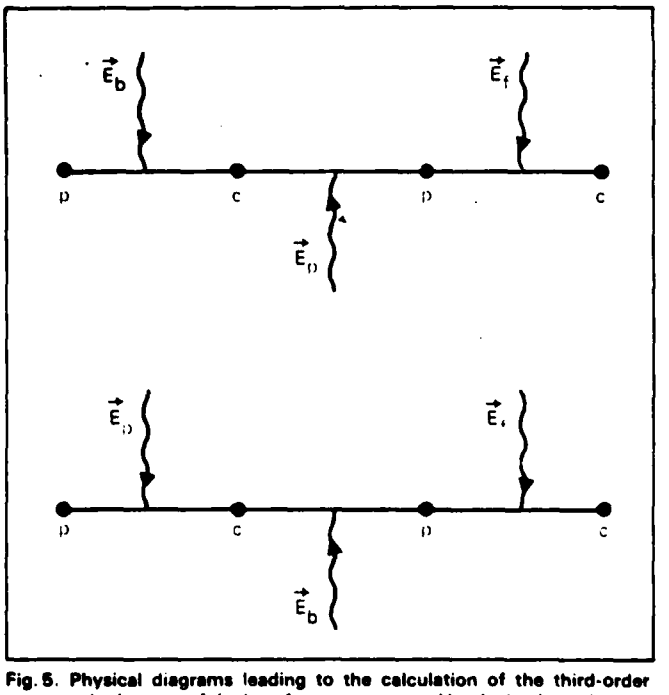

Fig. 5. Physical diagrams leading to the calculation of the third-order response in the case of the interference generated by the backward pump and probe.

The phase-conjugate signal is produced via the probe field induced two-photon parametric process as shown in Fig. 7. One should remember that no population is involved in this physical mechanism. The absence of the spatial modulation contribution arises from the fact that the input fields are far detuned from the intermediate level resonance, and the laser detuning is large compared to the Doppler width.

The calculation of the polarization proceeds in the same manner

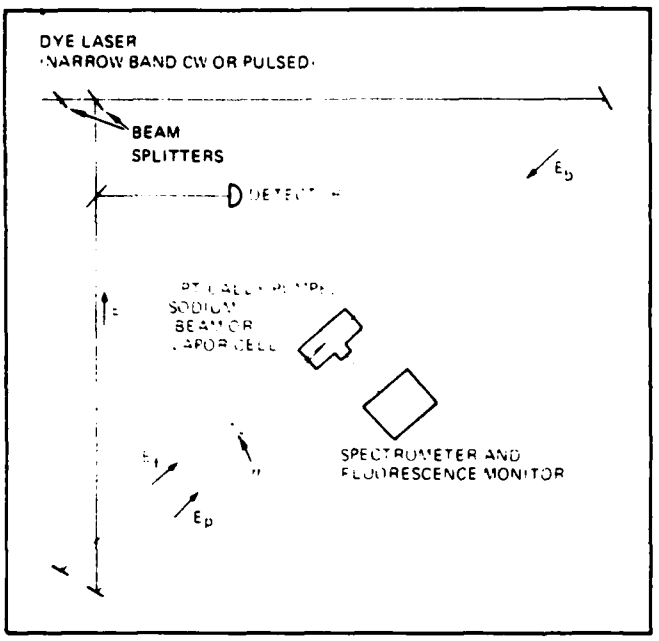

Fig. 6. A typical experimental set-up in DFWM experiments.

as before. Figure 8 shows the physical schemes (Feynman-type diagrams) leading to the phase-conjugate signal. In the extreme Doppler limit, the result is given by

$$P(\vec{r},t) = \frac{\text{constant}}{\gamma_2 + i(2\omega - \Omega)} \xi_f \xi_b \xi_p^* e^{i(\omega t + \vec{k}_p \cdot \vec{r})} , \qquad (6)$$

where γ_2 is the two-photon linewidth. Again, in the small signal regime, the generated signal is proportional to the RHS of Eq. (6).

The first experimental observation of two-photon DFWM was performed in atomic rubidium whose detuning from intermediate level $|2\rangle$ was small ($\sim 20\,cm^{-1}$).[26] The variation of this technique for small probe field detuning was also demonstrated as a powerful tool for studying metastable transitions.[26]

III. TRANSIENT DFWM

We shall now consider an experimental situation for which the duration of the input pulses is short compared to all relevant characteristic relaxation time of the medium.

In this regime, the density matrix equation acquires a temporal dependence. The set of equations (1) now takes the following form

$$i\hbar\left(\frac{\partial}{\partial t} + \gamma_\alpha + \vec{V}\cdot\nabla\right)\rho_{\alpha\alpha} = \lambda_\alpha + [H,\rho]_{\alpha\alpha} \qquad (7a)$$

$$i\hbar\left(\frac{\partial}{\partial t} + \gamma_{\alpha\beta} + i(\omega - \omega_{\beta\alpha}) + \vec{V}\cdot\nabla\right)\rho_{\alpha\beta} = [H,\rho]_{\alpha\beta} . \qquad (7b)$$

and the computation of the quantum mechanical scattering amplitudes proceeds along the same line as shown in Figs. (4), (5), and (8) while keeping the time of the interaction in the proper context. In essence of this approach is to construct the required excitation by means of two overlapping pulses (within the dephasing time) and time-delay the third pulse or sequence of pulses. The generation of the sequence of signal pulses yields direct information on the characteristic (e.g., energy and dephasing) decay rate. In the case of a two-level system, Fig. 9 shows the required sequence of fields. The purpose of the excitation sequence is to measure the energy decay rate of the population grating generated by the interference of the forward pump and probe pulses. Specifically, the population grating generated by the forward pump and probe pulses at time $t = 0$ will

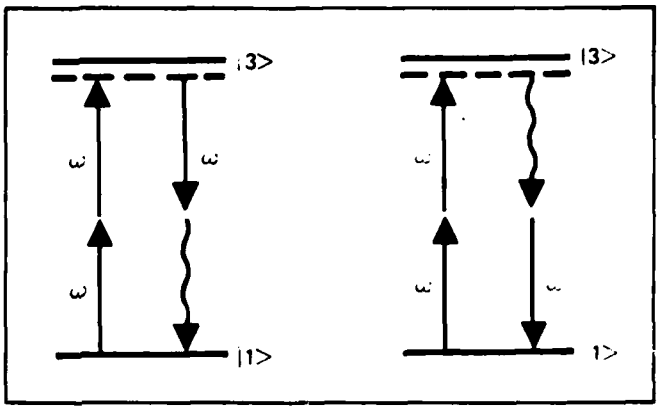

Fig. 7. Parametric processes leading to phase-conjugate signal in the three-level system.

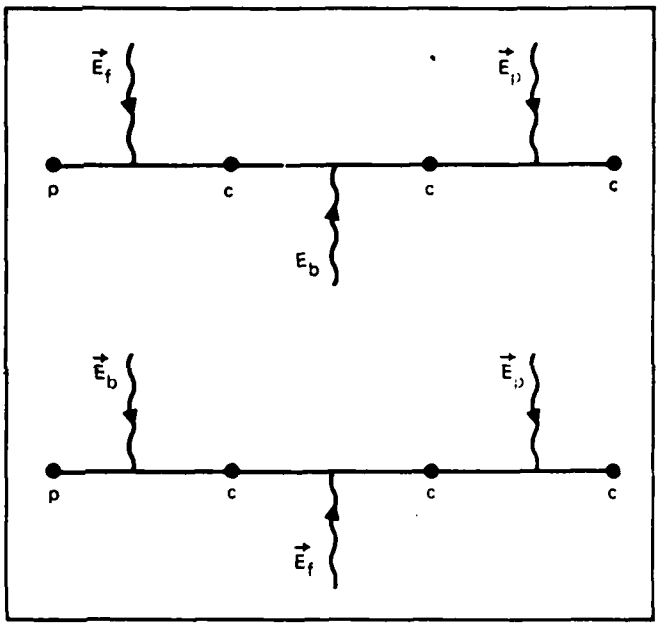

Fig. 8. Physical diagrams leading to the calculation of the third-order response in the case of the two-photon coherence generated by the counterpropagating pump waves.

start relaxing with an energy decay rate

$$\Gamma = 1/T_1, \text{ i.e., population} = \text{constant } e^{-t/T_1} . \qquad (8)$$

The sequence of backward pump pulses examines the energy decay phenomena by generating a sequence of signal pulses

$$\text{signal} \propto \sum_{i=1}^{n} e^{-t_i/T_1} . \qquad (9)$$

where n is the number of backward pump pulses, t_i denotes the time of action of the ith backward pump pulse; and, as an example, t_1 is the time delay between the creation of the population grating and the arrival of the first backward pump pulse.

This technique was used in the measurement of the collisional relaxation rates of the 5896 Å line of sodium atoms, using nanosecond pulses.[27] In this experiment a buffer gas (argon) was introduced in the sodium cell. For the case in which the forward pump is linearly polarized and 90° cross polarized with respect to the backward pump and probe, it was found that phase-interrupting collisions dominate over velocity-changing collisions. A similar method

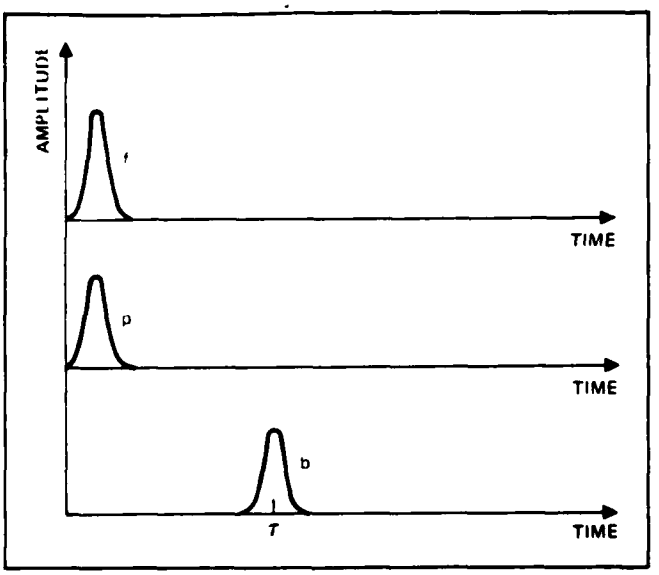

Fig. 9. A time delayed set-up for measuring the energy relaxation rate.

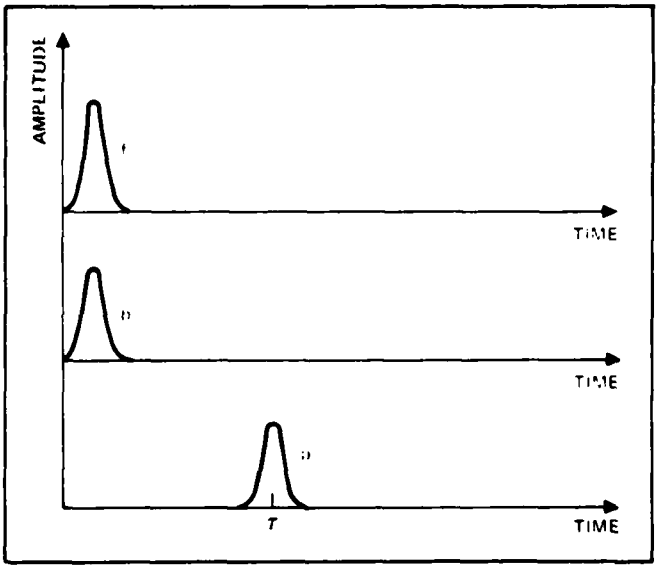

Fig. 10. A time delayed set-up for measuring the two-photon coherence dephasing rate.

was applied to the study of the mechanisms of energy transport in molecular solids by using picosecond pulses.[28] Using a variation of the geometry of DFWM, the measurement of thermal diffusion processes and electronic lifetimes were also made.[29]

In the case of three-level systems, Fig. 10 shows the required sequence of pulses for measuring the two-photon dephasing rates.[13] Again, the simultaneous action of the counterpropagating waves generates a two-photon coherence at time $t = 0$. The two-photon coherence relaxes with a characteristic time T_2; i.e.,

$$\text{Two-photon coherence} = \text{constant}\, e^{-t/T_2}. \tag{10}$$

A time-delayed sequence of probe pulses generates a sequence of signal pulses which provides a measurement of a dephasing time T_2, i.e.,

$$\text{signal} \propto \sum_{i=1}^{n} e^{-t_i/T_2}. \tag{11}$$

where the notation follows as before.

As mentioned, this technique has been applied to the measurement of the two-photon dephasing rate of Na in the presence of collisions.[13] These measured pressure-broadened coefficients for neon, helium, and argon are 16 ± 3 MHz torr, 36 ± 3 MHz torr, and 47 ± 3 MHz torr, respectively. Its application to the molecular system SF_6 yielded additional information concerning the intramolecular relaxation processes.[30] It was found that the collisionless dephasing rate was 0.17 GHz. Changing the pressure of SF_6 did not change the measured rate.

IV. CONCLUSIONS

We have shown that the basic physics of DFWM provides a new technique of studying the atomic and molecular spectra. The Doppler-free nature of the generated signal in the steady-state regime (cw laser sources) allows one to measure various atomic dephasing times. In the transient and time-delayed regimes, both the energy relaxation and dephasing rates can be measured by an appropriate temporal sequencing of the input pulses.

In our discussion, we have neglected the effects of saturation due to high intensity pump waves. Although preliminary experimental data exist in that regime, little is understood in the inhomogeneously broadened system. Furthermore, the complications due to the interaction length and self-focusing phenomena serve to obscure the basic physics of the nonlinear response. As yet no theory exists which describes these complications.

V. ACKNOWLEDGMENT

This work was supported in part by the Army Research Office under Contract No. DAAG29-81-C-0008.

VI. REFERENCES

1. R. A. McFarlane, W. R. Bennett, Jr., and W. E. Lamb, Jr., Appl. Phys. Lett. 2, 189(1963). A. Szoke and A. Javan, Phys. Rev. Lett. 10, 521(1963).
2. V. S. Letokhov and V. P. Chebotayev, Pis'ma Zh. Eksp. Ter. Fiz. 9, 364(1969). H. R. Schlossberg and A. Javan, Phys. Rev. 150, 267(1966).
3. L. S. Vasilenko, V. P. Chebotayev, and A. V. Shishaev, Pis'ma Zh. Eksp. Ter. Fiz. 12, 161(1970).
4. C. Wieman and T. W. Hansch, Phys. Rev. Lett. 36, 1170(1976).
5. I. D. Abella, N. A. Kurnit, and S. R. Hartmann, Phys. Rev. 141, 391(1966).
6. R. G. Brewer and R. L. Shoemaker, Phys. Rev. A 6, 2001(1972).
7. B. I. Stepanov, E. V. Ivakin and A. S. Rubanov, Sov. Phys. Doklady Tech. Phys. 16, 46(1971).
8. V. Wang and D. Close, invention disclosure, Hughes Research Laboratories (1974).
9. R. W. Hellwarth, J. Opt. Soc. Am. 67, 1(1977).
10. D. M. Bloom and G. Bjorklund, Appl. Phys. Lett. 31, 592(1977).
11. A. Yariv and D. M. Pepper, Opt. Lett. 1, 16(1977).
12. R. L. Abrams and R. C. Lind, Opt. Lett. 2, 94(1978); 3, 203(1978).
13. P. F. Liao, N. P. Economou, and R. R. Freeman, Phys. Rev. Lett. 39, 1473(1977).
14. A. Yariv and J. AuYeung, IEEE J. of Quant. Electron. QE-15, 224(1979).
15. D. G. Steel, J. F. Lam, and R. A. McFarlane, Laser Specroscpy V, A. R. W. McKellar, T. Oka and B. P. Stoicheff, editors, Springer Verlag, Berlin (1981).
16. S. M. Wandzura, Opt. Lett. 4, 208(1979).
17. D. M. Bloom, P. F. Liao, and N. P. Economou, Opt. Lett. 2, 158(1978).
18. J. F. Lam, D. G. Steel, R. A. McFarlane, and R. C. Lind, Appl. Phys. Lett. 38, 977(1981).
19. P. Aubourg, J. P. Bettini, G. P. Agrawal, P. Cottin, D. Guenin, O. Meunier, and J. L. Boulnois, Opt. Lett. 6, 383(1981).
20. D. G. Steel and J. F. Lam, Opt. Commun. 40, 77(1981).
21. R. K. Raj, D. Bloch, J. J. Snyder, G. Camy, and M. Ducloy, Phys. Rev. Lett. 44, 1251(1980).
22. D. Bloch and M. Ducloy (private communications).
23. M. Matsuoka, Opt. Commun. 15, 84(1975).
24. D. C. Hauensen, Opt. Commun. 28, 183(1979).
25. A. K. Popov and V. M. Shalaev, Appl. Phys. 21, 93(1980).
26. D. Bloch, E. Giacobino, and M. Ducloy, J. Phys. B At. Mol. Phys. 14, L819(1981).
27. M. Fujita, H. Nakatsuka, H. Nakanishi, and M. Matsuoka, Phys. Rev. Lett. 42, 974(1979).
28. J. R. Salcedo, A. E. Siegman, D. D. Dlott, and M. D. Fayer, Phys. Rev. Lett. 41, 131(1978).
29. H. J. Eichler, Optica Act. 24, 631(1977).
30. D. G. Steel and J. F. Lam, Phys. Rev. Lett. 43, 1588(1979).

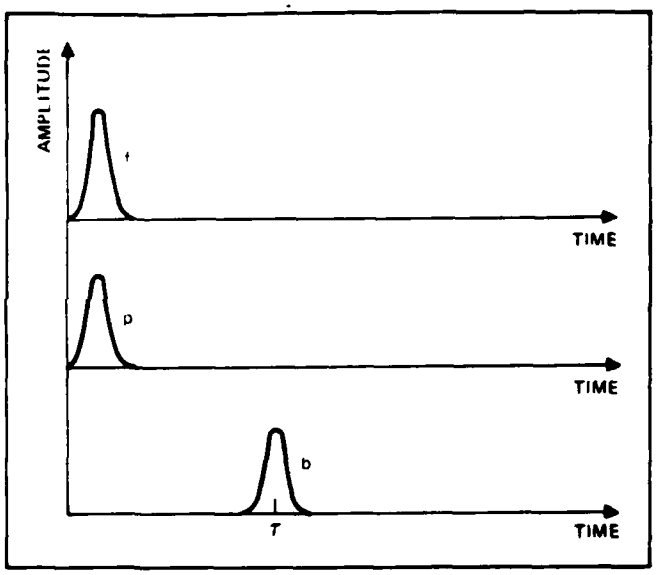

Fig. 9. A time delayed set-up for measuring the energy relaxation rate.

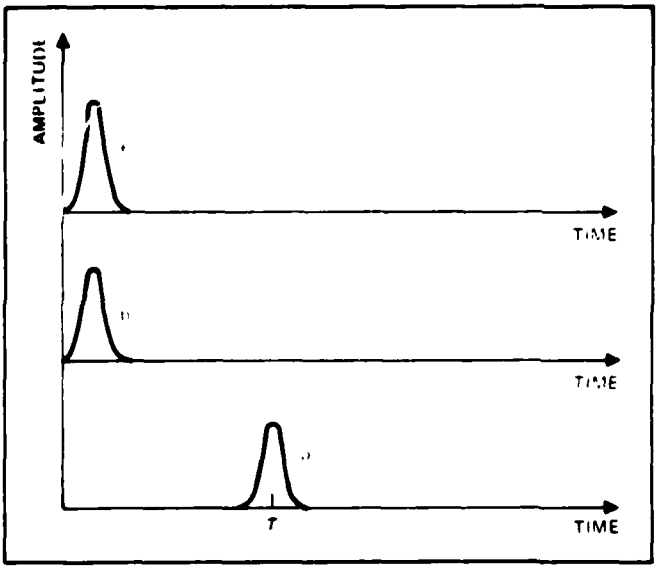

Fig. 10. A time delayed set-up for measuring the two-photon coherence dephasing rate.

was applied to the study of the mechanisms of energy transport in molecular solids by using picosecond pulses.[28] Using a variation of the geometry of DFWM, the measurement of thermal diffusion processes and electronic lifetimes were also made.[29]

In the case of three-level systems, Fig. 10 shows the required sequence of pulses for measuring the two-photon dephasing rates.[13] Again, the simultaneous action of the counterpropagating waves generates a two-photon coherence at time $t = 0$. The two-photon coherence relaxes with a characteristic time T_2; i.e.,

$$\text{Two-photon coherence} = \text{constant } e^{-t/T_2}. \tag{10}$$

A time-delayed sequence of probe pulses generates a sequence of signal pulses which provides a measurement of a dephasing time T_2, i.e.,

$$\text{signal} \propto \sum_{i=1}^{n} e^{-t_i/T_2}. \tag{11}$$

where the notation follows as before.

As mentioned, this technique has been applied to the measurement of the two-photon dephasing rate of Na in the presence of collisions.[13] These measured pressure-broadened coefficients for neon, helium, and argon are 16 ± 3 MHz torr, 36 ± 3 MHz torr, and 47 ± 3 MHz torr, respectively. Its application to the molecular system SF_6 yielded additional information concerning the intramolecular relaxation processes.[30] It was found that the collisionless dephasing rate was 0.17 GHz. Changing the pressure of SF_6 did not change the measured rate.

IV. CONCLUSIONS

We have shown that the basic physics of DFWM provides a new technique of studying the atomic and molecular spectra. The Doppler-free nature of the generated signal in the steady-state regime (cw laser sources) allows one to measure various atomic dephasing times. In the transient and time-delayed regimes, both the energy relaxation and dephasing rates can be measured by an appropriate temporal sequencing of the input pulses.

In our discussion, we have neglected the effects of saturation due to high intensity pump waves. Although preliminary experimental data exist in that regime, little is understood in the inhomogeneously broadened system. Furthermore, the complications due to the interaction length and self-focusing phenomena serve to obscure the basic physics of the nonlinear response. As yet no theory exists which describes these complications.

V. ACKNOWLEDGMENT

This work was supported in part by the Army Research Office under Contract No. DAAG29-81-C-0008.

VI. REFERENCES

1. R. A. *McFarlane*, W. R. *Bennett*, Jr., and W. E. Lamb, Jr., Appl. Phys. Lett. 2, 189(1963). A. Szoke and A. Javan, Phys. Rev. Lett. 10, 521(1963).
2. V. S. Letokhov and V. P. Chebotayev, Pis'ma Zh. Eksp. Ter. Fiz. 9, 364(1969). H. R. Schlossberg and A. Javan, Phys. Rev. [illegible], 267(1966).
3. L. S. Vasilenko, V. P. Chebotayev, and A. V. Shishaev, Pis'ma Zh. Eksp. Ter. Fiz. 12, 161(1970).
4. C. Wieman and T. W. Hansch, Phys. Rev. Lett. 36, 1170(1976).
5. I. D. Abella, N. A. Kurnit, and S. R. Hartmann, Phys. Rev. 141, 391(1966).
6. R. G. Brewer and R. L. Shoemaker, Phys. Rev. A 6, 2001(1972).
7. B. I. Stepanov, E. V. Ivakin and A. S. Rubanov, Sov. Phys. Doklady Tech. Phys. 16, 46(1971).
8. V. Wang and D. Close, *invention disclosure*, Hughes Research Laboratories (1974).
9. R. W. Hellwarth, J. Opt. Soc. Am. 67, 1(1977).
10. D. M. Bloom and G. Bjorklund, Appl. Phys. Lett. 31, 592(1977).
11. A. Yariv and D. M. Pepper, Opt. Lett. 1, 16(1977).
12. R. L. Abrams and R. C. Lind, Opt. Lett. 2, 94(1978); 3, 203(1978).
13. P. F. Liao, N. P. Economou, and R. R. Freeman, Phys. Rev. Lett. 39, 1473(1977).
14. A. Yariv and J. AuYeung, IEEE J. of Quant. Electron. QE-15, 224(1979).
15. D. G. Steel, J. F. Lam, and R. A. McFarlane, Laser Specroscpy V, A. R. W. McKellar, T. Oka and B. P. Stoicheff, editors, Springer Verlag, Berlin (1981).
16. S. M. Wandzura, Opt. Lett. 4, 208(1979).
17. D. M. Bloom, P. F. Liao, and N. P. Economou, Opt. Lett. 2, 158(1978).
18. J. F. Lam, D. G. Steel, R. A. McFarlane, and R. C. Lind, Appl. Phys. Lett. 38, 977(1981).
19. P. Aubourg, *J. P. Bettini, G. P. Agrawal, P. Cottin, D. Guenin*, O. Meunier, and J. L. Boulnois, Opt. Lett. 6, 383(1981).
20. D. G. Steel and J. F. Lam, Opt. Commun. 40, 77(1981).
21. R. K. Raj, D. Bloch, J. J. Snyder, G. Camy, and M. Ducloy, Phys. Rev. Lett. 44, 1251(1980).
22. D. Bloch and M. Ducloy (private communications).
23. M. Matsuoka, Opt. Commun. 15, 84(1975).
24. D. C. Hauensen, Opt. Commun. 28, 183(1979).
25. A. K. Popov and V. M. Shalaev, Appl. Phys. 21, 93(1980).
26. D. Bloch, E. Giacobino, and M. Ducloy, J. Phys. B: At. Mol. Phys. 14, L819(1981).
27. M. Fujita, H. Nakatsuka, H. Nakanishi, and M. Matsuoka, Phys. Rev. Lett. 42, 974(1979).
28. J. R. Salcedo, A. E. Siegman, D. D. Dlott, and M. D. Fayer, Phys. Rev. Lett. 41, 131(1978).
29. H. J. Eichler, Optica Act. 24, 631(1977).
30. D. G. Steel and J. F. Lam, Phys. Rev. Lett. 43, 1588(1979).

Submitted to IQEC '82

PRESSURE INDUCED EFFECTS ON CW DEGENERATE AND NEARLY DEGENERATE FOUR-WAVE MIXING

D.G. Steel, R.A. McFarlane and J.F. Lam

Hughes Research Laboratories
3011 Malibu Canyon Road
Malibu, California 90265
213-456-6411

ABSTRACT

Noble gas collisions on the $3s^2S_{1/2} - 3p^2P_{3/2}$ transition in sodium are studied. Effects of collisions on fine structure, hyperfine structure, and velocity are considered theoretically and collisionally enhanced nonlinear response and bandwidth effects including collisional narrowing are demonstrated experimentally.

PRESSURE INDUCED EFFECTS ON CW DEGENERATE AND NEARLY DEGENERATE FOUR-WAVE MIXING

D.G. Steel, R.A. McFarlane, and J.F. Lam

Hughes Research Laboratories
3011 Malibu Canyon Road
Malibu, California 90265
213-456-6411

We report experimental and theoretical studies on the effect of buffer gas collisions with sodium atoms using nearly degenerate four-wave mixing (NDFWM) as well as degenerate four-wave mixing (DFWM) using the $3s^2S_{1/2} - 3p^2P_{3/2}$ transition. Our work demonstrates collisional narrowing of the pump-probe detuning bandwidth in NDFWM and collisional enhancement of certain optically pumped hyperfine components in DFWM.

The first set of experiments we describe involve NDFWM using two cw tunable stabilized dye lasers tuned to the 5890 Å transition. In the experiments, the backward pump (E_b) and forward pump (E_f) are supplied by the same laser and are arranged to be exactly counterpropagating. The probe is supplied by a second dye laser and is nearly collinear with the forward pump ($\theta < 1°$). In an earlier paper, we reported the multiresonant complex spectral structure observed in Doppler-broadened media when the probe frequency is tuned with respect to the pump frequency.[1] If the pump frequency is detuned from the atomic resonance by an amount Δ and δ is the pump-probe detuning, then we find two resonances as the probe frequency is adjusted occurring at $\delta = 0$ and $\delta = 2\Delta$. The first resonance has a width determined by T_1 while the width of the second resonance is determined by T_2 as shown in Fig. 1a. Hence, it is expected that collisions should affect these two resonances quite differently. Indeed, as buffer gas is added, we observe that the width and relative amplitude of the second resonance changes as expected due to dephasing collisions (Fig. 1b). However, the first resonance is actually observed to experience narrowing. In fact, at high buffer gas pressures when $\Delta = 0$, we observe that the pump-probe detuning bandwidth decreases from roughly 20 MHz to less than 10 MHz (Fig. 1c).

The theoretical work to describe these collisional effects in NDFWM uses a collision model which includes phase interrupting collisions affecting the optical coherence and velocity changing collisions (vcc) which affect

the populations.[2] The phase interrupting collisions give rise to pressure broadening and a pressure induced shift in the resonance frequency. Vcc lead to a thermalization of the velocity distribution in the limit of the strong vcc approximation. As indicated above there are two components to the phase conjugate signal. The first one (arising from the v = 0 velocity class) is strongly affected by vcc while the second component (arising from the $\omega_{forward} - \omega_o - \vec{k}_f \cdot \vec{v} = 0$ velocity class) is not affected by vcc but undergoes pressure broadening due to phase interrupting collisions. In addition, fine structure (fs) changing collisions (i.e., $^3P_{3/2} \leftrightarrow ^3P_{1/2}$) are included along with hyperfine structure (hfs) changing collisions in order to enable quantitative comparison between theory and experiment.[3]

In the absence of buffer gas, DFWM experiments in sodium on the 5890 Å transition have shown the importance of hfs optical pumping.[4] There are six dipole allowed hf transitions at 5890 Å. The ground state ($^2S_{1/2}$) is split into two hf levels with F = 2 and 1 (where F is the total angular momentum quantum number). The upper level ($^2P_{3/2}$) is split into four hf levels (F = 0 - 3). Because of optical pumping usually only the $^2S_{1/2}$ (F = 2) - $^2P_{3/2}$ (F = 3) and the $^2S_{1/2}$ (F = 0) - $^2P_{3/2}$ (F = 1) transitions are observed. The remaining four transitions are weak since optical pumping removes the ground state population from the desired F level to the remaining F level where the atoms are no longer resonant with the laser frequency. The two strong transitions (denoted 2-3 and 0-1, respectively) are not optically pumped since decay from F = 3 to F = 1 and F = 0 to F = 2 are dipole forbidden. However, in the presence of buffer gas, the above behavior is dramatically affected due to fs and hfs changing collisions and vcc. Our measurements show that at very low buffer gas pressures (a few tens of millitorr), the strength of the 2-3 transition is significantly reduced while the normally very weak signal on $^2S_{1/2}$(F = 1) - $^2P_{3/2}$ (F = 2) transition is enhanced. We presently believe that in the first case, diffusion coupled with fs and hfs changing collisions provides a strong optical pumping effect resulting in a significant depopulation of the F = 2 ground state. As indicated above in the second case, normal optical pumping depletes the F = 1 ground state. However, in the presence of buffer gas vcc are believed to play an important role in effectively increasing the steady-state population of the depleted ground state. Experimental data to support these explanations are presented for various buffer gases.

D.G. Steel, R.A. McFarlane, and J.F. Lam
Hughes Research Laboratories

The analysis of these effects in DFWM is based on both a simple rate equation model and a more detailed density matrix calculation. In the first case, both diffusion, fs and hfs changing collisions, and vcc are included but standing wave effects are ignored. A density matrix calculation is also described where standing wave effects are included.

This work was supported in part by the Army Research Office, Contract No. DAA529-81-C-0008.

References:

1. D.G. Steel and R.C. Lind, Opt. Lett. 6, 587 (1981).
2. J.F. Lam and P.R. Berman, "Theory of Collision Effect in Resonant DFWM I: Nondegenerate Energy Levels," submitted to Phys. Rev. A.
3. P.F. Liao, J.E. Bjorkholm, and P.R. Berman, Phys. Rev. 2, 20 1489 (1979).
4. D.M. Bloom, P.F. Liao, N.P. Economou, Opt. Lett. 2, 58 (1978).

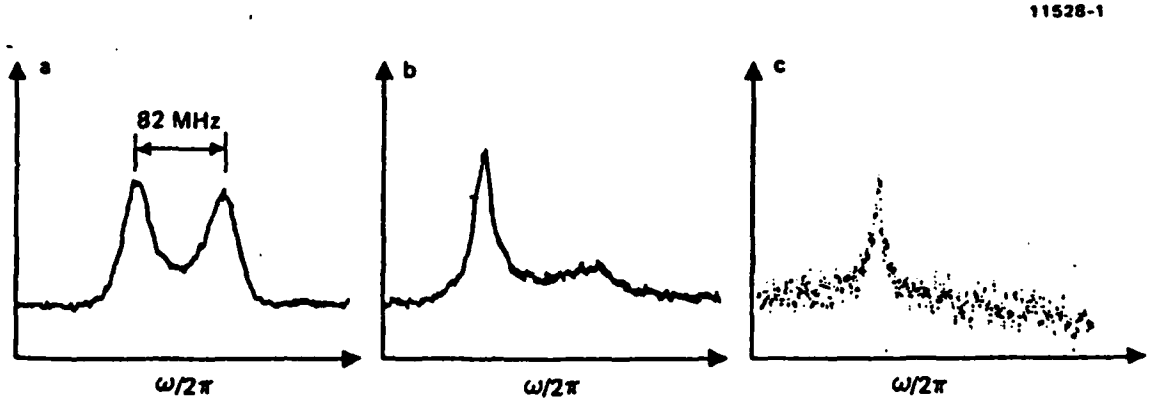

Figure 1: Pump-probe detuning response (a) $\Delta \tilde{-} 82$ MHz with no buffer gas; (b) $\Delta \tilde{-} 82$ MHz with 2 Torr of neon buffer-gas; (c) $\Delta = 0$ with 33 Torr of neon buffer gas.

Submitted to IQEC '82

COLLISION STUDIES OF HIGHLY EXCITED ATOMIC STATES USING A NEW CW FOUR-WAVE MIXING SPECTROSCOPY TECHNIQUE

J.F. Lam, D.G. Steel and R.A. McFarlane

Hughes Research Laboratories
3011 Malibu Canyon Road
Malibu, California 90265
213-456-6411

ABSTRACT

Theoretical and experimental results are presented describing a new Doppler-free spectroscopy technique using two wavelength 4-wave mixing coupling a 3-level system. Frequency domain measurements of noble gas dephasing cross-sections are made for high lying states of sodium.

COLLISION STUDIES OF HIGHLY EXCITED ATOMIC STATES USING A NEW CW FOUR-WAVE MIXING SPECTROSCOPY TECHNIQUE

J.F. Lam, D.G. Steel and R.A. McFarlane

Hughes Research Laboratories
3011 Malibu Canyon Road
Malibu, California 90265
213-456-6411

This paper describes measurements of buffer gas collision rates with high lying atomic states in sodium using a new Doppler free spectroscopy technique. The approach uses two narrow band stabilized tunable dye lasers at frequencies Ω_1 and Ω_2 in a two photon four-wave mixing experiment. With two separate wavelengths we are able to eliminate the usually large intermediate state detuning that results when two photon resonant degenerate four-wave mixing is used to study a three level system. By appropriate geometry, the signal in our approach is generated by a pure two-quantum excitation with no stepwise contribution. We are thus able to examine collision physics affecting the final state without being obscured by intermediate state effects. We anticipate that this technique will be extremely powerful in investigating collisional effects on the Rydberg series. The ability for this technique to produce large signals even for collision studies of highly excited states overcomes sensitivity problems due to large intermediate state detuning using degenerate two-photon absorption.[1] It also provides an important laser spectroscopy measurement of collisional effects giving rise to broadening and level shifts in the frequency domain in contrast to earlier measurements of broadening in the time domain using pulsed lasers.[2,3]

The analysis begins by assuming a cascade up three level system. The geometry involves a backward pump, E_b, at frequency Ω_1 (resonant with the first transition at frequency ω_{21}) and a forward pump, E_f, and probe, E_p, at frequency Ω_2 (resonant with the second transition out of level 2 at frequency ω_{32}). We assume that the forward and backward pumps are arranged to be counterpropagating and the probe beam is nearly collinear with the forward pump. We further assume that the level energies in the cascade-up three-level system are given by $E_3 > E_2 > E_1$. In this geometry the physical origin of the signal (which is nearly counterpropagating to the probe wave) arises from a four-wave mixing interaction generated by a two-photon coherence between levels 1 and 3 induced by the simultaneous interaction of E_f and E_b.

J.F. Lam, D.G. Steel, R.A. McFarlane
Hughes Research Laboratories

In collinear geometry the resonance condition that must be satisfied in order for all four waves to interact with the same velocity group is given by $\Omega_2 - \omega_{32} = -(k_2/k_1)\ (\Omega_1 - \omega_{21})$. Using the density matrix approach and calculating the polarization using perturbation theory to third order in the fields[4] we find in the Doppler limit the frequency response is a Lorentzian whose linewidth is given by the two-photon linewidth γ_{13} plus a normally small correction factor, $(k_2/k_1 - 1)\gamma_{12}$, which under certain conditions gives rise to subnatural linewidths.[5]

Effects of dephasing collisions are included phenomenologically to the density matrix by adding a pressure dependent complex parameter γ_{ij}^{ph} to γ_{ij} $(i \neq j)$. Hence the presence of buffer gas (in the form of ground state noble gas perturbers) will broaden and shift the Lorentzian profile, enabling a measurement of the two associated dephasing cross sections.

The experimental demonstration of this interaction was made in atomic sodium. Two cw narrow band dye lasers were used to couple the $3s^2S_{1/2} - 3p^2P_{3/2}$ transition (at λ = 5890 Å) to the $3p^2P_{3/2} - 4d^2D_{5/2}$ and $3p^2P_{3/2} - 4d^2D_{3/2}$ transitions at 5688 Å. The backward pump (at 5890 Å) was held fixed while the forward pump and probe (at 5688 Å) were scanned in frequency. An example of the resulting spectrum is shown in Fig. 1 along with a simplified energy level diagram of the transitions involved.

As indicated above, using this technique it is now possible to examine dephasing collisions giving rise to pressure broadening and level shifts. Experiments were conducted by introducing various noble gases into the cell containing sodium. The measurements show pressure broadening rates for helium, neon, and argon in good agreement with those obtained in previous cw[1] and pulsed experiments.[2,3] The measured line shifts were to the red with comparable cross sections as reported by Biraben for neon and argon but the transition shift for helium was also to the red in contrast with their earlier reported results. Experimental results of collisional effects on the Rydberg series ($\lambda \sim 4500$A) will also be described.

This work is supported in part by Army Research Office, No. DAA529-81-C-0008.

J.F. Lam, D.G. Steel, R.A. McFarlane
Hughes Research Laboratories

References:

1. F. Biraben, B. Cagnac, E. Giacobino, and G. Grynberg, J. Phys. B10, 2369 (1977).
2. P.F. Liao, N.P. Economou, and R.R. Freeman, Phys. Rev. Lett. 39, 1473 (1977).
3. A. Flusberg, R. Kachru, T. Mossberg, and S.R. Hartman, Phys. Rev. A, 1607 (1979).
4. D.G. Steel, J.F. Lam and R.A. McFarlane, "Atomic Coherence Effects in Resonant Four Wave Mixing," p. 260 in Laser Spectroscopy V edited by A.R.W. McKellar, T. Oka, B.P. Stoicheff, Springer-Verlag (1981).
5. Richard P. Hackel and Shaoul Ezekiel, Phys. Rev. Lett. 42, 1736 (1979).

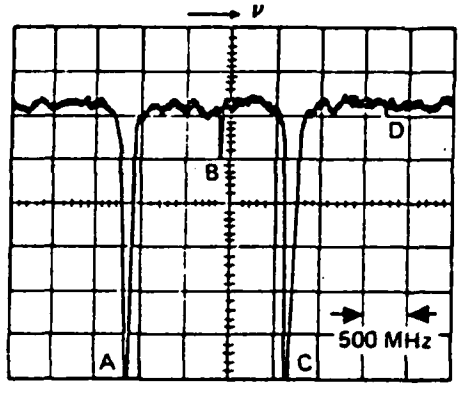

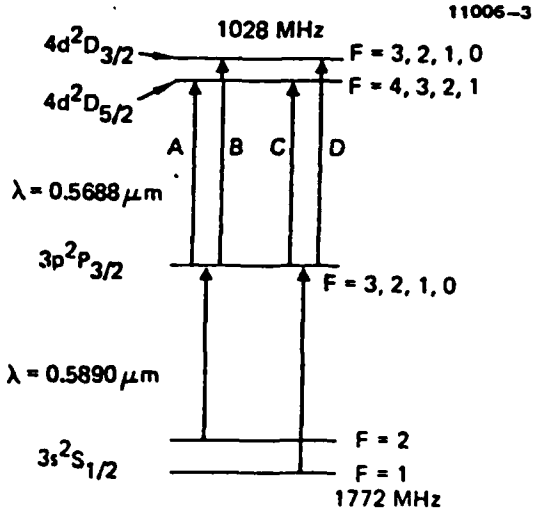

Fig. 1 Frequency spectrum of optically induced two-photon coherence as observed by non-degenerate FWM. Level diagram shows observed transitions.

PHYSICAL REVIEW A VOLUME 26, NUMBER 2 AUGUST 1982

High-resolution spectroscopy and collision studies of high-lying atomic states using four-wave mixing

D. G. Steel, J. F. Lam, R. A. McFarlane
Hughes Research Laboratories, Malibu, California 90265
(Received 9 February 1982)

This Communication describes a novel spectroscopic technique for studying high-lying atomic states. The approach uses two cw narrow-band stabilized dye lasers configured in a four-wave-mixing geometry. We demonstrate that the measurements are Doppler-free and the method is capable of high resolution. Using this technique we examine the complex dephasing parameter γ_{ij} associated with buffer-gas collisions in atomic sodium. Rates for pressure-induced broadening and resonance shifts are reported for neon.

We present experimental results describing a new nonlinear-spectroscopic technique which we have applied to high-resolution spectroscopic and collision studies of high-lying excited atomic states. Using two cw narrow-band tunable stabilized dye lasers in a four-wave-mixing (FWM) geometry we are able to make nonlinear spectroscopy measurements of collision-induced broadening and frequency shifts. This contrasts with earlier measurements in the time domain using pulsed lasers.[1,2] Furthermore, by using two tunable lasers (at frequency Ω_1 and Ω_2) in a three-level system we avoid signal-to-noise problems associated with large intermediate-state detuning in degenerate two-quantum absorption when atomic states of large principle quantum number n are examined.[3] The geometry assures a pure two-quantum coherent interaction with no contribution from stepwise excitation characteristic of nondegenerate two-photon absorption measurements.[4] Hence, collision measurements reflect interactions associated only with the upper level of the two-quantum transition.

A density-matrix calculation of the interaction was performed with the assumption of the geometry and cascade-up three-level system shown in Fig. 1. The transitions from the ground state to the intermediate state and from the intermediate state to the final state are assumed to have resonances at frequencies ω_1 and ω_2, respectively. Two cw monochromatic electromagnetic waves E_b and E_f (backward and forward pump beams) at frequency Ω_1 and Ω_2, respectively, are assumed to be counterpropagating with respect to each other. It is assumed that $\Omega_1(\Omega_2)$ is tuned near $\omega_1(\omega_2)$ in order to be consistent with the rotating wave approximation used in the calculation. A third wave E_p (the probe beam) is also at frequency Ω_2 and is nearly collinear with E_f. These three waves act to induce a nonlinear polarization in the medium via a third-order susceptibility. This polarization gives rise to a nearly phase-matched signal in a direction almost counterpropagating to the input signal wave E_s. Physically, the signal arises from a Doppler-free two-quantum coherence induced by the simultaneous action of the forward and backward pump waves. The coherence oscillates in time at the sum frequency of the two pump waves $\Omega_1+\Omega_2$. In the presence of the probe wave, this two-quantum coherence gives rise to the nonlinear polarization. The calculation, using the density-matrix approach, is performed using perturbation theory to third order in the applied fields.[5] The results show that the polarization is given by

$$P(z,t) = -\frac{N_0}{(2\hbar^3)}\frac{|\mu_{12}|^2|\mu_{23}|^2}{k_1 u_0}E_f E_b E_p^* \exp(-i\Omega_1 t - ik_1 z)\left[\gamma_{13}+\left(\frac{k_2}{k_1}-1\right)\gamma_{12}-i\left(\Delta_2+\frac{k_2}{k_1}\Delta_1\right)\right]^{-1}$$
$$\times\left\{-\frac{i}{k_1 u_0}Z'\left(-\frac{\Delta_1+i\gamma_{12}}{k_1 u_0}\right)+\left(\frac{k_2}{k_1}-1\right)\left[\gamma_{13}+\left(\frac{k_2}{k_1}-1\right)\gamma_{12}-i\left(\Delta_2+\frac{k_2}{k_1}\Delta_1\right)\right]^{-1}\right.$$
$$\left.\times\left[Z\left(\frac{\Delta_1+\Delta_2+i\gamma_{13}}{(k_2/k_1-1)k_1 u_0}\right)-Z\left(-\frac{\Delta_1+i\gamma_{12}}{k_1 u_0}\right)\right]\right\},$$

where $\gamma_{ij}=\frac{1}{2}(\gamma_i+\gamma_j)$ and represents the linewidth associated with the i-j transition, $k_i=\Omega_i/c$, μ_{ij} is dipole moment of the i-j transition, u_0 is the thermal velocity, $\Delta_j=\Omega_j-\omega_j$, and Z is the plasma dispersion function where the prime denotes the derivative with respect to its argument. From this expression the resonance condition is given by $\Omega_2-\omega_2=-(k_2/k_1)(\Omega_1-\omega_1)$. The linewidth is the sum of the two-photon linewidth and a small correction factor $\gamma_{13}+(k_2/k_1-1)\gamma_{12}$. We note that if k_2 is less than k_1 the linewidth will be less than the two-photon linewidth, providing a means for achieving subnatural

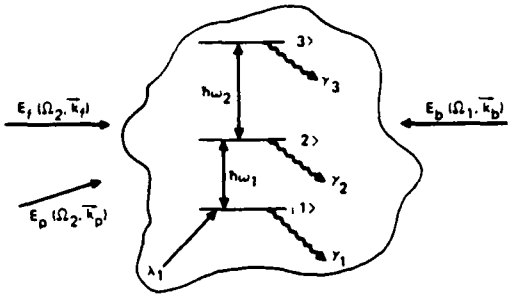

FIG. 1. Description of the cascade-up three-level system and related geometry for studying two-quantum FWM spectroscopy. E_f and E_b are assumed to be counterpropagating. E_b is nearly resonant with the first transition at frequency ω_1, and E_f and E_p are nearly resonant with the second transition at frequency ω_2. The frequency of the signal produced by the two quantum nonlinear interaction is given by $\Omega_1 + \Omega_2 - \Omega_2 = \Omega_1$.

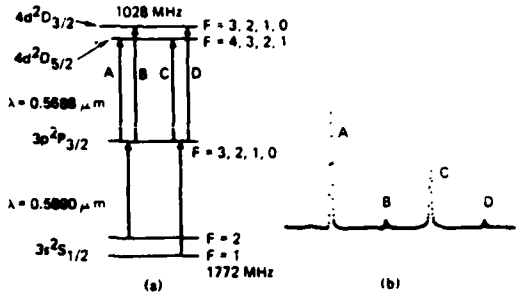

FIG. 2. (a) Simplified energy-level diagram for atomic sodium. The hyperfine splitting in the ground state is designated by $F = 2$ and 1, and the fine-structure splitting in the upper level is designated by $J = \frac{3}{2}$ and $\frac{5}{2}$. (b) An example of the signal produced by the FWM interaction when Ω_1 is tuned between the $3s\ ^2S_{1/2}(F=2)-3p\ ^2P_{3/2}(F=3)$ transition and the $3s\ ^2S_{1/2}(F=1)-3p\ ^2P_{3/2}(F=0)$ transition.

linewidth spectroscopy.[6] The correction arises because, in the moving reference frame of the atom, the perceived change in the laser frequency as the laser is tuned is dependent on k_f. This magnification or demagnification of the actual change in the laser frequency leads both to the linewidth correction and to the k_f-dependent resonance condition.

This interaction differs from earlier nondegenerate two-photon spectroscopy because there is no stepwise contribution to the polarization. Hence, assuming the lower level is a ground state or metastable, the linewidth is determined predominantly by the upper-level lifetime with a very reduced contribution from the intermediate state. As we demonstrate below, this property makes this spectroscopic technique very well suited for collision studies of high-lying atomic states.

The above expression for the polarization shows that the strength of the signal (in the small signal limit) depends only on the ground-state to intermediate-state electric dipole strength (μ_{12}) and on the Rabi frequencies given by $\mu_{ij}E/\hbar$. Hence, if the various $\mu_{ij}E/\hbar$'s are held constant, the signal will not decrease as transitions to higher principle quantum numbers in the Rydberg series are studied. This provides a considerable improvement over degenerate two-photon absorption spectroscopy where the signal decreases with increasing principle quantum number due to increasing intermediate-state detuning.

An experimental study of this type of nonlinearity was performed using atomic sodium. Two Coherent Radiation Model 699-21 stabilized cw dye lasers were configured for the interaction indicated in Fig. 1. One laser provided the backward wave and was tuned to the $3s\ ^2S_{1/2}-3p\ ^2P_{3/2}$ transition at 589 nm. The second laser was tuned to the $3p\ ^2P_{3/2}-4d\ ^2D_{5/2,3/2}$ transition at 568.8 nm. Figure 2(a) shows a simplified energy-level diagram for these transitions in sodium. The hyperfine splitting is shown for the ground state but is omitted in the intermediate and upper states. In the experiments the frequency of the backward beam at 589 nm is held fixed while the frequency of the forward pump and probe is scanned. Figure 2(b) shows a typical scan. The frequency of the laser at 589 nm has been adjusted to lie between the $3s\ ^2S_{1/2}(2)-3p\ ^2P_{3/2}(3)$ transition and $3s\ ^2S_{1/2}(1)-3p^2P_{3/2}(0)$ transition. The number in parentheses represents the total angular momentum quantum number. The signals are not at an optimum level under this condition but all of the observed resonances are simultaneously displayed. The two large resonances arise from transitions terminating on the $D_{5/2}$ state and are separated by the ground-state hyperfine splitting. Similarly, the two weaker resonances terminate on the $D_{3/2}$ state. The splitting between the adjacent strong $D_{5/2}$ line and the weaker $D_{3/2}$ line to the left is given by the fine-structure splitting of the $4d\ ^2D$ state.[7] Intensities for each of the pump waves and probe waves were adjusted to be less than the saturation intensity for the respective transition in order to avoid power broadening and ac Stark splitting. The two-photon linewidth inferred from the A coefficient of the ^2D state is 3 MHz. The observed linewidth is 6 MHz consistent with the relative laser jitter which was measured independently.

The experiment could have been configured differently but would have produced significantly different results. Suppose the forward pump and probe had been tuned to the ground-state–to–intermediate-state resonance and the backward pump had been tuned to the intermediate- to upper-state resonance. The signal produced in this interaction would consist of the sum of a two-quantum interaction as above and also a stepwise interaction. In the latter interaction the forward pump and probe interact simultaneously to produce a spatial modulation of the intermediate-state population similar to a volume

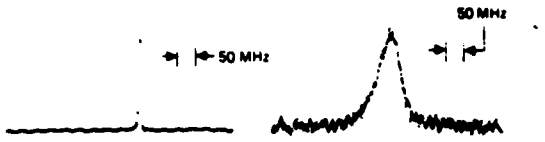

FIG. 3. Example of pressure broadening on the two-quantum line shape. (a) No buffer gas; (b) 3.1 Torr of neon buffer gas.

hologram. This hologram is then "read out" by the backward pump which sees the medium as a spatial modulation of absorption and dispersion at a resonant frequency determined by the intermediate- to final-state energy separation. A slight phase mismatch occurs, as above, because the frequency of the backward pump is not Bragg matched to the spatial periodicity of the forward pump and probe interference.

To demonstrate the usefulness of this new two-photon spectroscopy technique we have measured the pressure-broadening rates for the sodium $4d\ ^2D_{5/2}$ state in the presence of buffer-gas collisions. In the presence of buffer gas, optical pumping due to hyperfine- and fine-structure changing collisions reduces the signal considerably in atomic sodium. However, this effect was minimized and strong signals were obtained when the backward pump was detuned by about 1800 MHz to the low-frequency side of the $3s\ ^2S_{1/2}-3p\ ^2P_{3/2}(3)$ transition. In these experiments the two-photon linewidth was measured as a function of buffer-gas pressure. Shown in Fig. 3 is a comparison of the two-photon linewidth without buffer gas and a typical pressure-broadened linewidth. In these measurements a pressure-induced frequency shift was also observed. Figure 4 shows a plot of the linewidth as a function of buffer-gas pressure using neon. From the relationship that $\Delta\nu_{1/2} = N_0 u \sigma/\pi$, where $\Delta\nu_{1/2}$ is the full width at half maximum of the line (in Hz) and u is the center-of-mass thermal velocity given by $\sqrt{8kT/\mu}$ (μ is the reduced mass), we find that the pressure-broadening cross section for neon is 380 ± 37 Å^2. This is in excellent agreement with previously reported measurements (see tabulation in Ref. 2). Measurements of pressure-broadening rates for helium and argon have also

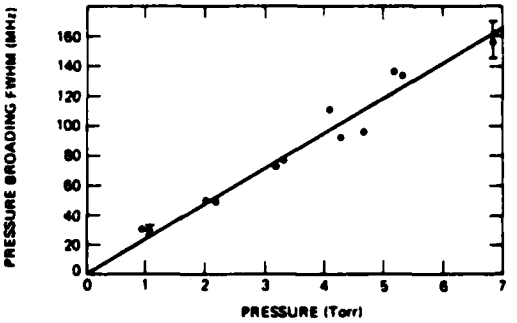

FIG. 4. Measurement of the pressure-broadened linewidth as a function of neon gas pressure for the 4*d* state in sodium.

been made and are in reasonable agreement with those tabulated in Ref. 2. More precise measurements of these are presently being made. The only measurements of pressure-induced shifts for the 4*d* level of sodium that have been reported were made using degenerate two-photon absorption.[3] Consistent with the measurements reported in Ref. 3 we have also observed red shifts for both neon and argon. However, we observed a red shift for helium as well in contrast to the reported blue shift found by Biraben.[3]

These experiments show the viability of performing detailed collision experiments on higher-lying n states in the Rydberg series for both s and d configurations. In particular, this technique will provide pressure-broadening rates from measurements in the frequency domain using cw lasers in contrast to the detailed work of Ref. 2 using pulsed lasers to make the measurements in the time domain. Furthermore, frequency domain measurements enable a determination of the pressure-induced frequency shift which was not possible in the earlier pulsed measurements.[1,2] These methods will enable us to measure the asymptotic limit of the cross section as a function of n as was done in the pioneering work of Füchtbauer and Shulz,[8] who used classical spectroscopy techniques for such pressure-broadening studies.

This work was supported in part by the Army Research Office under Contract No. DAAG29-81-C-0008.

[1]P. F. Liao, N. P. Economou, and R. R. Freeman, Phys. Rev. Lett. 39, 1473 (1977).
[2]A. Flusberg, R. Kachru, T. Mossberg, and S. R. Hartman, Phys. Rev. A 19, 1607 (1979).
[3]F. Biraben, B. Cagnac, and G. Grynberg, Phys. Lett. 36, L41 (1975).
[4]See, for example, P. F. Liao, J. E. Biorkholm, and P. R. Berman, Phys. Rev. A 21, 1927 (1980).
[5]D. G. Steel, J. F. Lam, and R. A. McFarlane, in *Laser Spectroscopy V*, edited by A. R. W. McKellar, T. Oka, and B. P. Stoicheff (Springer-Verlag, Berlin, 1981), p. 260.
[6]Richard P. Hackel and Shaoul Ezekiel, Phys. Rev. Lett. 42, 1736 (1979).
[7]W. Hänsch, K. C. Harvy, G. Meisel, and A. L. Schawlow, Opt. Commun. 11, 50 (1974).
[8]C. Füchtbauer and P. Schulz, Z. Phys. 97, 699 (1935); 93, 648 (1935); 113, 323 (1939).

PHYSICAL REVIEW A VOLUME 26, NUMBER 3 SEPTEMBER 1982

Theory of nonlinear optical coherences in resonant degenerate four-wave mixing

Juan F. Lam and Richard L. Abrams
Hughes Research Laboratories, Malibu, California 90265
(Received 16 February 1982)

A theory of resonantly enhanced degenerate four-wave mixing in two-level systems including the effects of atomic and photon angular momentum is presented in the absence of pump-induced saturation of the transition. It is shown that there exist three distinct quantum-mechanical amplitudes leading to the third-order polarization density. These quantum-mechanical amplitudes are shown to be sensitive to the states of polarization of the incident fields. The quantum-mechanical transport equation in the m representation is used to calculate the output signal in the various regimes of laser detuning, atomic linewidth, and polarization states of the radiation field for collinear interaction.

I. INTRODUCTION

The phenomenon of degenerate four-wave mixing (DFWM) has been a popular research subject recently due to its potential application to laser spectroscopy,[1] wave-front compensation,[2] and signal processing.[3] In the case of resonantly enhanced excitation, degenerate four-wave mixing provides a powerful tool to study the physical properties of atomic and molecular systems.[4] Pressure-broadened linewidths have been measured in both two- and three-level atomic systems.[5] Degenerate four mixing shares the same important feature with saturated absorption or two-photon spectroscopy, i.e., it yields Doppler-free spectra. Current theories have treated the atomic system as having nondegenerate energy levels, an approximation valid only for the case when the polarization state of all radiation fields are equal. In this regime, the mechanism for the generation of the signal via DFWM arises from spatial modulation of the population difference.[6] However, in general, real atoms possess angular momentum which arises, for example, from spatial symmetry of the potential energy. The effect of the existence of angular momentum leads to the violation of the assumption of nondegenerate energy levels. In this case, the relative orientation of the polarization state of the radiation fields leads to the existence of new physical mechanisms giving rise to the four-wave mixing signal.[7,8] The same mechanisms are present in the study of the Zeeman laser[9] and polarization spectroscopy.[10] The generalization of quantum levels to include magnetic degeneracies allows the possibility of studying depolarizing collision effects in resonantly enhanced degenerate four-wave mixing.[11]

We present in this paper a study of the amplitude, polarization, and spectral properties of the four-wave mixing signal generation by the nonlinear interaction of three input fields in a resonant two-level system with degenerate states. In Sec. II, we outline the approximations and model used in the description of the physics. Section III presents a qualitative picture of the fundamental physics that arise owing to the several choices of electric field polarization. Section IV presents a detailed calculation of the third-order response of the medium in the perturbation regime, i.e., the intensities of the applied and generated fields are assumed to be below saturation. Section V provides illustrative examples of the dependence of the signal on the relative orientation of the input field polarization states as well as the choice of angular momenta for the energy levels. We conclude by summarizing the main results in Sec. VI.

II. APPROXIMATION AND MODEL

We shall assume the following.

(a) The radiation field can be described in the classical picture and be written as

$$\vec{\mathbf{E}}(\vec{r},t)=\frac{1}{2}\sum_n \hat{e}_n \mathcal{E}_n \exp i(\omega_n t-\vec{k}_n\cdot\vec{r})+\text{c.c.}\ , \tag{2.1}$$

where $\hat{e}_n$ is the unit vector describing the polarization state of the field. $\mathcal{E}_n$ is a slowly varying envelope such that

$$|\hat{k}_n\cdot\vec{\nabla}\mathcal{E}_n| \ll k_n|\mathcal{E}_n|\ . \tag{2.2}$$

ω_n and $\vec{k}_n$ are the frequency and wave vector, respectively. $\hat{k}_n$ is the unit wave vector.

(b) The atom is described by a two-level system

with degenerate states (an example of which is shown in Fig. 1). The frequency difference between the upper and lower states is ω_0. The states are labeled by its total angular momentum J and z component M_j of the angular momentum.

(c) The interaction of radiation with the quantum system is described via an electric dipole coupling of the form

$$V(\vec{r},t) = -\vec{\mu}\cdot\vec{E}(\vec{r},t)\ , \tag{2.3}$$

where $\vec{\mu}$ is the electric dipole moment operator. The interaction process is near resonant so that the rotating-wave approximation is valid throughout, i.e.,

$$|\omega_n - \omega_0| \ll \omega_n + \omega_0\ . \tag{2.4}$$

(d) The lower state is populated initially by incoherent pumping processes. Relaxation processes are taken into account via effective decay rates. The spontaneous emission processes from the upper to the lower state are neglected in our description. The inclusion of such processes, which leads to optical pumping phenomena, necessitates a more elaborate description of the response of the medium as observed by Omont.[12] This work does not take into account the effects of optical pumping.

Taking these assumptions into account, the density-matrix equations which described the response of the medium to external fields are given by the following.[7]

Population:

$$\{\gamma_1 + \vec{v}\cdot\vec{\nabla}\}\rho_{J_1M_1J_1M_1} = \lambda_1(\vec{v}) + \frac{1}{i\hbar}\sum_{M_2}\{V_{J_1M_1J_2M_2}\tilde{\rho}_{J_2M_2J_1M_1} - \tilde{\rho}_{J_1M_1J_2M_2}V_{J_2M_2J_1M_1}\}\ , \tag{2.5}$$

$$\{\gamma_2 + \vec{v}\cdot\vec{\nabla}\}\rho_{J_2M_2J_2M_2} = \frac{1}{i\hbar}\sum_{M_1}\{V_{J_2M_2J_1M_1}\tilde{\rho}_{J_1M_1J_2M_2} - \tilde{\rho}_{J_2M_2J_1M_1}V_{J_1M_1J_2M_2}\}\ ; \tag{2.6}$$

atomic coherences:

$$\{\gamma_{12} + i\Delta + \vec{v}\cdot\vec{\nabla}\}\tilde{\rho}_{J_1M_1J_2M_2} = \frac{1}{i\hbar}V_{J_1M_1J_2M_2}\{\rho_{J_2M_2J_2M_2} - \rho_{J_1M_1J_1M_1}\} + \frac{1}{i\hbar}\sum_{M_2'}V_{J_1M_1J_2M_2'}\rho_{J_2M_2'J_2M_2}$$

$$-\frac{1}{i\hbar}\sum_{M_1'}\rho_{J_1M_1J_1M_1'}V_{J_1M_1'J_2M_2}\ , \tag{2.7}$$

$$\rho_{J_2M_2J_1M_1} = \rho^{*}_{J_1M_1J_2M_2}\ ; \tag{2.8}$$

Zeeman coherences:

$$\{\gamma_1' + \vec{v}\cdot\vec{\nabla}\}\rho_{J_1M_1J_1M_1'} = \frac{1}{i\hbar}\sum_{M_2}\{V_{J_1M_1J_2M_2}\tilde{\rho}_{J_2M_2J_1M_1'} - \tilde{\rho}_{J_1M_1J_2M_2}V_{J_2M_2J_1M_1'}\}\ , \tag{2.9}$$

$$\{\gamma_2' + \vec{v}\cdot\vec{\nabla}\}\rho_{J_2M_2J_2M_2'} = \frac{1}{i\hbar}\sum_{M_1}\{V_{J_2M_2J_1M_1}\tilde{\rho}_{J_1M_1J_2M_2'} - \tilde{\rho}_{J_2M_2J_1M_1}V_{J_1M_1J_2M_2'}\}\ ; \tag{2.10}$$

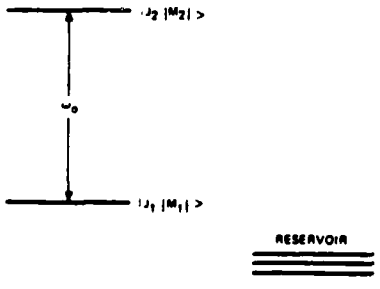

FIG. 1. Two-level system with degenerate states as a model of a resonant transition. ω_0 is the transition frequency, and J_α and M_α are the total and Z projection of the angular momentum of level α, respectively.

where $\vec{v}\cdot\vec{\nabla}$ describes the effect of atomic motion and gives rise to such effects as Doppler shifts and spatial hole burning. $\lambda_1(\vec{v})$ is the velocity-dependent incoherent pumping rate to level $|J_1\rangle$. γ_n and γ_n' are the effective decay rates of the population and Zeeman coherence, respectively. γ_{12} is the effective linewidth of the transition $|J_1\rangle \rightarrow |J_2\rangle$. $\Delta = \omega - \omega_0$ is the laser detuning from resonance. Also,

$$V_{J_1M_1J_2M_2} = -\tfrac{1}{2}\vec{u}_{J_1M_1J_2M_2}\cdot\sum_n \hat{e}_n\mathscr{E}_n\ , \tag{2.11}$$

$$\tilde{\rho}_{J_1M_1J_2M_2} = \rho_{J_1M_1J_2M_2}e^{-i\omega t}\ . \tag{2.12}$$

We have used the simplified notation that given any operator $\mathcal{Q}$,

$$\mathcal{Q}_{J_1M_1J_2M_2}=\langle J_1M_1 \mid \mathcal{Q} \mid J_2M_2\rangle \tag{2.13}$$

is the matrix element of $\mathcal{Q}$ between states $|J_1M_1\rangle$ and $|J_2M_2\rangle$. The set of equations (2.5)–(2.10) describe the response of the medium to external radiation fields.

The geometry of the interaction process is chosen to be collinear, i.e., the input and generated waves propagate along a line (Fig. 2). The input fields consist of the forward pump $\mathcal{E}_f$, backward pump $\mathcal{E}_b$, and the probe $\mathcal{E}_p$. The generated field is denoted by the signal $\mathcal{E}_s$. We shall be interested in those terms for which the phase of $\mathcal{E}_s$ is the complex conjugate of $\mathcal{E}_p$. One should note that in the fully collinear geometry, there are additional waves that will not be considered in this work[13] and, in principle, they can be isolated by choosing a nearly collinear geometry. Ducloy and Bloch[14] showed that the nearly collinear assumption is valid provided that $\theta < 2\gamma/ku_0$ (natural linewidth/Doppler width). For the case of sodium atoms confined to a cell at room temperature, the acceptance angle θ is 0.1°.

III. PHYSICAL PICTURE

We shall consider the physical picture of the nonlinear interaction process in both the lower and upper level of the quantum system. Each level will be characterized by its effective energy decay rate γ_J to the reservoir. The discussion to be followed is valid for any of the two energy levels.

First, consider the choice of polarization state of the radiation fields illustrated in Fig. 3. The electric dipole selection rule implies that only $\Delta M = +1$ transitions are allowed with σ_+ polarization. There exist two distinct physical contributions to the generated signal $\mathcal{E}_s$. The first one arises from a spatial modulation of the population in magnetic state $M+1$ of level $|J_2\rangle$ generated by the interference of the forward pump $\mathcal{E}_f$ and probe $\mathcal{E}_p$. The coherent

FIG. 2. Interaction geometry. $\mathcal{E}_f$ and $\mathcal{E}_b$ form a set of counterpropagating waves. Resonant medium is composed of a set of two-level systems.

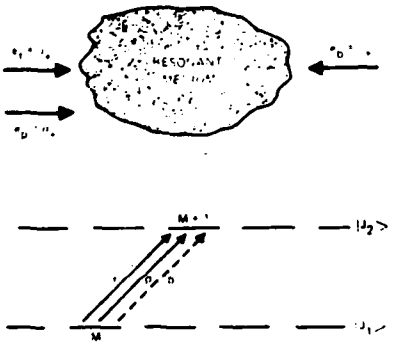

FIG. 3. Quantum-mechanical path giving rise to the normal population mechanism.

scattering of the backward pump $\mathcal{E}_b$ off the spatial modulation yields a signal field $\mathcal{E}_s$ with polarization state σ_+. The second contribution arises from the spatial modulation generated by the backward pump $\mathcal{E}_b$ and probe $\mathcal{E}_p$, and the coherent scattering is performed by the forward pump $\mathcal{E}_f$. Again, the polarization state of the generated signal is identical to the forward pump, i.e., σ_+ radiation. Since both physical contributions involve the generation of population and scattering dynamics between only two magnetic states, we shall denote this type of physical mechanism as *normal population*.

Consider now the choice of polarization state illustrated in Fig. 4. There exist two additional dis-

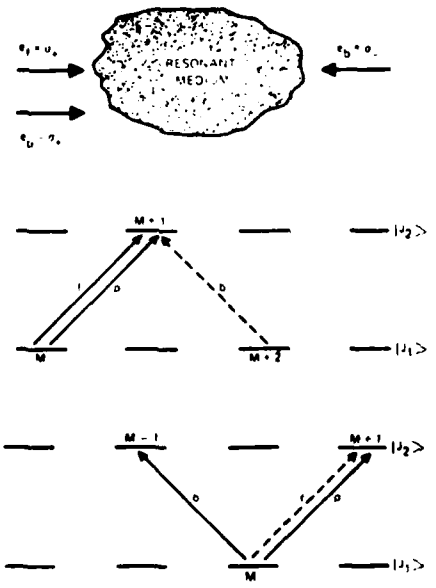

FIG. 4. Two quantum-mechanical paths giving rise to the cross-population and Zeeman-coherence mechanisms.

tinct physical contributions. The first one arises from the generation of a spatial modulation of the population in the $M+1$ state of level $|J_2\rangle$ via the interference of the forward pump $\mathscr{E}_f$ and probe $\mathscr{E}_p$. However, the coherent scattering of the backward pump $\mathscr{E}_b$ proceeds along a different channel. It excites an optical coherence between $|J_2M+1\rangle$ and $|J_1M+2\rangle$ which generates a σ_- radiation field. Since it couples a different channel we shall denote this physical mechanism as *cross population* [Fig. 4(a)]. The second physical mechanism arises from the generation of a spatial modulation of the Zeeman coherence between $|J_2M-1\rangle$ and $|J_2M+1\rangle$ by means of the action of the backward pump $\mathscr{E}_b$ and probe $\mathscr{E}_p$. The coherent scattering of the forward pump $\mathscr{E}_f$ yields a signal whose polarization state is σ_- [Fig. 4(b)]. It should be noted that the generated signal for this case has a polarization state which is the complex conjugate of the polarization state of the probe. We shall denote this physical mechanism as *Zeeman coherence.*

In the collinear geometry, these three physical mechanisms share an important property. They yield a Doppler-free spectrum for the generated signal if the resonant medium is Doppler broadened. To understand this characteristic, let us consider the dynamics of the interaction of moving atoms with the external radiation fields. The generation of the spatial modulation of either the population or Zeeman coherence involves the excitation of the quantum system by means of the pump $\mathscr{E}_n$ $(n=f,b)$ and the probe $\mathscr{E}_p$. In the language of Doppler shifts, the resonance conditions for the generation of the spatial modulation are

$$\omega-\omega_0-\vec{k}_n\cdot\vec{v}=0\,, \tag{3.1}$$

$$\omega-\omega_0-\vec{k}_p\cdot\vec{v}=0\,. \tag{3.2}$$

The coherent scattering of the other pump wave, which generates the signal wave, yields the resonance condition

$$\omega-\omega_0+\vec{k}_p\cdot\vec{v}=0\,. \tag{3.3}$$

In writing Eq. (3.3) we used the assumption of counterpropagating pump waves, i.e., $\vec{k}_f+\vec{k}_b=0$. The velocity group that satisfies the resonance condition (3.1), (3.2), and (3.3) are those with $\vec{v}=0$. Hence the spectrum of the generated signal is a Lorentzian centered at the transition frequency ω_0 and its width is determined by the natural or collision-broadened linewidth.

IV. NONLINEAR RESPONSE OF THE MEDIUM

The medium response is determined by the polarization

$$\vec{P}(\vec{r},t)=\int_{-\infty}^{\infty}d^3v\,\mathrm{tr}[\rho(\vec{r},\vec{v},t)\vec{\mu}]\,, \tag{4.1}$$

where ρ is the density matrix satisfying the evolution equations (2.5)–(2.10) in the case of two-level systems with degenerate states, and $\vec{\mu}$ is the electric dipole moment operator. The integration over velocity takes into account the averaging over the random motion of the atoms. We shall assume that the system is in thermal equilibrium and is described by the velocity-distribution function

$$W(\vec{v})=\left[\frac{1}{\pi u_0^2}\right]^{3/2}e^{-(\vec{v}/u_0)^2}\,, \tag{4.2}$$

where $u_0=(2k_BT/m)^{1/2}$, k_B is the Boltzmann's constant, T is the equilibrium temperature, and m is the mass of the atom.

In the unsaturated regime, the polarization (4.1) is obtained by means of the perturbation solution of the density-matrix equations (2.5)–(2.10). A set of perturbation chains, which identifies the three distinct physical mechanisms discussed in Sec. III can be written in the following manner.

Normal population:

$$\rho^{(0)}_{J_1M_1;J_1M_1}\rightarrow\begin{bmatrix}\tilde{\rho}^{(1)}_{J_1M_1;J_2M_2}\\ \tilde{\rho}^{(1)}_{J_2M_2;J_1M_1}\end{bmatrix}\rightarrow\begin{bmatrix}\rho^{(2)}_{J_2M_2;J_2M_2}\\ \rho^{(2)}_{J_1M_1;J_1M_1}\end{bmatrix}\rightarrow\begin{bmatrix}\tilde{\rho}^{(3)}_{J_1M_1;J_2M_2}\\ \tilde{\rho}^{(3)}_{J_2M_2;J_1M_1}\end{bmatrix}\,; \tag{4.3}$$

cross population:

$$\rho^{(0)}_{J_1M_1;J_1M_1}\rightarrow\begin{bmatrix}\tilde{\rho}^{(1)}_{J_1M_1;J_2M_2}\\ \tilde{\rho}^{(1)}_{J_2M_1;J_1M_1}\end{bmatrix}\begin{matrix}\nearrow\\ \searrow\end{matrix}\begin{matrix}\rho^{(2)}_{J_2M_2;J_2M_2}\rightarrow\begin{bmatrix}\tilde{\rho}^{(3)}_{J_1M_1';J_2M_2}\\ \tilde{\rho}^{(3)}_{J_2M_2;J_1M_1'}\end{bmatrix}\\ \rho^{(2)}_{J_1M_1;J_1M_1}\rightarrow\begin{bmatrix}\tilde{\rho}^{(3)}_{J_1M_1;J_2M_2'}\\ \tilde{\rho}^{(3)}_{J_2M_2';J_1M_1}\end{bmatrix}\end{matrix}\,; \tag{4.4}$$

Zeeman coherence:

$$\rho^{(0)}_{J_1M_1J_1M_1} \rightarrow \begin{bmatrix} \tilde{\rho}^{(1)}_{J_1M_1J_2M_2} \\ \tilde{\rho}^{(1)}_{J_2M_2J_1M_1} \end{bmatrix} \begin{matrix} \rightarrow \rho^{(2)}_{J_2M_2'J_2M_2} \rightarrow \begin{bmatrix} \tilde{\rho}^{(3)}_{J_1M_1J_2M_2} \\ \tilde{\rho}^{(3)}_{J_2M_2J_1M_1} \end{bmatrix} \\ \searrow \rho^{(2)}_{J_1M_1'J_1M_1} \rightarrow \begin{bmatrix} \tilde{\rho}^{(3)}_{J_1M_1J_2M_2} \\ \tilde{\rho}^{(3)}_{J_2M_2J_1M_1} \end{bmatrix} \end{matrix} ; \tag{4.5}$$

where the superscript denotes the order of the perturbation parameter which is given by the Rabi frequency $\vec{\mu}\cdot\vec{E}/h$. The primed superscript indicates the case for which $M \neq M'$.

If the input radiation fields are in arbitrary polarization states, then one can decompose them in terms of σ_+ and σ_- components and apply the three basic physical contributions (4.3) to (4.5) in order to generate the nonlinear polarization (4.1). Hence, it is necessary to know the strength and spectral behavior of each physical chain.

An intuitive approach can be presented to describe the essence of the spectral behavior of the normal population, cross population, and Zeeman-coherence terms. The basic dynamics of absorption and reemission processes are necessarily the same for all three mechanisms since they are insensitive to the angular momentum of the atomic species. However, the strength of the interaction in the presence of foreign perturbers is not the same for the population (normal or cross) and Zeeman-coherence contributions. In the case of the population, no changes in the projection of the angular momentum is involved, i.e., collision effects on the population are simply visualized as an effective decay rate accompanied by changes in velocity. However, collision effects on Zeeman coherence involves the dynamics of changes of the projection of the angular momentum of the system. Hence, in general, the pressure broadening contributions to the population and Zeeman-coherence term acquire different magnitude and are reflected in part by the effective energy decay rate γ_n and Zeeman dephasing rate γ_n'.[15] In the absence of foreign perturbers, the Zeeman dephasing rate γ_n' must be given by the spontaneous-emission rate Γ which is the same as the energy decay rate in the collisionless regime.

A direct application of the perturbation chains (4.3) to (4.5) yields the following expression for the polarization contribution to the degenerate four-wave mixing signal:

$$\vec{P}(\vec{r},t) = (\vec{S}_N + \vec{S}_C + \vec{S}_Z)\mathscr{E}_f\mathscr{E}_b\mathscr{E}_p^* \exp i(\omega t + \vec{k}_p\cdot\vec{r}) , \tag{4.6}$$

where

$$\vec{S}_N = R^{(2)}_{fp}\sum_{M_1}\sum_{M_2}\vec{\mu}_{J_2M_2J_1M_1}(\vec{\mu}_{J_1M_1J_2M_2}\cdot\hat{e}_b)(\vec{\mu}_{J_2M_2J_1M_1}\cdot\hat{e}_p^*)(\vec{\mu}_{J_1M_1J_2M_2}\cdot\hat{e}_f)$$
$$+ R^{(1)}_{fp}\sum_{M_1}\sum_{M_2}(\vec{\mu}_{J_1M_1J_2M_2}\cdot\hat{e}_f)(\vec{\mu}_{J_2M_2J_1M_1}\cdot\hat{e}_p^*)(\vec{\mu}_{J_1M_1J_2M_2}\cdot\hat{e}_b)\vec{\mu}_{J_2M_2J_1M_1} + (b\rightleftharpoons f) \tag{4.7a}$$

is the contribution due to the normal population mechanism,

$$\vec{S}_c = R^{(2)}_{fp}\sum_{\substack{M_1,M_1' \\ M_1\neq M_1'}}\sum_{M_2}\vec{\mu}_{J_2M_2J_1M_1'}(\vec{\mu}_{J_1M_1'J_2M_2}\cdot\hat{e}_b)(\mu_{J_2M_2J_1M_1}\cdot\hat{e}_p^*)(\vec{\mu}_{J_1M_1J_2M_2}\cdot\hat{e}_f)$$
$$+ R^{(1)}_{fp}\sum_{\substack{M_2,M_2' \\ M_2\neq M_2'}}\sum_{M_1}(\vec{\mu}_{J_1M_1J_2M_2}\cdot\hat{e}_f)(\vec{\mu}_{J_2M_2J_1M_1}\cdot\hat{e}_p^*)(\vec{\mu}_{J_1M_1J_2M_2'}\cdot\hat{e}_b)\vec{\mu}_{J_2M_2'J_1M_1} + [b\rightleftharpoons f] \tag{4.7b}$$

is the contribution due to the cross population mechanism, and

$$\vec{S}_Z = R_{fp}^{(2')} \sum_{M_1} \sum_{\substack{M_2,M_2' \\ M_2 \neq M_2'}} \vec{\mu}_{J_2M_2J_1M_1}(\vec{\mu}_{J_1M_1J_2M_2'}\cdot\hat{e}_b)(\vec{\mu}_{J_2M_2'J_1M_1}\cdot\hat{e}_p^*)(\vec{\mu}_{J_1M_1J_2M_2}\cdot\hat{e}_f)$$

$$+ R_{fp}^{(1')} \sum_{M_2} \sum_{\substack{M_1,M_1' \\ M_1 \neq M_1'}} (\vec{\mu}_{J_1M_1J_2M_2}\cdot\hat{e}_f)(\vec{\mu}_{J_2M_2J_1M_1'}\cdot\hat{e}_p^*)(\vec{\mu}_{J_1M_1'J_2M_2}\cdot\hat{e}_b)\vec{\mu}_{J_2M_2J_1M_1} + \{b \rightleftarrows f\} \tag{4.7c}$$

is the contribution due to the Zeeman-coherence mechanism.

The frequency-dependent factor $R_{np}^{(m)}$ is defined as

$$R_{np}^{(m)} = \frac{N_0}{(2i\hbar)^3} \int_{-\infty}^{\infty} d\vec{v}\, W(\vec{v}) \frac{1}{\gamma_{12}+i(\Delta+\vec{k}_p\cdot\vec{v})} \left[\frac{1}{\gamma_{12}+i(\Delta-\vec{k}_n\cdot\vec{v})} + \frac{1}{\gamma_{12}-i(\Delta-\vec{k}_p\cdot\vec{v})} \right] \times \left[\frac{1}{\gamma_m+i(\vec{k}_p-\vec{k}_n)\cdot\vec{v}} \right], \quad n=f,b \text{ and } m=1,2 \tag{4.7d}$$

$$R_{np}^{(m)} \rightarrow R_{np}^{(m')} \text{ if } \gamma_m \rightarrow \gamma_m' , \tag{4.7e}$$

and for the case of collinear interaction, it reduces to the following expression:

$$R_{np}^{(m)} = \frac{1}{iku_0}\frac{N_0}{(2i\hbar)^3} \left\{ \frac{1}{(1+\epsilon)(\gamma_{12}+i\Delta)} \left\{ \frac{1}{\gamma_m-(1-\epsilon)(\gamma_{12}+i\Delta)} \left[Z\left[\frac{i\gamma_{12}-\Delta}{ku_0}\right] - Z\left[\frac{i\gamma_m}{(1-\epsilon)ku_0}\right] \right] \right.\right.$$
$$\left.\left. - \frac{\epsilon}{\gamma_m+(1-\epsilon)(\gamma_{12}+i\Delta)} \left[Z\left[-\frac{i\gamma_{12}-\Delta}{ku_0}\right] - Z\left[\frac{i\gamma_m}{(1-\epsilon)ku_0}\right] \right] \right\}$$
$$- \frac{1}{2i\Delta} \left\{ \frac{1}{\gamma_m-(1-\epsilon)(\gamma_{12}+i\Delta)} \left[Z\left[\frac{i\gamma_{12}-\Delta}{ku_0}\right] - Z\left[\frac{i\gamma_m}{(1-\epsilon)ku_0}\right] \right] \right.$$
$$\left. \left. - \frac{1}{\gamma_m-(1-\epsilon)(\gamma_{12}-i\Delta)} \left[Z\left[\frac{i\gamma_{12}+\Delta}{ku_0}\right] - Z\left[\frac{i\gamma_m}{(1-\epsilon)ku_0}\right] \right] \right\} \right\}, \tag{4.8}$$

where $\epsilon=+1$ if $n=f$ and $\epsilon=-1$ if $n=b$. $Z(a+ib)$ is the plasma-dispersion function. Expression (4.8) is valid over all regimes of detuning and linewidth, from homogeneous to Doppler-broadened quantum systems.

Let us consider the frequency dependence of $R_{np}^{(m)}$ in the following regimes.

(a) γ_{12}, γ_m and $\Delta \gg ku_0$. These conditions are satisfied by a homogeneously broadened system, so velocity effects play no role in determining the form of $R_{np}^{(m)}$, i.e.,

$$R_{np}^{(m)} = \frac{N_0}{(2i\hbar)^3}\frac{1}{\gamma_m}\frac{2\gamma_{12}}{\gamma_{12}^2+\Delta^2}\frac{1}{\gamma_{12}+i\Delta} . \tag{4.9}$$

(b) γ_{12} and $\Delta \gg ku_0$ but $\gamma_m < ku_0$. These conditions imply that the frequency dependence of $R_{np}^{(m)}$ will not be affected by the effect of atomic motion. However, the strength of the signal is determined by the ratio of $\gamma_m/(1-\epsilon)ku_0$. This conclusion reflects the fact that atomic motion can lead to the destruction of the spatial grating generated by the interference of $\mathscr{E}_n$ and $\mathscr{E}_p$.[16] In this case,

$$R_{np}^{(m)} = \frac{N_0}{(2i\hbar)^3}\frac{2\gamma_{12}}{\gamma_{12}^2+\Delta^2}\frac{1}{\gamma_{12}+i\Delta} \times \frac{1}{iku_0} Z\left[\frac{i\gamma_m}{(i-\epsilon)ku_0}\right] \tag{4.10}$$

and one can show that ratio of $R_{bp}^{(m)}$ to $R_{fp}^{(m)}$ is given by

$$\gamma_m Z\left[\frac{i\gamma_m}{2ku_0}\right] \Big/ iku_0 .$$

(c) γ_{12}, γ_m, and $\Delta \ll ku_0$. These conditions are satisfied by an extreme Doppler-broadened system. In this regime velocity effects play a substantial role in determining the frequency dependence and amplitude of $R_{np}^{(m)}$. In particular,

$$R_{fp}^{(m)} \simeq \frac{N_0}{(2i\hbar)^3}\frac{\sqrt{\pi}}{\gamma_m ku_0(\gamma_{12}+i\Delta)} \tag{4.11a}$$

and

$$R_{bp}^{(m)} \simeq \frac{N_0}{(2i\hbar)^3} \frac{\sqrt{\pi}}{(ku_0)^3} . \tag{4.11b}$$

Furthermore, the ratio of $R_{bp}^{(m)}$ to $R_{fp}^{(m)}$ at $\Delta=0$ is given by

$$\gamma_m \gamma_{12}/(ku_0)^2$$

which reflects the fact that the contribution of the spatial interference generated by $\mathscr{E}_b$ and $\mathscr{E}_p$ is negligible compared to the one generated by $\mathscr{E}_f$ and $\mathscr{E}_p$, i.e., atomic motion leads to a washout of the grating generated by $\mathscr{E}_b$ and $\mathscr{E}_p$.[17]

Now consider the properties of the polarization states $\hat{e}_s$ of the generated signal for a given set of polarization states of the input fields. In the SVEA, the evolution of $\mathscr{E}_s$ is governed by

$$\mathscr{E}_s = i\frac{\omega}{2c\epsilon_0} l \mathscr{E}_f \mathscr{E}_b \mathscr{E}_p^* \hat{e}_s^* \cdot (\vec{S}_N + \vec{S}_C + \vec{S}_Z) , \tag{4.12}$$

where l is the nonlinear interaction length. We have assumed that absorption effects are negligible (absorption coefficient multiplied by l is much less than 1). The polarization state of $\mathscr{E}_s$ depends only on the couplings of the matrix elements of the dipole moments with the polarization states radiation fields. This coupling reflects the fact that there are three distinct quantum-mechanical paths leading to the third-order polarizations as discussed in Sec. III. Furthermore, the couplings depend only on the magnitude of the angular momenta J_1 and J_2, and the dipole moment for transition. They are given by the following.

Normal population:

$$I_n = \sum_{M_1 M_2} \langle M_2 | \vec{\mu}\cdot\hat{e}_s^* | M_1 \rangle \langle M_1 | \vec{\mu}\cdot\hat{e}_m | M_2 \rangle \langle M_2 | \vec{\mu}\cdot\hat{e}_p^* | M_1 \rangle \langle M_1 | \vec{\mu}\cdot\hat{e}_n | M_2 \rangle ; \tag{4.13}$$

cross population:

$$I_C^{(1)} = \sum_{\substack{M_1, M_2, M_2' \\ M_2 \neq M_2'}} \langle M_1 | \vec{\mu}\cdot\hat{e}_n | M_2 \rangle \langle M_2 | \vec{\mu}\cdot\hat{e}_p^* | M_1 \rangle \langle M_1 | \vec{\mu}\cdot\hat{e}_m | M_2' \rangle \langle M_2' | \vec{\mu}\cdot\hat{e}_s^* | M_1 \rangle , \tag{4.14a}$$

$$I_C^{(2)} = \sum_{\substack{M_2, M_1, M_1' \\ M_1 \neq M_1'}} \langle M_2 | \vec{\mu}\cdot\hat{e}_s^* | M_1' \rangle \langle M_1' | \vec{\mu}\cdot\hat{e}_m | M_2 \rangle \langle M_2 | \vec{\mu}\cdot\hat{e}_p^* | M_1 \rangle \langle M_1 | \vec{\mu}\cdot\hat{e}_n | M_2 \rangle ; \tag{4.14b}$$

Zeeman coherence:

$$I_Z^{(1)} = \sum_{\substack{M_2, M_1, M_1' \\ M_1 \neq M_1'}} \langle M_1 | \vec{\mu}\cdot\hat{e}_n | M_2 \rangle \langle M_2 | \vec{\mu}\cdot\hat{e}_p^* | M_1' \rangle \langle M_1' | \vec{\mu}\cdot\hat{e}_m | M_2 \rangle \langle M_2 | \vec{\mu}\cdot\hat{e}_s^* | M_1 \rangle , \tag{4.15a}$$

$$I_Z^{(2)} = \sum_{\substack{M_1, M_2, M_2' \\ M_2 \neq M_2'}} \langle M_2 | \vec{\mu}\cdot\hat{e}_s^* | M_1 \rangle \langle M_1 | \vec{\mu}\cdot\hat{e}_m | M_2' \rangle \langle M_2' | \vec{\mu}\cdot\hat{e}_p^* | M_1 \rangle \langle M_1 | \vec{\mu}\cdot\hat{e}_n | M_2 \rangle , \tag{4.15b}$$

where we have used the fact that

$$\hat{e}_s^* \cdot \vec{S}_\alpha = \sum_{n=f}^{b} \sum_{\beta=1}^{2} R_{np}^{(\beta)} I_\alpha^{(\beta)}$$

with $\alpha = N$, C, or Z and noting that $I_N^{(1)} = I_N^{(2)} = I_N$. The quantities $I_\alpha^{(\beta)}$ depend on the total angular momenta J_1 and J_2 as well as the electric dipole moment of the transition. $I_\alpha^{(\beta)}$ can be calculated to yield exact analytical expressions given specific choice of input field polarization states, which will be the subject of the next section. Expression (4.12) can be rewritten as

$$\mathscr{E}_s = i\frac{\omega}{2c\epsilon_0} l \mathscr{E}_f \mathscr{E}_b \mathscr{E}_p^* \sum_{\alpha} \sum_{\beta=1}^{2} \sum_{n=f}^{b} R_{np}^{(\beta)} I_\alpha^{(\beta)} . \tag{4.16}$$

Equation (4.16) together with Eqs. (4.8) and (4.13)–(4.15) are the main results of this paper.

V. EXAMPLES

We shall consider several choices of the relative orientation of the radiation field polarization states

for the case of optical transition $J_1=J\rightarrow J_2=J+1$. Generalization to the other cases $J_1=J\rightarrow J_2=J$ and $J_1=J+1\rightarrow J_2=J$ are straightforward and the results will not be given here. We shall decompose the polarization states in terms of the circularly polarized components

$$\sigma_+=+(\hat{x}+i\hat{y})/\sqrt{2}$$

and

$$\sigma=(\hat{x}-i\hat{y})/\sqrt{2}\ .$$

This representation corresponds to the choice of the quantization axis along the propagation path.

The quantities $I_\alpha^{(\beta)}$ contain a combination of four inner products of the dipole moments operator with the polarization state of the radiation fields. The decomposition into circularly polarized components together with the selection rules for electric dipole transition lead to the result that there exists only three possible components of $I_\alpha^{(\beta)}$ which are finite in magnitude. They are

$$(\vec{\mu}\cdot\sigma_\pm)(\vec{\mu}\cdot\sigma_\mp)(\vec{\mu}\cdot\sigma_\pm)(\vec{\mu}\cdot\sigma_\mp)\ ,$$

$$(\vec{\mu}\cdot\sigma_\pm)(\vec{\mu}\cdot\sigma_\mp)(\vec{\mu}\cdot\sigma_\mp)(\vec{\mu}\cdot\sigma_\pm)\ ,$$

and

$$(\vec{\mu}\cdot\sigma_\pm)(\vec{\mu}\cdot\sigma_\pm)(\vec{\mu}\cdot\sigma_\mp)(\vec{\mu}\cdot\sigma_\mp)\ .$$

In writing these terms, we have assumed, for sake of simplicity, that the $\vec{\mu}$ represents matrix elements and the order of appearance of the inner product is preserved as they are shown. The finite magnitude of these three terms results from the requirement that the initial and final quantum states for the signal generation process must be identical, i.e., the expectation value of the electric dipole moment operator is the trace of the product of the density operator and the electric dipole moment. The existence of only these three terms is consistent with the fact that the third-order susceptibility tensor in an isotropic medium has three independent components.[18] To remind the reader once more that these three terms correspond to the three quantum-mechanical amplitudes discussed above. The quantities

$$\langle J_1M_1\,|\,\vec{\mu}\,|\,J_2M_2\rangle$$

are given in terms of the reduced matrix elements and the Clebsch-Gordon coefficients.[19] The reader is referred to Ref. 19 for details of the computation.

Example 1. Consider the case where the polarization states of all the input fields are σ_+. Then the physical mechanism giving rise to the four-wave mixing signal is due to normal population. The signal field is given by

$$\mathscr{E}_s=i\frac{\omega}{2c\epsilon_0}l\mathscr{E}_f\mathscr{E}_b\mathscr{E}_p^*F(J)\sum_{\beta=1}^{2}\sum_{n=f}^{b}R_{np}^{(\beta)}\ , \quad (5.1)$$

where

$$F(J)=\tfrac{1}{4}\sum_{M=-J}^{J}|\langle J+1M-1\,|\,\mu\,|\,JM\rangle|^4\ .$$

The polarization state of the four-wave mixing signal is σ_+.

Example 2. Consider the choice of polarization states such that

$$\hat{e}_f=\sigma_+=\hat{e}_p \text{ and } \hat{e}_b=\sigma_-\ .$$

Then the mechanisms are cross population and Zeeman coherence. The signal field is given by (in the absence of foreign perturbers)

$$\mathscr{E}_s=i\frac{\omega}{2c\epsilon_0}l\mathscr{E}_f\mathscr{E}_b\mathscr{E}_p^*[G(J)(R_{fp}^{(2)}+R_{bp}^{(1)})+H(J)(R_{fp}^{(1)}+R_{bp}^{(2)})]\ ,$$

where

$$G(J)=\tfrac{1}{4}\sum_{m=-J-1}^{J+1}|\langle J+1M\,|\,\mu\,|\,JM-1\rangle|^2\times|\langle J+1M\,|\,\mu\,|\,JM+1\rangle|^2$$

and

$$H(J)=\tfrac{1}{4}\sum_{M=-J}^{J}|\langle J+1M-1\,|\,\mu\,|\,JM\rangle|^2\times|\langle J+1M+1\,|\,\mu\,|\,JM\rangle|^2\ .$$

The polarization state of the four-wave mixing signal is σ_-.

For an inhomogeneous medium in the extreme Doppler limit, the contribution due to the Zeeman coherence is negligible due to atomic washout of $R_{bp}^{(\beta)}$. Hence, it is possible to isolate the cross-population term. One can choose the case for which $\hat{e}_p=\sigma_+=\hat{e}_b$ and $\hat{e}_f=\sigma_-$ which leads to the isolation of the Zeeman coherence component in the extreme Doppler limit.

Example 3. Now consider the case for which $\hat{e}_f=\hat{x}=\hat{e}_b$ and $\hat{e}_p=\hat{y}$. For this choice all three physical mechanisms contribute to the signal field, i.e.,

$$\mathscr{E}_s=i\frac{\omega}{2c\epsilon_0}l\mathscr{E}_f\mathscr{E}_b\mathscr{E}_p^*\{[\tfrac{1}{2}G(J)-\tfrac{1}{4}L(J)+\tfrac{1}{4}M(J)](R_{fp}^{(1)}+R_{bp}^{(1)})+[\tfrac{1}{2}G'(J)-\tfrac{1}{4}L'(J)+\tfrac{1}{4}M'(J)](R_{fp}^{(2)}+R_{bp}^{(2)})\}\ ,$$

where

$$L(J)=\frac{1}{4}\sum_{M=-J-1}^{J+1}(|\langle J+1M|\mu|JM+1\rangle|^4+|\langle J+1M|\mu|JM-1\rangle|^4),$$

$$M(J)=\frac{1}{4}\sum_{M=-J-1}^{J+1}(|\langle J+1M|\mu|JM+1\rangle|^2|\langle J+1M+2|\mu|JM+1\rangle|^2$$
$$+|\langle J+1M|\mu|JM-1\rangle|^2|\langle J+1M-2|\mu|JM-1\rangle|^2).$$

The prime quantities can be obtained from the unprimed quantities by the following transformation: (1) interchange M with $M\pm1$ inside the parentheses and (2) change the summation limits from $\mp J\mp1$ to $\mp J$. Unlike the previous example where the polarization characteristics yield positive definite quantities, we can find choices of angular momenta such that $\mathcal{S}_s=0$.

One finds that for transitions $J=0\rightarrow J=1$ and $J=1\rightarrow J=1$, the three quantum-mechanical amplitudes add up to give a total cancellation of the signal.[20] This prediction has been confirmed in degenerate four-wave-mixing experiments in sodium vapor,[7] involving a single-photon excitation of the $D2$ line. The laser was tuned to the

$$3^2S_{1/2}(F=1)\rightarrow 3^2P_{3/2}(F=0)$$

transition. With the choice of polarization states of the radiation field as presented above, no signal was observed in the detector.

VI. CONCLUSION

We have presented a description of the three quantum-mechanical amplitudes or nonlinear optical coherences responsible for the signal generated in a degenerate four-wave-mixing process. The amplitudes correspond to the distinct excitation paths that a set of three arbitrarily polarized radiation fields can interact with a quantum system whose Hamiltonian is spherically symmetric. In the collinear geometry, we found that in the extreme Doppler limit the spectral response of the signal is Doppler free. This property together with the inherently high signal-to-noise[21] makes the degenerate four-wave mixing a powerful tool for the studies of atomic and molecular spectra. With the choice of polarization states such that the counterpropagating pump fields are linearly copolarized and the probe field is cross polarized, we found that the generated signal is null for electric dipole transitions $J=1\rightarrow J=0$ and $J=1\rightarrow J=1$ (in the absence of buffer gases). This effect arises from a complete cancellation of the sum of the quantum-mechanical amplitudes providing a unique approach for the studies of collisions in these transitions.[11] And last, we also showed that it is possible to isolate each of the quantum-mechanical amplitudes by an appropriate selection of the polarization states of the radiation field in the inhomogeneously broadened regime.

ACKNOWLEDGMENTS

We extend our sincere thanks to Professor P. R. Berman, Professor M. Ducloy, Professor R. W. Hellwarth, Dr. P. F. Liao, Dr. R. C. Lind, Dr. R. A. McFarlane, and Dr. D. G. Steel for many stimulating discussions. This work was supported in part by the Army Research Office under Contract No. DAAG29-81-C-0008.

[1]D. G. Steel, J. F. Lam, and R. A. McFarlane, *Laser Spectroscopy V*, edited by A. R. W. McKellar, T. Oka, and B. P. Stoicheff (Springer, Berlin, 1981).

[2]B. I. Stepanov, E. V. Ivakin, and A. S. Rubanov, Dok. Akad. Nauk. SSSR 196, 567 (1971) [Sov. Phys.—Dokl. 16, 46 (1971)].

[3]D. M. Bloom and G. Bjorklund, Appl. Phys. Lett. 31, 592 (1977).

[4]P. F. Liao, N. P. Economou, and R. R. Freeman, Phys. Rev. Lett. 39, 1473 (1977).

[5]R. K. Raj, D. Bloch, J. J. Snyder, G. Camy, and M. Ducloy, Phys. Rev. Lett. 44, 1251 (1980).

[6]R. L. Abrams and R. C. Lind, Opt. Lett. 2, 94 (1978); 3, 205 (1978).

[7]J. F. Lam, D. G. Steel, R. A. McFarlane, and R. C. Lind, Appl. Phys. Lett. 38, 977 (1981); R. L. Abrams, J. F. Lam, R. C. Lind, D. G. Steel, and P. F. Liao, *Optical Phase Conjugation*, edited by R. A. Fisher

(Academic, New York, 1982), Chap. 8.

[8]D. Bloch, These de Troisiene Cycle, Université de Paris Nord, 1980 (unpublished).

[9]M. Sargent, M. O. Scully, and W. E. Lamb, Jr., *Laser Physics* (Addison-Wesley, Reading, Mass., 1974).

[10]C. Wieman and T. W. Hansch, Phys. Rev. Lett. 36, 1170 (1976).

[11]P. R. Berman and J. F. Lam (unpublished).

[12]A. Omont, *Progress in Quantum Electronics* (Pergamon, Oxford, 1976).

[13]J. H. Marburger and J. F. Lam, Appl. Phys. Lett. 35, 249 (1979).

[14]M. Ducloy and D. Bloch, J. Phys. (Paris) 42, 711 (1981).

[15]The assignment of an effective dephasing rate for the Zeeman coherence is only an approximation. An accurate description of collision effects in quantum systems with degenerate states necessitates the introduction of the irreducible representation of the density matrix (Ref. 12). In this representation, the effect of collisions on the Zeeman coherence is represented by a dephasing rate.

[16]An identical effect appears in an inhomogeneously broadened laser system [see W. E. Lamb, Jr., Phys. Rev. 134, A1429 (1964)]. For the case of two-level atoms, their translational motion leads to a washout of the spatial modulation generated by the interference of the counterpropagating waves inside the laser cavity.

[17]S. M. Wandzura, Opt. Lett. 4, 208 (1979).

[18]R. W. Hellwarth, *Progress in Quantum Electronics* (Pergamon, Oxford, 1977).

[19]E. U. Condon and G. H. Shortley, *The Theory of Atomic Spectra* (Cambridge University Press, Cambridge, 1935).

[20]In the presence of buffer gases, the quantum-mechanical amplitudes do not add up to zero due to the distinct values of the collisional induced rates for the population and Zeeman coherences [see Ref. 1, and D. Bloch and M. Ducloy, J. Phys. B 14, L471 (1981)]. This noncancellation of the amplitudes has also been observed in nonresonant four-wave-mixing experiments in sodium vapors [see Y. Prior, A. R. Bogdan, M. Dagenais, and N. Bloembergen, Phys. Rev. Lett. 46, 111 (1981); G. Grynberg, J. Phys. B 14, 2089 (1981)].

[21]The generated signal in degenerate four-wave-mixing processes is background-free contrary to saturated absorption techniques [see V. S. Letokhov and V. P. Chebotayev, Zh. Eksp. Teor. Fiz. Pis'ma Red. 9, 364 (1969) [JETP Lett. 9, 215 (1969)]; R. A. McFarlane, W. R. Bennett, Jr., and W. E. Lamb, Jr., Appl. Phys. Lett. 2, 189 (1963)] where one measures small changes in the absorption coefficient.

Collisionally Induced Narrowing of the Longitudinal Relaxation Linewidth in Nearly Degenerate Four-Wave Mixing

J. F. Lam, D. G. Steel, and R. A. McFarlane
Hughes Research Laboratories, Malibu, California 90265
(Received 19 July 1982)

This paper reports the observation of collisionally induced spectral narrowing of the longitudinal relaxation linewidth with use of the nearly degenerate four-wave mixing process. A theoretical model, which takes into account strong velocity-changing collisions for the population and phase-interrupting collisions for the optical coherence, leads to a good qualitative understanding of this new effect.

PACS numbers: 34.90.+q, 42.65.Cq

This communication describes the first observation of a collisonal narrowing of the longitudinal relaxation linewidth which we observe using nearly degenerate four-wave mixing (NDFWM). The origin of the effect is explained by an analytical treatment of NDFWM which includes spontaneous emission and the effects of collisions due to ground-state perturbers. The results show that a direct measurement of velocity-changing collision rates may be possible with this method.

We consider the nonlinear interaction between three input fields denoted by $\vec{E}_f$, $\vec{E}_b$, and $\vec{E}_p$ oscillating at frequencies ω, ω, and $\omega+\delta$, respectively, and a set of moving two-level atoms having transition frequency ω_0. $\vec{E}_f$ and $\vec{E}_b$ are counterpropagating pump fields and $\vec{E}_p$ is the probe field which is nearly collinear to $\vec{E}_f$.[1] The physical process giving rise to a four-wave mixing signal in such a system can be described as follows. The interference of the fields $\vec{E}_f$ and $\vec{E}_p$ generates a nonequilibrium population difference which propagates in space with phase velocity $\delta/|\vec{K}_f - \vec{K}_p|$. The population difference provides a moving grating from which the field $\vec{E}_b$ scatters, generating a signal wave propagating in the opposite direction to $\vec{E}_p$. Conservation of energy imposes the condition that the frequency of the signal field is given by $\omega - \delta$. As a result of Doppler broadening, two resonances are observed, corresponding to two distinct velocity groups: The first occurs at $\delta = 0$ when the forward pump and probe are resonant with one velocity group of atoms, and the second occurs at $\delta = -2\Delta$ ($\Delta = \omega_0 - \omega$) when the forward pump and backward propagating signal are resonant with the second velocity group of atoms. The linewidths of the two resonances are given by the energy relaxation time (T_1) and the dipole dephasing time (T_2), respectively.[2,3]

Because of the distinct nature of the processes determining the bandwidths of the resonances at $\delta = 0$ and $\delta = -2\Delta$, collisions due to ground-state perturbers affect the linewidths of the two resonances differently. The bandwidth associated with the dephasing of the optical coherence in the presence of buffer gases is affected by phase-interrupting collisions and gives rise to collisional broadening of the $\delta = -2\Delta$ resonance.[4] The bandwidth associated with the population relaxation in the presence of buffer gases is a manifestation of velocity-changing collisional processes in addition to radiative decay processes. This paper shows that these effects give rise to collisional narrowing of the $\delta = 0$ resonance. In principle, NDFWM permits a simultaneous examination of collisional dynamics for each of these processes, leading to independent measurements of velocity-changing and phase-interrupting pressure-dependent cross sections.

The origin of collisional narrowing of the longitudinal (T_1) relaxation linewidth arises from the physical decoupling of the ground and excited states in the presence of buffer gases. In the absence of foreign perturbers, the ground and excited states are coupled together by means of the vacuum radiation field (the strength of this coupling is measured by the spontaneous decay rate γ). As a result of this coupling, both quantum states evolve as a single entity even in the presence of applied radiation fields, and this entity has a unique spectral response, i.e., the bandwidth is determined by γ. In the presence of foreign perturbers, the ground and excited states experience different collisional interactions which effectively decouples them even in the presence of the vacuum radiation field. In this case, the responses of the ground and excited states to applied radiation fields reflect their evolution as distinct entities. Hence, the NDFWM signal has contributions arising from both the ground and excited states separately. The spectral response of the individual contribution is characterized by

the respective collisional cross section. For the signal arising from the ground state, the bandwidth is determined by $\gamma_t + \Gamma_1$ while that of the excited state is determined by $\gamma + \gamma_t + \Gamma_2$. Γ_n is the velocity-changing collisional decay rate and γ_t is the reciprocal of the transit time. For low pressures, one notes that $\gamma_t + \Gamma_1 \ll \gamma + \gamma_t + \Gamma_2$. Hence, the contribution from the ground state will dominate over that from the excited state. The bandwidth is determined by $\gamma_t + \Gamma_1$ which is much narrower than γ. A measurement of the bandwidth at the resonance line $\delta = 0$ will provide a direct measurement of the ground-state decay rate Γ_1 provided that the transit time is known accurately.

To test this physical picture we have calculated the effect of collisions on the spectral response of NDFWM, in the impact regime. We have chosen a collision regime which entails a complete thermalization of the velocity distribution upon each scattering event, i.e., the strong-collision model. The third-order optical polarization obtained with a perturbation solution of the density-matrix equations is given by

$$P(\vec{r},t) = -N_0 \frac{|\mu_{21}|^4}{(2i\hbar)^3} E_f E_b E_p^* \{\exp[-i\vec{K}_p \cdot \vec{r} - i(\omega - \delta)t]\} \sum_{n=1}^{2} \{S_n + R_n\}, \tag{1}$$

where N_0 is the initial population of the ground state and μ_{21} is the dipole moment between the ground and excited states. In the extreme Doppler limit, S_n and R_n are given by

$$S_n = \left| 1 + \frac{\gamma}{\gamma + \Gamma_2 - \Gamma_1} (-1)^n \right| I_n + \frac{\gamma}{\gamma + \Gamma_2 - \Gamma_1} (-1)^n N_2 \left| \frac{\gamma + \Gamma_2 + i\delta}{\gamma n + i\delta} \right|, \tag{2a}$$

$$R_1 = N_1, \quad R_2 = N_2, \tag{2b}$$

$$I_n = -2\pi^{1/2} (Ku_0)^{-1} (\gamma_n + i\delta)^{-1} (2\gamma_e + i[2\Delta + \delta])^{-1} \tag{2c}$$

$$N_n = \frac{\Gamma_n}{Ku_0} \left(\frac{6\pi}{Ku_0} \right) \left(\frac{1}{\gamma_n + i\delta} \right) \left(\frac{1}{\Gamma_n + i\delta} \right), \tag{2d}$$

where $\gamma_e = \gamma/2 + \Gamma_{12}$, $\gamma_1 = \Gamma_1$, and $\gamma_2 = \gamma + \Gamma_2$. Γ_{12} is the pressure-dependent dephasing rate and Ku_0 is the Doppler width. We assume that $\delta \ll \omega$ and transit-time effects have been included phenomenologically.

The quantities S_n and R_n have simple physical interpretations. S_n has two contributions. The first one, proportional to I_n, arises from the dynamics that gives rise to the resonances at $\delta = 0$ and $\delta = -2\Delta$ with their respective linewidths modified by collisions. The second contribution, proportional to γ, is due to the existence of spontaneous decay from the velocity-redistributed excited state to the ground state. R_n, proportional to Γ_n / Ku_0 as shown in Eq. (2d), is due to velocity redistribution of the population in the presence of buffer gases. In the absence of buffer gases (turn off Γ_1, Γ_2, and Γ_{12}) the spectral response is given by the term proportional to I_n in Eq. (2a).

The calculated spectral response for various buffer-gas pressures is shown in Fig. 1. As buffer gas is added, we find that the amplitude at $\delta = -2\Delta$ decreases as a function of pressure, while the linewidth of that resonance broadens in accordance with the phase-interrupting collision model. However, we observe that the linewidth of the resonance at $\delta = 0$ narrows as a function of pressure and the magnitude of the signal increases. The narrowing yields a minimum width comparable to the value determined by transit-time effects (assumed to be 1 MHz in this calculation). An increase in magnitude of the response which was found at $\delta = 0$ arises from the tendency of collision processes to fill up the velocity hole "burned" by the radiation fields. (Magnitude changes are not indicated in the figures.)

As anticipated above, the narrowing of the linewidth at the resonance $\delta = 0$ in the presence of buffer gas is due to the appearance of distinct quantum mechanical scattering amplitudes for the excited and ground states. The distinct scattering amplitudes translate into different cross sections resulting in different decay rates Γ_n. Hence, collision effects lead to distinct bandwidths for both states.

The experimental configuration for these collision studies was identical to that used by Steel and Lind.[5] The counterpropagating pump fields were supplied by one stabilized cw dye laser (CR699-21) while the nearly collinear probe wave was supplied by a second stabilized cw dye laser (also CR699-21). The lasers were tuned to the $3s^2S_{1/2}(F = 2)$-$3p^2P_{3/2}(F = 3)$ transition of the D_2 line in sodium at 589 nm. Beam intensities were on the order of 2 mW/cm^2. All three input beams

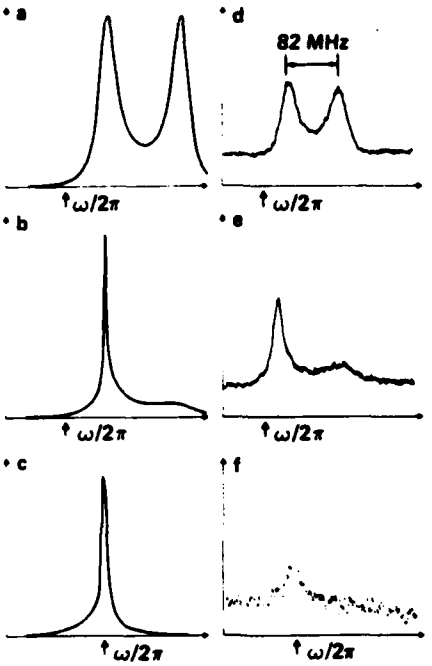

FIG. 1. Comparison between theory and experiment of the NDFWM spectral response for various neon buffer-gas pressures. The amplitude scaling varies with each figure. The separation between the double peaks is 82 MHz. (a) Theory, $\Delta = -41$ MHz, 0 Torr. (b) Theory, $\Delta = -41$ MHz, 2 Torr. (c) Theory, $\Delta = 0$, 10 Torr. (d) Experiment, $\Delta = -41$ MHz, 0 Torr. (e) Experiment, $\Delta = -41$ MHz, 2 Torr neon. (f) Experiment, $\Delta = 0$, 33 Torr neon.

were copolarized to avoid Zeeman coherence effects which are discussed elsewhere.[6]

Shown in Fig. 1(d) is a typical spectral response as the probe frequency is tuned near the pump frequency. These data are similar to those measured earlier.[5] In these experiments, it was important to tune the pump laser to the high-frequency side of the transition to avoid confusion with neighboring hyperfine levels in the upper state. Two resonances are observed occurring at $\delta = 0$ and at $\delta = -2\Delta$ as predicted in Fig. 1(a). As expected from the known lifetime of the transition, the widths of each peak were found to be approximately equal to 20 MHz. The width of the first peak is given by $1/\pi T_1$, while the width of the second peak is given by $2/\pi T_2$. The widths of the resonances are the same since we are using a ground-state transition for which $T_2 = 2T_1$ in the absence of collisions. In Fig. 1(e) we see the effect of adding a small amount (2 Torr) of neon buffer gas. As in the theoretical calculation of Fig. 1(b), there is a slight narrowing of the first peak at $\delta = 0$. The second peak has dropped in magnitude and broadened with respect to the first peak due to phase-interrupting collisions. The measured broadening of that peak is in agreement with the pressure-broadening rates tabulated by Lewis.[7] As the buffer-gas pressure is increased beyond a few Torr to the 30-Torr range, we see in Fig. 1(f) that the first peak is narrowed considerably. For these data, the pump frequency was adjusted to be coincident with the atomic resonance ($\Delta = 0$). However, similar narrowing behavior was observed when the pump frequency was tuned to the high-frequency side of the resonance, though the data were considerably noisier because of a reduced signal level. The narrowest linewidth measured was approximately 5 MHz but was limited by relative laser jitter.

The quantitative differences as a function of pressure between theory and experiments are most likely due to the collision model which assumes strong velocity-changing collisions. A more general description of collisions is presently being incorporated into the formalism. On the basis of this improved analysis and the above experiments we expect that by reducing the relative laser jitter and transit-time broadening, it should be possible to directly observe linewidths determined by velocity-changing collisions.

In conclusion, we have shown that in the presence of ground-state perturbers, the spectral response of the NDFWM signal shows a narrowing of the bandwidth of the longitudinal relaxation resonance ($\delta = 0$). We have presented a theory and a physical picture which qualitatively account for the observations showing the narrowing to be due to a collision-induced distinction between ground- and excited-state dynamics. These results demonstrate the possibility of determining the ground-state velocity-changing collision cross sections directly from the spectral response of NDFWM.

This work was supported in part by the U. S. Army Research Office under Contract No. DAAG29-81-C-008.

[1]D. M. Pepper and R. L. Abrams, Opt. Lett. 3, 212 (1978).

[2]R. K. Raj, D. Bloch, J. J. Snyder, G. Camy, and M. Ducloy, Phys. Rev. Lett. 44, 1251 (1980).

[3]J. Nilsen and A. Yariv, J. Opt. Soc. Am. 71, 180

(1980).

[4]P. R. Berman, in *Advances in Atomic and Molecular Physics*, edited by D. R. Bates and B. Bederson (Academic, New York, 1977), Vol. 13.

[5]D. G. Steel and R. C. Lind, Opt. Lett. 6, 387 (1981).

[6]NDFWM studies of collision effects using cross-polarized pump and probe show distinctly different behavior from that reported here. J. F. Lam, D. G. Steel, and R. D. McFarlane, to be published.

[7]E. L. Lewis, Phys. Rep. 58, 1 (1980).

PHYSICAL REVIEW A VOLUME 27, NUMBER 2 FEBRUARY 1983

Enhancement of four-wave mixing signals due to velocity-changing collisions

D. G. Steel and R. A. McFarlane
Hughes Research Laboratories, 3011 Malibu Canyon Road, Malibu, California 90265
(Received 28 June 1982)

We present experimental data showing the first observation of large enhancement of four-wave mixing signals due to velocity-changing collisions. The results are explained with a simple model which describes the population distributions in the presence of velocity-changing collisions and optical pumping, allowing relative velocity-changing collision rates to be inferred from the data.

The effect of velocity-changing collisions (VCC) by ground-state perturbers on the velocity distribution of atoms interacting with a monochromatic laser beam has been demonstrated by numerous experiments using saturation spectroscopy.[1,2] The purpose of this Communication is to describe a new manifestation of VCC which gives rise to enhancement of four-wave mixing signals. The enhancement is brought about by a collisional redistribution of the velocities which offsets the effects of velocity hole burning due to hyperfine optical pumping. We show how VCC rates may be inferred from the data using a simple model for the equilibrium population distribution.

The principal distinction between four-wave mixing and saturation spectroscopy using cw lasers in a multilevel system is that four-wave mixing signals increase with a pump induced increase in the ground-state number density while saturation spectroscopy signals increase with a pump induced decrease in the ground-state number density. Hence, cw four-wave mixing experiments tend to emphasize transitions which are not optically pumped, while in saturation spectroscopy the largest signals are observed on optically pumped transitions. The above description is true unless the pump beam laser intensity (I) is much less than I'_{sat}, where the saturation intensity I'_{sat} is calculated to account for optical pumping, spatial diffusion, and wall relaxation.[3,4] Typically, I'_{sat} is much less than the usual I_{sat}. In the first cw degenerate four-wave mixing (DFWM) experiments on the D_2 line in atomic sodium, the only strong signals observed using a cw dye laser were obtained on the $3s\,^2S_{1/2}(F=1)-3p\,^2P_{3/2}(F=3)$ transition and on the $3s\,^2S_{1/2}(F=1)-3p\,^2P_{3/2}(F=0)$ transition.[5] Of the six dipole allowed transitions on the D_2 line in atomic sodium, these two transitions are the only transitions that are not optically pumped. The remaining four transitions are indeed observed but only at intensities comparable to I'_{sat}. On these transitions at intensities larger than I'_{sat}, atoms in the $F=2$ ground state are quickly pumped into the $F=1$ ground state while atoms in the $F=1$ ground state are quickly pumped into the $F=2$ ground state. This paper demonstrates that at pump intensities comparable to I_{sat}, the normally very weak signal on the optically pumped transition given by $3s\,^2S_{1/2}(F=1)-3p\,^2P_{3/2}(F=2)$ can be considerably enhanced in the presence of VCC by ground-state perturbers. The physical origin of this enhancement is easily understood by considering the effect of VCC on velocity hole burning caused by the pump beams and optical pumping. In the absence of optical pumping, a pump beam generates a hole in the velocity distribution of the ground state by exciting atoms to the upper level in a very narrow velocity distribution determined by the natural linewidth of the transition. The depth of the hole in the ground-state velocity distribution is equal to the height of the spike in the upper-state velocity distribution and is determined by the strength of the laser-atom coupling. The maximum depth of the velocity hole would be equal to one-half the equilibrium ground-state population in the absence of the laser, corresponding to complete saturation of the transition. However, in an inverted V-type three-level system shown in Fig. 1, where optical pumping is present, it is possible to increase the hole depth in the ground-state population distribution to the point where the depletion of the population of that velocity group is

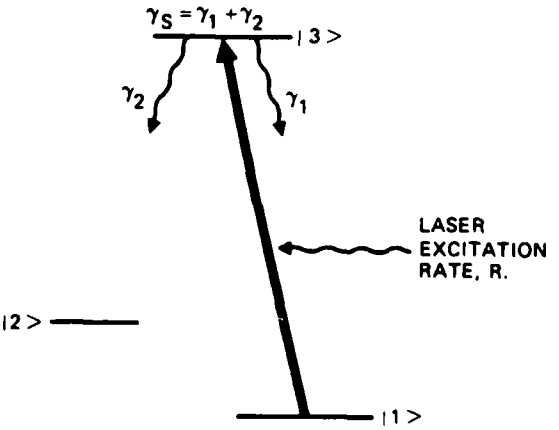

FIG. 1. Inverted V-type three-level system used to describe the effects of VCC on four-wave mixing signals generated on optically pumped transitions.

almost complete. At the same time, the height of the spike in the upper level is also reduced, being determined by the final equilibrium population distribution and the strength of the laser-atom coupling. However, atoms which have not been optically pumped out of level 1 because they are Doppler shifted out of resonance can be shifted into resonance if they experience an appropriate velocity-changing collision. This has the effect of increasing the equilibrium population density of level 1 in the specific velocity group interacting with the laser. As shown in the experiments below, this effect can be very pronounced. A simple analytical solution to the population rate equations has been obtained for this three-level system shown in Fig. 1 where a hard-sphere collision model has been assumed. In this model, the effects of the standing wave in the experiment have been ignored and strong collisions have been assumed, i.e., the velocity distribution is thermal after a collision. Nevertheless, we show that the four-wave mixing signal is an excellent indicator for the resonant population distribution and the VCC rate for various ground-state perturber gases can be estimated from the data.

The experimental approach to demonstrate this effect is based on DFWM in atomic sodium vapor. The geometry for DFWM is discussed in the literature.[6] The cw dye laser was tuned to the 589 nm resonance of the D_2 line. In Doppler-broadened media this interaction is Doppler free since only the zero-velocity group (whose width is determined by the natural linewidth) can interact simultaneously with all three beams.[7] Figure 2 (dotted line) shows the DFWM signal produced as the laser is tuned through the resonances of the D_2 line. As indicated above, while there are six dipole allowed transitions, only two are usually observed at convenient power levels because of optical pumping.[8] However, as a small amount of buffer gas is added, there is a pronounced change in the spectral behavior of DFWM. Figure 2 (solid line) shows that transitions A and B, which are not optically pumped, are reduced due to fine-structure changing collisions,[9] while transitions $3s\,^2S_{1/2}(F=1)-3p\,^2P_{3/2}(F=1)$ and $3s\,^2S_{1/2}(F=1)-3p\,^2P_{3/2}(F=2)$ (denoted by C in the figure and unresolved in this display) are enhanced. The points in Fig. 3 show the observed dependence of the $3s\,^2S_{1/2}(F=1)-3p\,^2P_{3/2}(F=2)$ DFWM signal level as a function of buffer gas pressure for helium. Similar data were also obtained in argon and xenon. As anticipated by our arguments given above, the data show that DFWM signals that are normally weak due to optical pumping are considerably enhanced by the presence of only a few hundred millitorr of buffer gases.

In the absence of pump absorption, DFWM signals vary as the square of the ground-state population density. Hence we expect that a simple rate equation

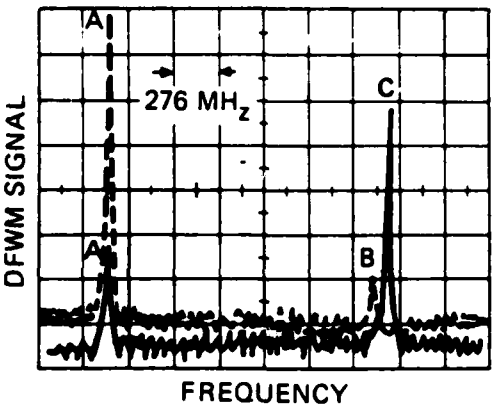

FIG. 2. Spectral structure of the DFWM signal as the cw dye laser is tuned across the D_2 line. The dashed line shows strong signals observed on the $3s\,^2S_{1/2}(F=2)-3p\,^2P_{3/2}(F=3)$ transition (A) and the $3s\,^2S_{1/2}(F=1)-3p\,^2P_{3/2}(F=0)$ transition (B). The solid line shows the effect of adding 200 mTorr of helium buffer gas. We see that the signal denoted by C in the vicinity of the three dipole allowed transitions originating out of the $F=1$ ground state is considerably enhanced. A high-resolution display of this spectral region shows that, in fact, the signal appearing is due to collisional enhancement of the $3s\,^2S_{1/2}(F=1)-3p\,^2P_{3/2}(F=1)$ transition and the $3s\,^2S_{1/2}(F=1)-3p\,^2P_{3/2}(F=2)$ transition.

model predicting the equilibrium population densities would explain the DFWM signal level dependence on buffer gas pressure.[10] The rate equations for levels 1 and 3 are shown below:

$$\dot{n}_1(v) = -D(n_1 - n_1^0) - Rn_1 + Rn_3 + \gamma_1 n_3 + \Gamma_{VCC}[N_1 f(v) - n_1] ,$$

$$\dot{n}_3(v) = -Dn_3 - Rn_3 + Rn_1 - \gamma_s n_3 + \Gamma_{VCC}[N_3 f(v) - n_3] .$$

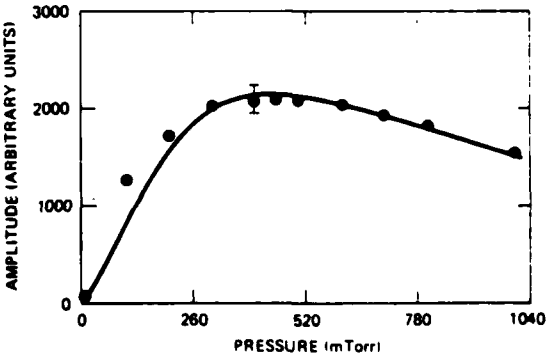

FIG. 3. Comparison between theory ($\Gamma_{VCC}^0 = 1.5 \times 10^{-}$ sec^{-1} $Torr^{-1}$) and experiment showing the dependence of the DFWM signal on buffer gas pressure. Comparison is made with the theory by assuming that the DFWM signal is linearly proportional to the square of the calculated population density at $v=0$.

The effects of velocity-changing collisions are accounted for by assuming the distribution to be thermal after a collision. Such strong collisions are described by a term like $\Gamma_{VCC}[N_i f(v) - n_i(v)]$, where $N_i = \int n_i(v)\,dv$, $f(v)$ is a Maxwellian velocity distribution, and Γ_{VCC} is the pressure dependent velocity-changing collision rate. For simplicity, Γ_{VCC} has been assumed to be the same for both the upper and lower levels of the transition. State-changing collision effects in this pressure range are negligible compared to radiative processes for the transitions under investigation and are not included in this model. In these rate equations, D is the diffusion rate ($\sim p^{-1}$ where p is the buffer gas pressure), γ_1 is the decay rate of level 3 back to level 1, γ_s is the spontaneous emission rate for level 3, n_i^0 is the unperturbed velocity distribution [given by $N_i^0 f(v)$], and R is the velocity dependent laser excitation rate given by $R_0/[1+(\omega-\omega_0-kv)^2/\gamma^2]$, where ω is the laser frequency and kv is the Doppler shift. R_0 is the resonance excitation rate given by $\gamma_s(I/I_{sat})$. These equations may be solved to yield the modified velocity distribution for the ground-state population by assuming only that the natural linewidth and $|\omega-\omega_0|$ are small compared to the Doppler linewidth in order to carry out the velocity integrals analytically:

$$n_1(v) = \frac{N_1^0 f(v)}{1+(R_0/R_1)/(\tau R_0+1)^{1/2}}\left[1+\frac{R_0/R_2}{(\tau R_0+1)^{1/2}}\right] \times\left[1-\left[\frac{\gamma_s'-\gamma_1}{D'}\right]\left[\frac{1}{1+(R_0/R_2)/(\tau R_0+1)^{1/2}}\right]\left[\frac{R_0/\gamma_s'}{\tau R_0+(\omega-\omega_0-kv)^2/\gamma^2}\right]\right],$$

where

$$R_0 = \gamma_s(I_0/I_{sat}),\quad \tau = (\gamma_s'-\gamma_1+D')/(D'\gamma_s'),$$

$$R_1 = (\gamma_s'/F)(D'/\Gamma_{VCC}'),\quad R_2 = (\gamma_s'/F)(\gamma_s'-\Gamma_{VCC}')/\Gamma_{VCC}',$$

$$\Gamma_{VCC}' = \Gamma_{VCC}\frac{[\gamma_s'(\gamma_s'-\gamma_1-\Gamma_{VCC}')-(\gamma_1-D')(D'-\Gamma_{VCC}')]}{(\gamma_s'-\Gamma_{VCC}')(D'-\Gamma_{VCC}')},$$

$$\gamma_s' = \gamma_s+\Gamma_{VCC}'+D,\quad D' = D+\Gamma_{VCC}',$$

and F is proportional to the ratio of the natural linewidth to the Doppler linewidth and is given by $(\pi^{1/2}/2)(\gamma/ku_0)\exp[-(\omega-\omega_0)^2/k_BT]$.

The calculated behavior of this population dependence on Γ_{VCC} for various buffer gas pressures is compared with experiment by plotting $n_1^2(v=0)$ as a function of buffer gas pressure p. Values for the diffusion rate D were taken from the literature.[11] The calculation was multiplied by a constant to enable direct comparison with the DFWM signal. Hence the only adjustable physical parameter was the collison rate Γ_{VCC}^0, where $\Gamma_{VCC} = \Gamma_{VCC}^0 p$. The results from helium are shown in Fig. 3 (solid lines). Similar data and comparison with theory were obtained with argon and xenon. The values used for Γ_{VCC}^0 were 1.5×10^7, 1×10^7, and 0.9×10^7 for helium, argon, and xenon, respectively, in units of $sec^{-1}Torr^{-1}$.[12] The value for helium is in surprisingly good agreement with that by Liao and colleagues,[2,13] considering our use of the strong collision model. To the best knowledge of the authors the values for argon and xenon are presented here for the first time. The effect of decreasing the value for Γ_{VCC}^0 is to increase the value of the pressure for maximum signal enhancement. The fit of the model to the data made a 20% change in Γ_{VCC}^0 easily observable. This model is a rate equation approximation and we have not included the effects of VCC on the third order optically induced coherence in degenerate four-wave mixing. In this case, Lam and Berman[14] have shown theoretically that in contrast to our intrinsically intensity dependent collisional enhancement, a small intensity independent collisional enhancement can be observed assuming strong collisions and no optical pumping or diffusion only if Γ_{VCC} for the lower level greatly exceeds Γ_{VCC} for the upper level. If the collision rates are assumed to be equal, as they are in our model, then they predict a small collisionally induced decrease in the signals due to a reduction in the degree of spatial modulation.[14] In fact, experimentally, we do observe a slight collision induced signal reduction at very low pump intensities.

In conclusion, we have demonstrated a new form of collisional enhancement of four-wave mixing signals. This effect has been demonstrated to be a useful signature of velocity-changing collisions and is a totally different approach to the study of VCC from the usual saturation spectroscopy approach.

The authors wish to acknowledge useful discussion with Dr. Juan F. Lam and the valuable assistance of John Shuler. This work was supported in part by the U.S. Army Research Office under Contract No. DAAG29-81-C-0008.

[1]C. Brechignac, R. Vetter, and P. R. Berman, Phys. Rev. A 17, 1609 (1978).
[2]P. F. Liao, J. E. Bjorkholm, and P. R. Berman, Phys. Rev. A 21, 1927 (1980).
[3]M. S. Feld, M. M. Burns, T. U. Kuhl, P. G. Pappas, and D. E. Murnick, Opt. Lett. 5, 79 (1980).
[4]P. G. Pappas, M. M. Burns, D. D. Hinshelwook, M. S. Feld, and D. E. Murnick, Phys. Rev. A 21, 1955 (1980).
[5]P. F. Liao, D. M. Bloom, and N. P. Economou, Appl. Phys. Lett. 32, 813 (1978).
[6]R. L. Abrams, J. F. Lam, R. C. Lind, D. G. Steel, and P. F. Liao, in *Phase Conjugation*, edited by Robert Fisher (Academic, New York, 1983).
[7]M. Ducloy and D. Bloch, J. Phys. (Paris) 42, 711 (1981).
[8]As the unfocused pump power is reduced to the 100-μW range, we have no problem observing all six of the dipole allowed transitions and most of the allowed crossovers.
[9]In the vicinity of the D_2 line on sodium, laser excitation of a nonoptically pumped transition [e.g., $3s\,^2S_{1/2}(F=2) - 3p\,^2P_{3/2}(F=3)$] can still result in a redistribution of the ground-state equilibrium population density due to state-changing collisions involving the upper state. For example, the fine-structure changing collision $3p\,^2P_{3/2} \rightarrow 3p\,^2P_{1/2}$ enables a net transfer of population from the $3s\,^2S_{1/2}(F=2)$ state to the $3s\,^2S_{1/2}(F=1)$ state.
[10]Similar studies have been performed to examine the efficiency of optically pumped nuclear polarization. P. G. Pappas, R. A. Forber, W. W. Quiver, Jr., R. R. Dasari, M. S. Feld, and D. E. Murnick, Phys. Rev. Lett. 47, 236 (1981).
[11]L. C. Balling, in *Advances in Quantum Electronics*, edited by D. W. Goodwin (Academic, New York, 1975), Vol. 3, p. 1. The diffusion rate is approximated by $D^1 = D_0(2.4/a)^2/p$ where D_0 is tabulated and varies as the square root of the mass ratios. Application of the diffusion approximation places several requirements on the experimental configuration, but most important is the requirement that the beam size be much smaller than the cell size.
[12]The relative accuracy for these numbers seems limited only by the relative accuracy of the diffusion rates given in Ref. 10.
[13]P. R. Berman, P. F. Liao, and J. E. Bjorkholm, Phys. Rev. A 20, 2389 (1979).
[14]J. F. Lam and P. R. Berman (unpublished).

Collisional destruction of four-wave-mixing signals in sodium in the presence of low-pressure buffer gas

D. G. Steel and R. A. McFarlane
Hughes Research Laboratories, 3011 Malibu Canyon Road, Malibu, California 90265
(Received 15 July 1982)

We present experimental data showing destruction of degenerate four-wave-mixing signals by collisions at extremely low pressures of added buffer gases (~100 mtorr). These experiments are performed on the $3s\,^2S_{1/2}(F=2)-3p\,^2P_{3/2}(F=3)$ transition of the D_2 line in atomic sodium for which, in the absence of buffer gases, the lower state is not optically pumped to the $3s\,^2S_{1/2}(F=1)$ ground state. However, using a simple rate equation model we are able to qualitatively explain the observed behavior by showing that state-changing collisions have the effect of generating a collision-induced optical pumping. This transfers the $F=2$ ground-state population to the $F=1$ ground state, thus reducing the density of atoms available for generating a signal.

Recently, degenerate four-wave mixing (DFWM) using cw narrow-band tunable dye lasers has been used as an alternative to saturation spectroscopy for high-resulution spectroscopy. For a pure two-level system the two methods are quite similar in their Doppler-free behavior and their dependence on various physical parameters.[1] However, in a multilevel system complicated by hyperfine-structure optical pumping, four-wave mixing and saturation spectroscopy (using cw lasers) become distinct. In particular, four-wave-mixing signals increase with a pump-induced increase in the ground-state number density while saturation spectroscopy signals increase with a pump-induced decrease in the ground-state number density. To be specific we consider the D_2 line in atomic sodium shown in Fig. 1. There are six dipole-allowed components of this transition owing to hyperfine splitting of the upper ($3p\,^2P_{3/2}$) state and lower ($3s\,^2S_{1/2}$) state. Of the six transitions, four are susceptible to hyperfine optical pumping and are shown as dotted lines in Fig. 1. The remaining two transitions designated A and B are unaffected by such hyperfine-structure optical pumping due to the dipole selection rules. Hence, for pump intensities comparable to the transition saturation intensity, these latter two transitions give rise to the two strong DFWM signals observed in cw experiments in atomic sodium as reported earlier.[2] The remaining transitions are considerably weaker because the ground-state population is transferred by optical pumping from one ground state to the other ground state. In saturation spectroscopy, just the opposite happens, with the transitions shown with dotted lines in Fig. 1 giving rise to the strongest signals. This optical pumping effect can be avoided in these experiments if the pump intensity is reduced well below the saturation intensity as described by Feld and Pappas.[3]

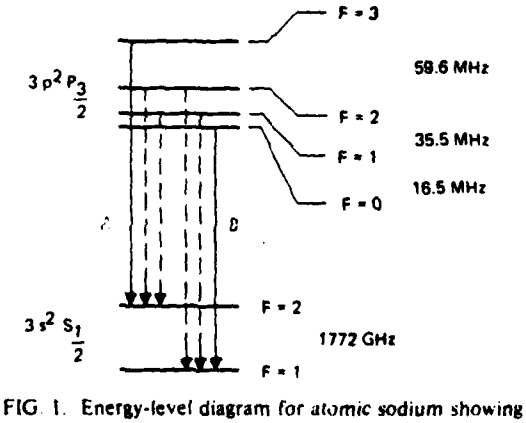

FIG. 1. Energy-level diagram for atomic sodium showing the D_2 line at 589 nm. Dotted lines show transitions susceptible to optical pumping.

In this paper we describe experimental studies using DFWM on the $3s\,^2S_{1/2}(F=2)-3p\,^2P_{3/2}(F=3)$ transition in sodium at 589 nm (the D_2 line). Our results show that while this transition is easily observed as previously discussed, a small quantity of buffer gas completely eliminates the observed signal. We believe this effect is due to collision-induced optical pumping caused by state-changing collisions involving both hyperfine-state-changing collisions and fine-structure–state-changing collisions.[4] These collisions have the effect of transferring the population to another atomic state which can then decay to the $F=1$ ground state. Using this model we show that a simple rate equation solution for the populations shows good qualitative agreement with the experiment. These results are important in that they strongly affect the interpretation of collision experiments performed using such transitions.

The origin of the nonlinear response in resonant DFWM is discussed by numerous authors.[1] We can consider the signal to arise from the scattering of a backward pump wave (E_b) from a spatial modulation

of the absorption and dispersion generated by the simultaneous interaction of a forward pump wave (E_f) and nearly collinear probe beam (E_p). Phase-matching conditions indicate (if the forward and backward pumps are counterpropagating) that the signal k vector will be oppositely directed to the k vector of the input probe wave. Typically, the angle between the forward pump and probe is very small, of order 1°. The interaction is Doppler free since only the $v=0$ velocity group can interact simultaneously with all three beams.

For these experiments a stabilized tunable dye laser was operated at 589 nm with pump intensities of order a few mW/cm^2 comparable to the saturation intensity. The interaction region was 1 cm and the sodium density was maintained so as to keep the inverse absorption length less than 1 cm^{-1}. Figure 2(a) shows the entire spectrum when the dye laser is scanned through the D_2 line. As expected, two transitions are observed corresponding to transitions A and B given above. Figure 2(b) shows the effect of adding 200 mtorr of argon buffer gas to the cell showing transitions A and B considerably reduced. Buffer gas pressures are measured outside the cell at room temperature while the cell temperature was near 150 °C. (Transition C is a collisionally *enhanced* signal arising from the optically pumped transitions terminating on the $F=2$ and $F=1$ upper states and is discussed elsewhere.[5]) The parametric behavior of the A transition as a function of gas pressures was recorded for three buffer gases and is shown in Fig. 3. There are slight variations for the various gases. To ensure the signals were not the results of collisions with large molecules, an additional precaution was taken by passing the buffer gases through a liquid-nitrogen-cooled coil prior to pumping them

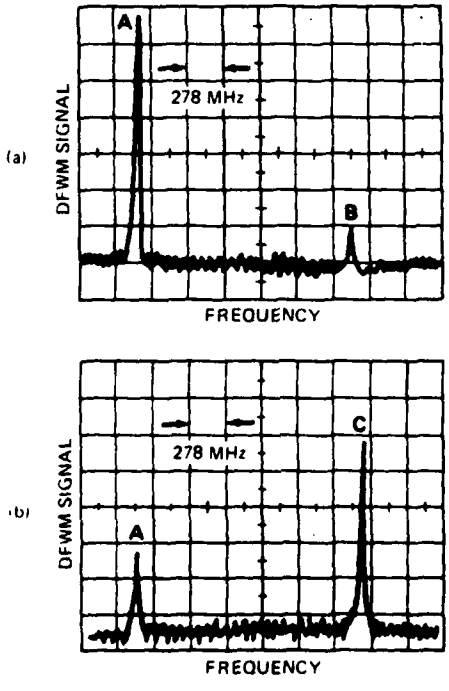

FIG. 2. (a) DFWM signal observed in the absence of buffer gases as the cw dye laser is tuned across the D_2 line. (b) DFWM signal as shown in (a) but in the presence of 200 mtorr of argon buffer gas showing that transitions A and B are considerably reduced. [Transition C is a collisionally enhanced transition discussed elsewhere (Ref. 4)].

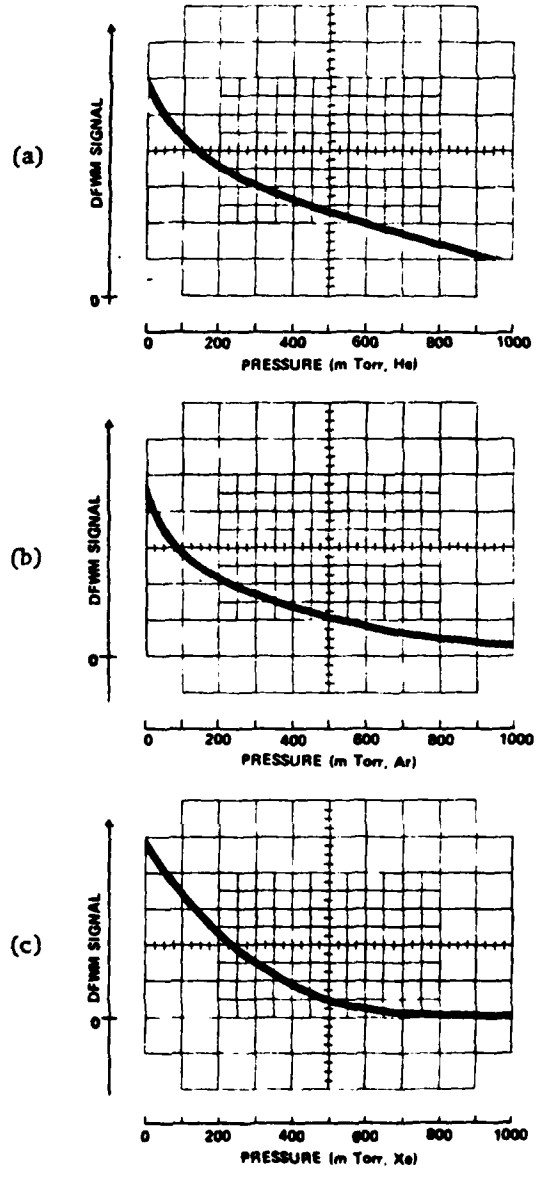

FIG. 3. The parametric dependence of the DFWM signal as a function of gas pressure for (a) helium, (b) argon, and (c) xenon.

into the cell to ensure that any impurities would be condensed out of the system.

To explain the above behavior a simple rate equation model was solved based on Fig. 4(a). Level 4 is any level which can decay to level 2 by spontaneous dipole emission and is coupled to level 3 by state-changing collisions. Qualitatively, level 4 represents the $3p\,^2P_1$ state of sodium as well as the $F=2$, $F=1$, and $F=0$ levels of the $3p\,^2P_{3/2}$ state. The only optical coupling allowed is between levels 1 and 3. To understand the observed behavior, it is important to include the effects of diffusion. Diffusion limits the rate at which pumped atoms can leave and unpumped atoms can enter the interaction region and thus enhances the effect of any optical pumping mechanism.

The important rate equations are given by

$$\dot{n}_1 = D(n_1 - n_1^0) - R(n_1 - n_3) + \alpha_1\gamma_4 n_4 + \gamma_3 n_3 \ ,$$

$$\dot{n}_3 = -Dn_3 - R(n_3 - n_1) - \gamma_3 n_3 - \Gamma_{34} n_3 + \Gamma_{43} n_4 \ ,$$

$$\dot{n}_4 = -Dn_4 + \Gamma_{34} n_3 - \Gamma_{43} n_4 - \gamma_4 n_4 \ .$$

In these equations, n_i is the population of level i in the presence of the radiation field, n_i^0 is the level population in the absence of the field, α_i is the branching ratio, R is the laser excitation rate assumed to be on resonance given by $\gamma_s I/I_{sat}$ ($\gamma_s = \gamma_3$ is the A coefficient), D is the diffusion rate given by $D_0(2.4/a)^2/p$ where values for D_0 are taken from the literature,[6] a is the beam radius, and p is the pressure, and Γ_{ij} is the pressure-dependent state-changing collision rate from level i to level j. These equations may be solved for the time-independent equilibrium solution for the population in level 1:

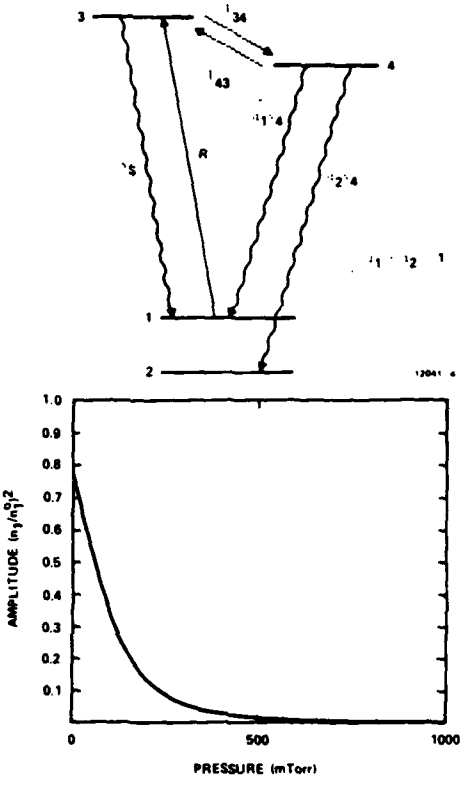

FIG. 4. (a) Model assumed to describe the effect of state-changing collisions. The laser is tuned to be resonant with levels 1 and 3. Level 3 can decay by dipole radiation to level 1 or in the presence of buffer gas collisions can be transferred to level 4. Level 4 can decay by spontaneous dipole emission to either level 1 or level 2. (b) The equilibrium solution to the rate equation model for the population of level 1. The value n_1^2 is plotted rather than n_1 since the DFWM signal is proportional to the square of the atomic density.

$$n_1 = n_1^0 = \left\{1 - \frac{I}{I_{sat}}\left[\frac{1 + \frac{\Gamma_{34}}{D}\left[1 - \frac{\Gamma_{43} + \alpha_1\gamma_4}{\gamma_4'}\right]}{1 + \frac{\Gamma_{34}}{\gamma_s}\left[1 - \frac{\Gamma_{43}}{\gamma_4'}\right] + \frac{D}{\gamma_s}}\right]\right\}\left\{1 + \frac{I}{I_{sat}}\left[\frac{2\frac{\Gamma_{34}}{D}\left[1 - \frac{\Gamma_{43} + \alpha_1\gamma_4}{\gamma_4'}\right]}{1 + \frac{\Gamma_{34}}{\gamma_s}\left[1 - \frac{\Gamma_{43}}{\gamma_4'}\right] + \frac{D}{\gamma_s}}\right]^{-1}\right\} \ .$$

where $\gamma_4' = \gamma_4 + \Gamma_{43} + D$. By noting that the expression in the denominator multiplying I/I_{sat} is usually much greater than 1, we see that in the presence of state-changing collisions the effective saturation intensity is decreased. This result is similar to that obtained for estimating the effects of ordinary optical pumping on saturation as discussed in Ref. 3. For $I/I_{sat} = 0.5$, and the values for an effective Γ_{31}^0 and Γ_{34}^0 estimated from the literature[7] to be of order 2×10^7 sec^{-1} and 1×10^7 sec^{-1} torr^{-1}, respectively, we find the predicted behavior for $(n_1/n_1^0)^2$ shown in Fig. 4(b). We plot the value $(n_1/n_1^0)^2$ since the nonlinear DFWM signal is proportional (in the absence of pump absorption) to the square of the population density. The model shows the predicted behavior to be in good qualitative agreement with the experiments. Note, however, that the model is overly pessimistic on the effects of collision-induced reduction

of the population in the ground state. We believe that this is due to the fact that we have ignored the effects of velocity-changing collisions.

In conclusion, we have presented experimental data showing the effects on DFWM signals of small amounts of added buffer gases. We believe these are the result of state-changing collision-induced optical pumping. While these experiments have been performed using DFWM, they clearly apply to any nonlinear spectroscopy technique using cw lasers including nondegenerate four-wave-mixing spectroscopy to study excited states.[8] The effects of these collisions diminish as the laser interacting with the ground-state resonance is detuned by an amount large with respect to hyperfine splittings and the Doppler width.

This work was supported in part by Army Research Office Contract No. DAAG29-81-C-0008.

[1]R. L. Abrams, J. F. Lam, R. C. Lind, D. G. Steel, and P. F. Liao, in *Phase Conjugation*, edited by Robert Fisher (Academic, New York, 1983), and references contained therein.

[2]P. F. Liao, D. M. Bloom, and N. P. Economou, Appl. Phys. Lett. 32, 813 (1978).

[3]M. S. Feld, M. M. Burns, T. U. Kuhl, P. G. Pappas, D. E. Murnick, Opt. Lett. 5, 79 (1980); P. G. Pappas, M. M. Burns, D. D. Hinshelwood, M. S. Feld, and D. E. Murnick, Phys. Rev. A 21, 1955 (1980).

[4]P. F. Liao, J. E. Bjorkhom, and P. R. Berman, Phys. Rev. A 20, 1489 (979).

[5]D. G. Steel and R. A. McFarlane, Phys. Rev. A (in press).

[6]L. C. Balling, in *Advances in Quantum Electronics*, edited by D. W. Goodwin (Academic, New York, 1975), Vol. 3, p. 1.

[7]E. L. Lewis, Phys. Rep. 58, 1 (1980).

[8]D. G. Steel, R. A. McFarlane, and J. F. Lam, Phys. Rev. A 26, 1146 (1982).

SPECTRAL NARROWING AND RELATED EFFECTS OF COLLISION DYNAMICS IN RESONANT DEGENERATE FOUR-WAVE MIXING*

J.F. Lam, D.G. Steel and R.A. McFarlane
Hughes Research Laboratories
Malibu, California 90265
U.S.A.

We have undertaken a detailed study of the effect of ground state perturbers on the magnitude and spectral response of degenerate and nearly degenerate four-wave mixing signals. The results, as described below, point out the possibility of measuring ground state velocity changing collision cross sections and that it is possible to enhance the degenerate four-wave mixing signal in the presence of buffer gases.

The theoretical model consists of a set of 2-level atoms interacting with the external radiation fields in the degenerate four-wave mixing (DFWM) geometry [1]. There is a frequency shift of the probe wave with respect to the two counterpropagating pump waves such that $\delta=0$ for degenerate operation while $\delta\neq0$ for nearly degenerate operation. We have introduced appropriate collision-induced decay and pumping channels to account for the existence of fine and hyperfine structure components. In the impact regime, optical coherences undergo phase interrupting collisions with ground state perturbers while populations undergo velocity changing collisions (VCC). Experiments using sodium were carried out for comparison with the theoretical model. Two stabilized cw lasers were tuned to the $3s^2S_{1/2}$-$3p^2P_{3/2}$ transition. A nearly collinear pump and probe insures that the spectrum of the DFWM signal is Doppler-free.

We consider the situation where the frequency shift δ is allowed to vary with respect to constant pump frequency and the polarization state of all radiation fields is the same. The analysis shows the spectrum of the FWM signal has two resonances due to resonant excitation of two velocity groups. The first resonance occurs at $\delta=0$ when the forward pump and probe are resonant with one velocity group. Its linewidth is determined by the longitudinal relaxation rate, $1/T_1$. The second resonance occurs at $\delta=-2\Delta$ ($\Delta=\omega_0-\omega$. ω_0 and ω are the transition and laser frequencies, respectively) when the forward pump and generated signal are resonant with the other velocity group. The linewidth of this resonance is determined by the transverse relaxation rate $1/T_2$. Hence, in the presence of buffer gas, the resonance at $\delta=0$ experiences VCC while the resonance at $\delta=-2\Delta$ undergoes phase interrupting collisions. Fig. 1 shows the spectral response in the presence of Ne buffer gas. Figs. 1a, 1b, and 1c illustrate the results of the theoretical analysis using the quantum mechanical transport equation while Figs. 1d, 1e and 1f are the corresponding experimental results. The narrowing and enhancement of the $\delta=0$ linewidth arises from the collision-induced decoupling of the ground and excited states. This decoupling occurs because the ground state ($3s^2S_{1/2}$) and excited state ($3p^2P_{3/2}$) are characterized by different trajectories due to VCC resulting in $\Gamma_1\neq\Gamma_2$. Γ_n is the VCC rate for level n. For the ground state, the bandwidth is determined by $\gamma_t+\Gamma_1$, while for the excited state, it is $\gamma_t+\Gamma_2+\gamma$. γ_t is the inverse of the transit time and γ is the spontaneous decay rate. Since $\gamma_t+\Gamma_1 \ll \gamma_t+\Gamma_2+\gamma$, one finds that for low buffer gas pressure, the magnitude of the signal generated by the ground state dominates that due to the excited state and the linewidth is determined by $\gamma_t+\Gamma_1$. By choosing large enough optical beams, γ_t can be made sufficiently small such that $\Gamma_1 \gg \gamma_t$ and the linewidth becomes a direct measure of Γ_1. The arrow in Fig. 1 corresponds to the location of the

atomic transition frequency. The broadening of the $\delta=-2\Delta$ linewidth as a function of pressure is due to collisionally induced dephasing. Figure 2 shows the ratio of the magnitude of the peak at $\delta=-2\Delta$ to that at $\delta=0$. The dotted curve represents the experimental data while the solid curve is obtained from the analysis. The ratio is reduced at a rate faster than that due to pressure broadening of the T_2 peak and is the result of the predicted enhancement of the T_1 peak [2].

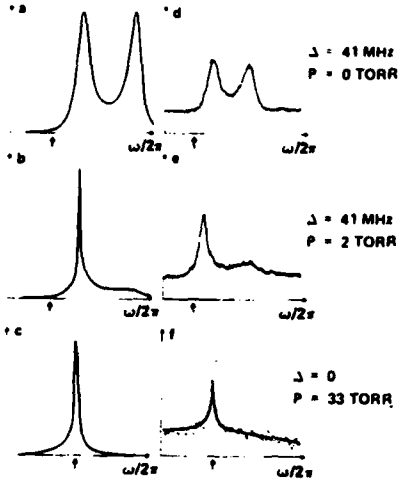

Fig. 1 Spectra of FWM for different values of pressure and Δ

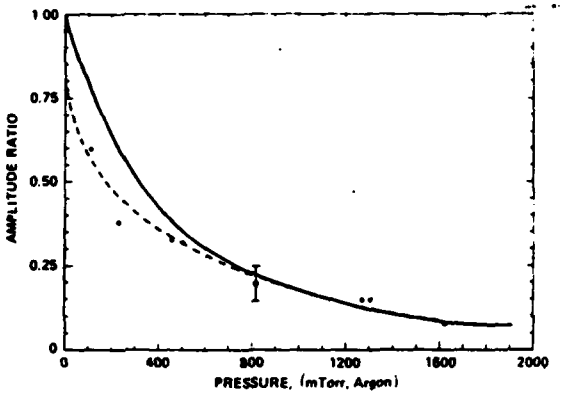

Fig. 2 Ratio of the peak amplitudes of the T_2 to T_1 resonances vs. pressure

Next, we consider the effect of buffer gases on the DFWM spectrum when $\delta=0$. Fig. 3a shows the spectrum of the DFWM signal as the laser is tuned through the D_2 line of sodium in the absence of buffer gases. The signals A and B arise from the $3s^2S_{1/2}(F=2)$-$3p^2P_{3/2}(F=3)$ and $3s\,^2S_{1/2}(F=1)$-$3p\,^2P_{3/2}(F=0)$, respectively. These transitions do not experience optical pumping. When a small amount of buffer gas is added (~30mTorr), the spectrum exhibits significant changes as depicted in Fig. 3b. The decrease in the magnitude of the signals A and B is due to collision induced ground state optical pumping arising from fine and hyperfine structure changing collisions in the excited state. There are two hyperfine split ground state levels. Calculations show that the population of the particular ground state excited by the laser can be almost completely transferred to the remaining ground state when ground state relaxation is limited by spatial diffusion. The new structure (C) is unresolved in this display but involves transitions from $3s^2S_{1/2}(F=1)$ to $3p^2P_{3/2}(F=1$ and 2). The transitions are strongly optically pumped and at convenient laser powers ($I\sim I_{sat}$) are very weak. However, in the presence of small amounts of buffer gas these transitions are considerably enhanced as shown. The physical origin of this enhancement is understood by considering the effect of VCC on velocity hole burning caused by the pump beams and ground state optical pumping. In the absence of optical pumping, the pump beams generate a hole in the ground state velocity distribution. The depth of this hole is limited by saturation to one half the equilibrium value in the absence of the laser field. However, in sodium as indicated above, the ground state is hyperfine split into two levels separated by 1.77 GHz. Optical pumping results in a transfer of population from the ground state level involved in the optical excitation to the

remaining level. This results in a much deeper velocity hole and a very weak DFWM signal due to the depleted ground state population. However, in the presence of buffer gas, atoms which have not been optically pumped because of their Doppler shift can be shifted into resonance if they experience an appropriate VCC. These collisions have the effect of thermalizing the population, washing out the velocity hole. The signal is thus enhanced because of the increase in the ground state population for that velocity class. Fig. 4 shows a comparison between theory and experiment for helium buffer gas [3]. At higher pressures the signal begins to fall off because the entire velocity distribution becomes optically pumped.

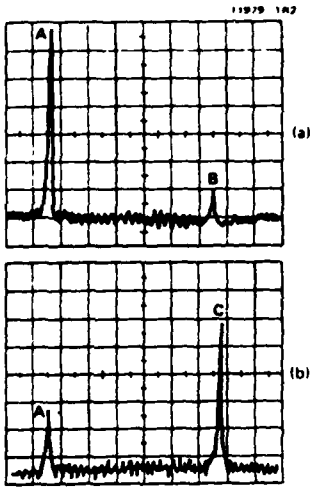

Fig. 3 DFWM spectra of sodium (a) no buffer gases (b) in the presence of buffer gas

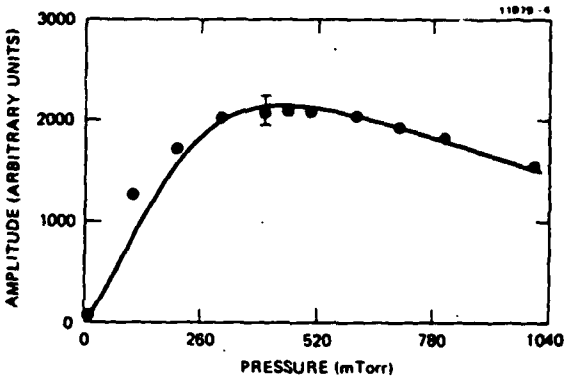

Fig. 4 DFWM signal vs. pressure of He buffer gas

*Work supported in part by the U.S. Army Research Office under contract No. DAAG29-81-C-008

References

1. R.L. Abrams, et al: in Optical Phase Conjugation, edited by R.A. Fisher (New York, Academic Press 1983) pp. 211-284

2. J.F. Lam, D.G. Steel and R.A. McFarlane: Phys. Rev. Lett. 49, 1628 (1982)

3. D.G. Steel and R.A. McFarlane: Phys. Rev. A 27, 1217 (1983)

Collision Effects on Zeeman Coherences

using

Nearly Degenerate Four-Wave Mixing

J.F. Lam, D.G. Steel and R.A. McFarlane
Hughes Research Laboratories
Malibu, California 90265
(213) 456-6411

Abstract

We report experimental and theoretical studies of collisional processes on Zeeman coherences using polarization sensitive nearly degenerate four-wave mixing. The detuning characteristic of the signal allows a direct measurement of the magnitude of the m-mixing collisional rates.

Collision Effects on Zeeman Coherences using Nearly Degenerate Four-Wave Mixing

J.F. Lam, D.G. Steel, and R.A. McFarlane
Hughes Research Laboratories
Malibu, California 90265
(213) 456-6411

Recently, we have shown that the nearly degenerate four-wave mixing (NDFWM) process can provide a direct and simultaneous measurement of the longitudinal ($1/T_1$) and transverse ($1/T_2$) relaxation rates of a resonant two-level atom. Furthermore, we observed that in the presence of buffer gases, the linewidth of the resonance describing the longitudinal relaxation process experiences a significant narrowing, below that of the natural width. Using a theoretical model, the narrowing was accounted for as arising from collisional effects in the ground state population[1]. These observations were made for the case where the radiation fields are co-polarized and we concluded that NDFWM offers a unique technique for the measurement of the ground state velocity changing cross section[2].

This paper discusses our ongoing studies on collision dynamics in Zeeman coherences using NDFWM. The production of such coherences is achieved by having the pump fields be 90^{o} cross polarized with respect to the probe field. This scheme provides a truly phase and polarization conjugation in a resonant medium[3].

The results of our studies can be summarized as follows. In the Doppler limit and in the absence of buffer gases, the spectrum of the generated signal shows two resonances having equal linewidths (given by the spontaneous emission rate). The first resonance is centered at the pump frequency ω and reflects the fact that the forward pump and probe excite the same velocity group. This resonance is centered at $3\omega-2\omega.$, ω_o being the transition frequency. This resonance reflects the fact that the forward pump and the generated signal

shares the same velocity group and describes the nonlinear response of the optical coherence. The equality in the linewidths is a consequence of the resonant atom behaving as closed quantum system. In the presence of buffer gases, the two resonances remain with the distinction that the linewidths are no longer equal in magnitude. The linewdith of the first resonance is influenced by collisionally induced changes in the Zeeman coherence of the ground state. Its magnitude is determined by angular momentum changing collisions. The linewidth of the second resonance is broadened as a function of buffer gas pressure. This is a manifestation of the effects of phase interrupting collisions on the optical coherence. The predominance of ground state dynamics in determining the details of the first resonance is a consequence of the fact that the resonance atom behaves like an open quantum system in the presence of foreign perturbers.

The theoretical lineshape was obtained using a perturbative solution of the density matrix equations, taking into account the random motion of the atoms. In the Doppler regime with the pump frequency within the Doppler linewidth, the results of the computation agree well with the physical processes discussed above. A novel feature appears when the laser is tuned outside the Doppler width. Figure 1 shows the theoretical spectral lineshape of the generated signal as a function of probe-pump frequency offset. In this example, the pump detuning from the atomic resonance is set at 4 GHz and the Ar buffer gas pressure is 700 Torr. The narrow dip arises from the quantum interference between ground and excited state dynamics. And the width of the dip is determined by collisional effects on Zeeman coherences. A value of

collision cross section was employed in the calculation which reproduced the form of the lineshape structure observed by Bloembergen and coworkers on their recent studies of atomic sodium.[4] Structure associated with the second resonance disappears at such high buffer gas pressures.

Measurements are underway in our laboratory using pump detunings less than the Doppler width and our results will be compared with the theoretical modeling for this case.

*Work supported in part by the Army Research Office under Contract No. DAAG29-81-C-0008

REFERENCES

1. J.F. Lam, D.G. Steel and R.A. McFarlane, Phys. Rev. Lett. 49, 1628 (1982).
2. J.F. Lam, D.G. Steel and R.A. McFarlane, in Laser Spectroscopy VI, H.P. Weber and W. Luthy, editors, Springer-Verlag (1983) p. 315.
3. J.F. Lam and R.L. Abrams, Phys. Rev. A 26, 1539 (1982).
4. L. J. Rothberg and N. Bloembergen, in Laser Spectroscopy VI, H.P. Weber and W. Luthy, eds., Springer Verlag 1983.

FIGURE CAPTION

Fig. 1. NDFWM Theoretical Lineshape with $\omega-\omega_o$ = 4 GHz and P = 700 Torr of Ar

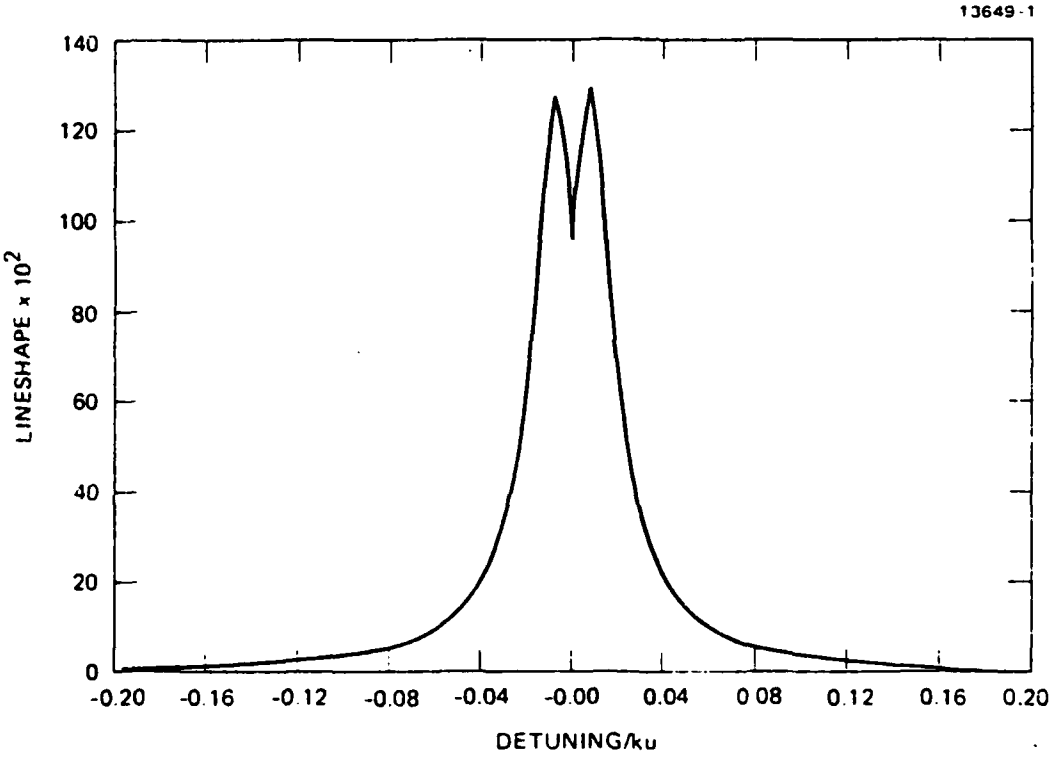
13649-1
140
120
100
80
60
40
20
0
LINESHAPE x 10^2
-0.20
-0.16
-0.12
-0.08
-0.04
-0.00
0.04
0 08
0.12
0.16
0.20
DETUNING/ku

SUBMITTED TO PHYS. REV. A

HIGH RESOLUTION SPECTROSCOPY AND COLLISION STUDIES OF RYDBERG STATES BY FREQUENCY DOMAIN THREE STATE SPECTROSCOPY (FDTS)

Duncan G. Steel and Ross A McFarlane
Hughes Research Laboratories
3011 Malibu Canyon Road
Malibu, CA 90265
213-456-6411

We descibe an experimental study of collision induced frequency shift and line broadening on transitions between the 3s ground state and ns and nd excited states of atomic sodium due to rare gas collisions. These studies are made in the frequency domain using a new kind of four-wave mixing spectroscopy which we designate frequency domain three state spectroscopy (FDTS). Such a frequency domain study of collisions permits both the frequency shift and line broadening to be simultaneously measured. The simultaneous measurement of both of these parameters is important since the shift is due to long range type collisions and the broadening is due to short range dephasing type collisions.

1. Introduction

An atom undergoing a resonant transition from a high lying state to the ground state experiences a shift and a broadening of its spectral line profile in the presence of collisions with neutral perturbers. The profile is given by $I(\omega)=(I_o/\pi)(\gamma_o+\gamma_c)/[(\omega-\omega_o-\epsilon_c)^2+(\gamma_o+\gamma_c)^2]$, where ϵ_c and γ_c are the collision induced pressure dependent frequency shift and line broadening, respectively. In the case of alkali-noble gas collisions, the spectral shift of an alkali atom transition taking place between the ground state and a state n when n is large (n is the principal quantum number) is dominated by scattering of the outer alkali atom electron by the neutral ground state perturber. The line broadening is dominated by the polarizabiity of the perturber. The shift was first analyzed by Fermi[1]. The frequency shift and line broadening were experimentally examined in the classic work of Fuchtbäuer and his co-workers[2-5] who studied absorption by the principal series of several metals in the presence of various noble and molecular gases. The experimental results show that as the principal quantum number increases, the collisional cross section increases as one would expect from geometrical considerations and then approaches an asymptotic value, independent of the principal quantum number. The data suggests that the asymptotic values depend only on the perturber, and not on the particular species of the absorbing atom. Following these studies, additional experimental observations were made in the extensive work of Mazing[6] and Alekseev[7]. There have been numerous theoretical works attempting to provide quantitative understanding of this behavior[8-10].

More recently, using the techniques of conventional spectroscopy and laser spectroscopy, collision studies have been extended to series other than the principal series. Doppler free two-photon absorption has been used to study the collisional broadening and shift of the 3s-4d[11-13] and 3s-5s[12,13] transitions in sodium. The broadening behavior was verified using transient techniques based on the measurement of the temporal decay of the two-photon coherence[14]. Further measurements of the two-photon coherence have been made using cw techniques based on observations in the frequency domain[15]. In an extensive experimental study, Flusberg, Kachru, Mossberg, and Hartman, carried out their measurements of the pressure broadening for the 3s-ns and 3s-nd superposition state series of atomic sodium[16]. Using the tri-level echo technique, they measured the temporal decay of the two-photon coherence, ρ_{13} in the density matrix formalism, between the excited state, 3, and the ground state, 1, via a coupling through a resonant intermediate state, 2. (Because these measurements were in the time domain, measurements of the pressure induced spectral shift were not readily obtained.) Using two pulsed dye lasers, this technique has enabled them to explore the series well beyond n=5, extending to n=34. They were able to compare their results with the collision theory of Omont [10] and showed good qualitativie agreement for the 3s-ns series. Agreement between theory and experiment for the 3s-nd series was not obtained and is not really expected since Omont's analysis includes only elastic collisions, while inelastic collisions are known to play an important role in collisions involving higher angular momentum states[17].

Using resonant two-photon absorption, Krebs and Schearer[18] have measured the collision induced shifts of the 3p-nd transitions in atomic sodium. Currently no analysis exists for the collision induced shifts for intermediate values of n. For large n, they obtained an asymptotic value for the cross section similar to the results of Fuchtbauer and in good agreement with the asymptotic theory of Alekseev and Sobelman[8] and Ivanov[9]. The work of Brillet and Gallagher[19] on rubidium using two-photon absorption showed that while the collision induced shifts were in agreement with the theory for large n, the collision broadening was larger than expected.

In this paper we describe frequency domain measurements using two stabilized tunable dye lasers and the method of nonlinear four-wave mixing of the pressure induced shift and broadening of the 3s-ns transitions and pressure induced broadening of the 3s-nd transitions in sodium due to rare gas collisions. The experimental and theoretical basis for these measurements was described earlier[15]. We designate it frequency domain three-state spectroscopy (FDTS) to distinguish it from time domain type measurements such as the tri-level echo or two-photon coherent transient measurements or from frequency domain absorption measurements. The important distinction between FDTS and other two-photon frequency domain spectroscopy techniques is that FDTS generates a line profile characterizing the ground state to final state transition, but remains resonant through the intermediate state by using two independently tunable frequencies. Hence, the FDTS signal strength does not decrease due to intermediate state detuning as the final state principal quantum number increases. This is not the case in ordinary two-photon absorption signals. Time domain measurements

provide strong signals and do not requre narrowband lasers, however, usually they provide only line broadening information while FDTS provides measurements of both the spectral shift and the line broadening. This is important, since in the context of collision theory, it yields information about the imaginary and the real part of the scattering amplitude[8]. The time domain measurements give the signal decay (which relates directly to the broadening); thus, information is obtained primarily about the imaginary part of the scattering amplitude. Since narrowband lasers are used for FDTS and it is Doppler free, the pressure dependent effects can be observed at relatively low pressure (~1 Torr) ensuring measurements in the impact regime. This is in contrast to the work of Fuchtbauer indicated above where the pressures were high enough (in the range of several 100 Torr) to observe pressure broadening in excess of the combined Doppler and instrumentation width. In addition, FDTS also enables measurement of the fine structure of the high lying states. This will be briefly summarized in Section 3.

In section II of this paper we present the theoretical basis for this nonlinear spectroscopy technique and describe how collisions are included in the formalism. In Section III we present the experimental results and indicate how velocity changing collisions and state changing collisions affect the observed behavior in terms of signal strength. We describe the measurements of fine structure splitting and measured line shift and broadening rates and describe how cross-sections are inferred from the data. In Section IV we discuss the results and compare the measurements with existing analysis.

2. Theory

As we shall show in the following discussion, FDTS is a form of Doppler-free coherent four-wave mixing. The signal is a coherent collimated beam as opposed to fluorescence, and is produced by a two-photon induced optical coherence between the ground state and excited state. The nonlinear polarization is third order in the applied electric fields. The frequency and the direction of the signal are determined by conservation of energy and phase matching. The two-photon induced coherence is produced via coupling through a resonant intermediate state. Resonance at both the intermediate state and the excited state is guaranteed by using two independently tunable narrowband lasers at frequencies ω_1 and ω_2 and characterized by electric fields $E_1(\omega_1,\vec{k}_1)$ and $E_2\ (\omega_2,\vec{k}_2)$, respectively. In degenerate frequency two-photon absorption, the signal strength decreases as the principal quantum number of the excited state increases due to intermediate state detuning. This does not occur in FDTS since the intermediate state is always resonant. In fact, as shown below, for arbitrary field strength E_2, the signal strength can be made independent of the strength of the intermediate state to final excited state transition moment.

The analysis of FDTS follows from perturbation theory[15]. The geometry for the interaction is shown in Figure 1. Two counter propagating plane waves at frequencies ω_1 and ω_2 with fields $E_1(\omega_1,\vec{k}_1)$ and $E_2(\omega_2,\vec{k}_2)$ respectively, are incident on a cell containing the three state resonant system (atomic sodium) with the ground state to intermediate state resonance at Ω_1 and the intermediate state to excited state resonance at Ω_2. A third plane wave, $E_2'(\omega_2,\vec{k}_2')$,

intersects the interaction region at a very small angle with respect to E_2. The phase matched nonlinear interaction of interest produces a signal $E_1'(\omega_1,\vec{k}_1')$ counterpropagating to $E_2'(\omega_2,\vec{k}_2')$. While the resonant system is Doppler broadened, it is not hard to anticipate that the spectroscopy signals obtained by holding ω_1 fixed and tuning ω_2 are Doppler-free. The frequency ω_1 is tuned to the middle of the ground state to intermediate state absorption spectrum. Only those atoms satisfying the velocity dependent resonance conditions, $\omega_1-\Omega_1-\vec{k}_1\cdot\vec{v}=0$, will interact with E_1. Assuming fully collinear geometry then, there will be no velocity dependence in the atoms that interact with E_2 or E_2' since the velocity is fixed by the frequency of E_1.

To calculate the nonlinear polarization for FDTS, we recall that the polarization $\vec{P}=Tr\vec{\mu}\rho$ where $\vec{\mu}$ is the dipole moment operator and ρ is the density matrix. ρ is a solution of the velocity dependent quantum mechanical transport equation

$$i\hbar\left(\frac{\partial}{\partial t}+\vec{v}.\nabla\right)\rho=[H_o,\rho]+[V,\rho]-\frac{i\hbar}{2}\{\Gamma,\rho\}_+ +i\hbar\left.\frac{\partial\rho}{\partial t}\right|_{sp.em.}-i\hbar\left.\frac{\partial\rho}{\partial t}\right|_{coll} \qquad (1)$$

where H_o is the Hamiltonian of the unperturbed atom ($\langle i|H_o|j\rangle=E_i\delta_{ij}$) and V is the electromagnetic perturbation energy, $-\mu E$. The vector notation is dropped because we shall assume all fields are copolarized. The decay term is given by the anticommutator of Γ and ρ where Γ is assumed to be diagonal and represents decay from any level $\langle i|\Gamma|i\rangle=\Gamma_i$ due to spontaneous emission or inelastic collisions. $(\partial\rho/\partial t)|_{sp.em.}$ represents a source term due to sponaneous emission into a level. The last term represents dephasing collisions which give rise to a frequency shift ε_{ij} and an increased decay of the optical coherences, γ_{ij}^{ph}:

$\langle i|\frac{\partial\rho}{\partial t}|_{coll}|j\rangle = (-i\,\epsilon_{ij} + \gamma_{ij}^{ph})$ where the convention $\epsilon_{ij}>0$ for $j>i$ corresponds to a blue shift.

The three level system is shown in Figure 2. We assume that in the absence of the optical fields, only the ground state is populated. The nonlinear interaction originates with E_1 establishing an optical coherence, ρ_{12}, between the ground state and the intermediate state, 2, by the dipole interaction, $-\mu_{12}\,E_1$. The electric field, E_2, by the coupling $-\mu_{23}\,E_2$ to ρ_{12} establishes the two-photon optical coherence, ρ_{13}. The electric field E_2^* generates a third order contribution to ρ_{12} by coupling $\mu_{23}E_2^*$ with ρ_{13}. Recalling that in general $E_i=(1/2)\,\mathscr{E}_i \exp\, i(k_i x-\omega_i t) + c.c.$, the above description is in the context of density matrix perturbation theory where the order of the nonlinearity is determined by the order of electric field interaction. This is shown diagramtically in Figure 3 where the relevant fields have been determined by phase matching and conservation of energy. The relevant polarization is then given by $P=\int dv\,Tr\mu\rho=\int dv\,\mu_{12}\rho_{21}+c.c.$

The final result for the polarization is (in the rotating wave approximation) given by

$$P(x,t)= -\mu_{12}\left(\frac{N_o}{k_1U_o}\right)\left(\frac{\mu_{12}\mathscr{E}_1}{2\hbar}\right)\left(\frac{\mu_{23}\mathscr{E}_2}{2\hbar}\right)\left(\frac{\mu_{23}\mathscr{E}'^{*}_2}{2\hbar}\right)e^{-ik_1x-i\omega_1t}$$

$$\times\left[\Gamma_{13}+\gamma_{13}^{ph}+\left(\frac{k_2}{k_1}-1\right)(\Gamma_{12}+\gamma_{12}^{ph})-i\left(\Delta_2+\frac{k_2}{k_1}\Delta_1-\epsilon_{13}-\left(\frac{k_2}{k_1}-1\right)\epsilon_{12}\right)\right]^{-1}$$

$$\times\left\{\frac{2i}{k_1u_o}\left[1-\frac{\Delta_1-\epsilon_{12}+i(\Gamma_{12}+\gamma_{12}^{ph})}{k_1u_o}\sum\left(-\frac{\Delta_1-\epsilon_{12}+i(\Gamma_{12}+\gamma_{12}^{ph})}{k_1u_o}\right)\right]\right.$$

$$\left.+\left(\frac{k_2}{k_1}-1\right)\left[\Gamma_{13}+\gamma_{13}^{ph}+\left(\frac{k_2}{k_1}-1\right)\left(\Gamma_{12}+\gamma_{12}^{ph}\right)\right.\right.$$

$$-i\left(\Delta_2 + \frac{k_2}{k_1}\Delta_1 - \epsilon_{13} - \left(\frac{k_2}{k_1} - 1\right)\epsilon_{12}\right)\Bigg]^{-1} \cdot$$

$$\times \left[Z\left[\frac{\Delta_1+\Delta_2-\epsilon_{13}+i(\Gamma_{13}+\gamma_{13}^{ph})}{\left(\frac{k_2}{k_1}-1\right)k_1u_o}\right] - Z\left[\frac{\Delta_1-\epsilon_{12}+i(\Gamma_{12}+\gamma_{12}^{ph})}{k_1u_o}\right]\right]\Bigg\} \quad (2)$$

where

$Z(\xi) = \pi^{-1/2}\int_{\infty}^{\infty} dx\ e^{-x^2}(x-\xi)^{-1}$ is the plasma dispersion function, u_o is the thermal velocity, $\omega_i = ck_i$, and N_o is the ground state population density. The remaining symbols have the following definitions: $\Gamma_{13} = (\gamma_{23}^{sp} + \gamma_3)/2$, $\Gamma_{12} = (\gamma_{12}^{sp} + \gamma_2)/2$, $\Delta_i = \omega_i - \Omega_i$, γ_{ij}^{ph} is the line width contribution due to phase interrupting collisions between states i and j, and ϵ_{ij} is energy level shift due to collisions of level j with respect to level i. The resonance condition is given by

$$\Delta_2 + \frac{k_2}{k_1}\Delta_1 - \epsilon_{13} - \left(\frac{k_2}{k_2} - 1\right)\epsilon_{12} = 0 \quad (3)$$

and the linewidth is determined by

$$\gamma \equiv \gamma_{13} + \gamma_{13}^{ph} + \left(\frac{k_2}{k} - 1\right)(\Gamma_{12} + \gamma_{12}^{ph}) \quad (4)$$

In frequency units (Hertz), the FWHM is γ/π.

There are several interesting properties of this polarization which impact spectroscopy. First is that the interaction provides a nearly Doppler free linewidth. Since typically $(k_2/k_1)-1<1$, the contribution from the intermediate state is small leading to nearly state specific spectroscopy signatures. A second important property is that the signal strength is determined only by μ_{12} if the intermediate state to final state interaction $(\mu_{23}\mathscr{E}_2)$ $(\mu_{23}\mathscr{E}_2^{*})$ is held constant; i.e. as μ_{23}

decreases, $\mathscr{E}_2$ and $\mathscr{E}_2'$ increase. This leads to the interesting possibility of studying "forbidden transitions", typically weak and difficult to observe. Finally, because of the resonance condition, the tuning of ω_1 is not critical as long as $(\Delta_1-\epsilon_{12})/k_1u_o$ is small; i.e. ω_1 is tuned within the Doppler width. It should be noted, however, that the observed frequency dependent character of a complex spectroscopic structure generated as a function Δ_2 (for fixed Δ_1), can be very complicated if level 1 or level 2 is composed of nondegenerate states. In particular if the upper state has complex structre (e.g. fine structure or hyperfine structure), the splitting as measured by varying Δ_2 relates directly to the actual splitting of the level. However, in the absence of collisions ($\epsilon_{ij}=0$) a splitting δ in the intermediate state is observed as a splitting $\{(k_2/k_1)-1\}\delta$ splitting as a function Δ_2 and a splitting δ in the ground state is measured as $(k_2/k_1)\delta$. Hence, the significance of observed spectral structures must be carefully interpreted. It is interesting to consider the unusual dependence of the resonance condition and linewidth on k-vectors. Physically this dependence arises because in the rest frame of an atom moving in a Doppler broadened medium, the velocity dependent frequency shift is given by kv. For the k_1 beam, the frequency shift for a given velocity is different than the frequency shift observed by the atom for the k_2 beam.

In the above solution, a fully collinear geometry was assumed to make the velocity integrals simple. However, in the experiments, a small angle (θ~1°) exists between $\vec{k}_2$ and $\vec{k}_2'$. This leads to a propagating term exp $i[(\vec{k}_1 + \vec{k}_2' - \vec{k}_2)\cdot x-\omega t]$ rather than the simple term shown in Eq. 2. This term leads to a phase mismatch between the wave

vector, $\vec{k}_1$ of the signal generated by the nonlinear polarization and the net wave vector of the nonlinear polarization. The signal propagates in a direction to minimize this mismatch. The mismatch manifests itself in the solution for the intensity of the signal (in the slowly varying envelope approximation) as

$(\sin^2 \frac{|\Delta\vec{K}|L}{2})/(\frac{|\Delta\vec{K}|}{2})^2$ where L is the interaction length and $\Delta\vec{K}=\vec{k}_1+\vec{k}_2-\vec{k}_2'-\vec{k}_1'$. For small angles between $\vec{k}_2$ and $\vec{k}_2'$, this leads to a signal wave vector, $\vec{k}_1'$, almost counterpropagating to $\vec{k}_2'$. This has a tremendous impact on improving the signal-to-noise ratio since the signal at ω_1 is propagating in a direction different from the main pump beam which is also at frequency ω_1. Hence, one is looking for a signal on a nearly black background (limited only by incoherent scattering) in contrast to saturation spectroscopy where one is looking for a small signal on top of a large dc background due to the backward propagating probing beam. In principal, this mismatch also results in a reduction in signal. In practice, however, the magnitude of the mismatch is small except for $k_2/k_1 >> 1$ such as occurs at the ionization limit. Even there, the mismatch can be reduced to near zero at the expense of a slight increase in linewidth if the angle between $\vec{k}_2$ and $\vec{k}_1$ is adjusted to be slightly less than 180°.

3. Experimental Results

As indicated in Section I, one of the principal motivations for developing FDTS has been to enable collision studies of nS and nD Rydberg states with ground state perturbers. Such studies in the frequency domain will lead to information about the polarizability and effective electron scattering cross section for the perturber. This follows from extraction of the dephasing collision cross section, σ_{Br}^{13}, from the linewidth, γ, as is described below. Because stabilized narrowband dye lasers are used in FDTS, frequency domain measurement of fine structure in the Rydberg levels is also possible. This approach is in contrast to the earlier work using quantum beat spectroscopy to measure fine structure.

FDTS of atomic sodium is complicated by the fact that sodium has a nuclear spin of I=3/2 leading to significant hyperfine splitting of the $3s^2S_{1/2}$, $3p^2P_{1/2}$, and $3p^2P_{3/2}$ states. A simplified energy level diagram is shown in Figure 4. The splitting is easily resolved by cw narrowband dye lasers. Optical dipole selection rules for the total angular momentum, $\vec{F}=\vec{I}+\vec{J}$, are given by $\Delta F=0,\pm1$. Hence, for the D_2 line, there are a total of 6 dipole allowed transitions between various hyperfine split states. However, for the D_2 line, cw monochromatic radiation illuminating certain transitions causes a significant redistribution of the ground state population. This is due to hyperfine optical pumping and in some cases results in transferring almost all the population from the F=1 (F=2) ground state to the F=2 (F=1) ground state. The only 3s-3p transitions which are not optically pumped are the $3s^2S_{1/2}$ (F=2)-$3p^2P_{3/2}$ (F=3) transition and the $3s^2S_{1/2}$ (F=1)-$3p^2P_{3/2}$ (F=0) transition. Therefore, since the signal intensity

is proportional to the particular groundstate density, transitions to the excited state, nd or ns, are dominated by groundstate to intermediate state transitions involving these two unpumped transitions. This is convenient since it reduces secondary spectral structure associated with a given excited state due to the presence of various intermediate states. In general, each excited state appears twice in a scan of ω_2 separated by $(k_2/k_1)\Delta_{HFS}$ where Δ_{HFS} is the 1772 MHz associated with the ground state hyperfine splitting. This is unavoidable but poses no problem because of such a large ground state splitting. In the data discussed below, the total frequency scans are much less than this splitting and therefore this structure is not displayed.

The simple picture described above becomes much more complicated in the presence of collisions. The polarization shown in Eq. 2 shows that due to collision broadening, the signal decreases with increasing linewidth. Similarly, in the time domain, the optical coherence, decaying as exp-γt, results in a decrease in signal with increasing γ. This was the basis of the experimental technique used by Flusberg[16]. Since γ is a linear function of the pressure (cf Section 4), measuring the signal as a function of pressure yielded the pressure broadening coefficient in their paper (after some small corrections). Unfortunately, this direct measurement does not work in the cw case. As discussed in detail elsewhere, buffer gas collisions induce velocity changes in the sodium atoms[20] and also cause state changes[21]. The net result is that transitions which are normally weak and hard to observe due to optical pumping effects discussed above can become strong due to velocity changing collisions (vcc) which reduce the effects of ordinary

optical pumping. Similarly transitions which are strong because they are not optically pumped become less strong due to collision induced optical pumping arising from state changing collisions (scc). Scc transfer population from the excited state to another state whose dipole selection rules may allow decay to the other ground state. While cross sections for both kinds of collisions are small, their effects can be quite large (easily observed at 10's of mTorr) since spatial diffusion limits the effective ground state relaxation time. The dependence of the signal amplitude on buffer gas pressure is therefore very nonlinear. The implication for FDTS is that using the signal amplitude as a function of pressure to measure relaxation is not adequate. Rather, the width itself must be measured as the pressure is varied and interpreted using Eq. 2. The reader is referred to the above references for a complete discussion of vcc and scc in four-wave mixing.

The experimental configuration used for these spectroscopy studies is shown in Figure 5. The primary tools for the experiments were two Coherent Radiation CR-699-21 stabilized ring dye lasers pumped by two CR18 argon ion lasers. One dye laser was operated with R6G dye at λ=5890Å and pumped at 5145Å. The second dye laser operated with R6G for studies of the 4d state, but used UV argon ion pumping of stilbene 3 (Exciton 420) dye for studies of n=8-15. Studies beyond n=15 require Stilbene 1 which is unreliable with a very short lifetime. Studies of n=6 and 7 require a courmarin dye with a Krypton ion pump to achieve sufficient output power and were not feasible for lack of a Krypton laser. The linewidth of each laser (stabilized to its own reference cavity) was 200 KHz RMS with a relative peak-to-peak

linewidth of 2 MHz. This was measured by beating one laser against the other and observing the spectrum on an RF analyser.

An acousto-optic modulator driven at 40 MHz was amplitude modulated at 20 kHz and used to modulate beam k_2 and k_2'. This produced a 20 kHz modulation on the signal which enabled the use of phase sensitive detection. This was convenient since the modulation of ω_2 produced a modulation in signal at ω_1 but did not modulate scattered light at ω_1 due to window imperfections or sodium fluorescence.

Both beams k_2 and k_2' were lightly focused by two 1 meter lenses into the 1cm long quartz sodium cell. The cell temperature was 571°K but the sodium temperature in the side arm was adjusted to give 60% absorption of the unfocused 200 μW k_1 beam at 5890 Å. The power of the k_2 and k_2' beams was adjusted to give maximum signal without power broadening the spectrum. Typically this power was the order of 6 mW. The signal (at 5890 Å), in the absence of buffer gas, was easily visible on a white card. Due to collision induced optical pumping, however, the signal dropped several orders of magnitude in the presence of 1 Torr of buffer gas. Hence, phase sensitive detection was used to establish a good signal-to-noise ratio in spite of the collision induced signal reduction.

The signal, following phase sensitive detection, was digitized and averaged on a Tracor Northern 1710 signal averager and stored on disk or analyzed using a nonlinear least squares code on a VAX computer.

Figure 6 shows an example of typical data obtained on the $3s^2S_{1/2}$ $(F=2)$-$3p^2P_{3/2}(F=3)$-$8d^2D_J$ transition. Both the J=5/2 and J=3/2 components are easily resolved and can be contrasted to the earlier frequency domain measurements using a pulsed dye laser[22]. The total

angular momentum F is specified for the ground state and intermediate state because the different components are easily resolved. However, Δ_{HFS} is unresolved for the high lying states. The two primary resonances each show a secondary resonance to the low frequency side. This is the resonance due to transitions involving the $3p^2P_{3/2}$ (F=2) intermediate state. The spacing between the primary and secondary resonance is $\{(k_2/k_1)-1\}\delta$ where δ is the hyperfine splitting between the F=2 and F=3 intermediate state (59.6 MHz). The linewidth exceeds the natural linewidth and the profile deviates from a Lorentzian because the finite angle between $\vec{k}_1$, $\vec{k}_2$ and $\vec{k}_2'$ leads to a residual Doppler width.

Using FDTS and its ability to clearly resolve the excited state fine structure splitting, we have been able to measure Δ_{FS} for various nd states confirming the fine structure inversion for the observed states. The results are shown in Table 1 and compared to earlier measurements. As indicated in Figure 6, the low frequency structure results from coupling to the $^2D_{5/2}$ level and the higher frequency component results from coupling to the $^2D_{3/2}$ level. Verification of this inversion arises from consideration of the observed signal intensities. This is determined by the relative sizes of the transition line strengths between states i and j: $S(i,j) \alpha \mu_{ij}^2$ where S(i,j) is line strength. We are interested in the ratio $\mathcal{I}=S(^2D_{5/2}, ^2P_{3/2}[F=3])/S(^2D_{3/2}, ^2P_{3/2}[F=3])$ where the ratio has been summed over all F values of the ^2D_J state. The F states are summed since the hyperfine splitting is unresolved. To evaluate the ratio, note that the line strength between specific F states is given by[30]

$$S(\gamma SLIJF;\gamma' SL'IJ'F') \qquad (5)$$

$$= (2I+1)Q(IJF;IJ'F')Q(SLJ;SL'J')S(\gamma SL;\gamma' SL')$$

where $S(\gamma SL;\gamma' SL')$ is the line strength for transitions between $|\gamma SL\rangle$ and $|\gamma' SL'\rangle$ and Q is the relative intensity:

$$Q(J_1, J_2, J; J_1, J_2; J') = \frac{(2J_2-1)(2J_2'+1)}{2J_1+1} \begin{Bmatrix} J_2 & J & J_1 \\ J & J_2' & 1 \end{Bmatrix}^2 \qquad (6)$$

The number {} is the Wigner 6j symbol. Summing over F, the line strength is given by

$$S(\gamma SLIJ;\gamma SL'IJ'F') = \frac{(2F'+1)(2J+1)}{2S+1} \begin{Bmatrix} L & J & S \\ J' & L' & 1 \end{Bmatrix}^2 S(\gamma SL;\gamma' SL') \qquad (7)$$

The calculated ratio of intensities of the nonlinear response (varying as $\mathscr{E}^2$) is 81. This estimate ignores polarization effects since magnetic substate optical pumping redistributes the magnetic substate population and the rate equations have not been solved to evaluate this effect. In measurements shown in Figure 6, the ratio (29) is less than expected because of polarization effects and because saturation was occuring on the $^2D_{5/2}$ transition at ω_2 intensities strong enough to observe the $^2D_{3/2}$ component simultaneously with the $^2D_{5/2}$ component. However, this clearly demonstrates the fine structure inversion. To put the above results in perspective, we note that for ordinary hydrogen, the fine structure splitting results in a higher frequency component which arises from the transition to the larger j-value. In the alkali metals, even for large n-values, the components are inverted. This difference arises from relativistic corrections and is described by E. Luc-Koenig[29]. Her calculated values are included in Table 1.

The primary source of systematic error in these measurements is uncertainty in the dispersion. Calibration was achieved with a 1 GHz free spectral range Fabry-Perot interferometer. Considerable improvement in accuracy could be achieved by lengthening the Fabry-Perot cavity. This was not possible with the present equipment. It should be pointed out that location of the resonances must be checked as a function of beam intensities since any A.C. Stark splitting can lead to an apparent shift in the resonance position.

The collision studies were performed to measure both the collision induced shift and broadening of the resonance. While transitions to the $nd^2D_{5/2}$ were studied to evaluate collision induced broadening using helium, argon, and neon buffer gases, most of the work concentrated on measuring the collision induced broadening and shift of transitions to the ns states due to helium buffer gas. Helium was chosen for these first detailed measurements because it has the weakest collision induced optical pumping effect[21]. As indicated above in the limit of third order perturbation theory, collision induced optical pumping does not effect either γ_{ij}^{ph} or ϵ_{ij}, but it does decrease the signal-to-noise of the nonlinear interaction due to a reduction of the resonant ground state population.

An example of the pressure broadening observed on the transition to the $11d^2D_{5/2}$ state due to neon buffer gas is shown in Figure 7. The recorded signal is the result of signal averaging several frequency scans. The effect of the collision induced frequency shift is most easily seen in Figure 8 where the frequency shift shown is observed on the transition to the $9s^2S_{1/2}$ state with 1.8 Torr Helium. The frequency shifts are measured using a single scan on the Tracor signal

averager and a long time constant on the lockin to avoid any laser reset jitter. The laser scans slowly over the resonance at zero Torr. Buffer gas is added before the laser frequency changes significantly and the gain of lock-in amplifier is adjusted to give an easily detected signal on the pressure shifted resonance.

To extract the frequency shift rate and the broadening due to collisions we recall from Section II that the measured frequency shift follows from the resonance condition given by Eq. 3 and the linewidth is given by Eq. 4. In the binary approximation for collisions, the terms γ_{13}^{ph}, γ_{12}^{ph}, ϵ_{13}, and ϵ_{12} are linearly proportional to buffer gas pressure. Therefore, the pressure broadening rate, γ_o, is defined by $\gamma_o^{ph}p+\Gamma_o=\gamma$ where Γ_o is the pressure independent linewidth and the frequency shift rate is defined by $\epsilon_o p = \epsilon_{13}+\{(k_2/k_1)-1\}\epsilon_{12}$. The rates are obtained by measuring the width and shift as a function of buffer gas pressure and finding the slope by a least squares fit. Each data point of such a measured dependence is the result of performing a nonlinear least squares fit of a Lorentzian lineshape to the recorded data (see Fig. 7) and determining the full width at half maximum and the line center. Examples of the measured pressure dependence of both the line broadening and resonance shift are shown in Figure 9a and 9b, respectively. The error bars represent the statistical error based on the nonlinear least squares fit and do not include systematic errors. The straight line is the best fit through the points. Table 2 shows the pressure broadening rate (FWHM) γ_o/π (Hz/Torr) for argon, neon, and helium for the dephasing rate between the $3s^2S_{1/2}(F=2)$ state and the $nd^2D_{5/2}$ state. Table 3 shows the pressure broadening rate and the rate of frequency shift, $\epsilon_o/2\pi$,

(Hz/Torr) for transitions between the $3s^2S_{1/2}(F=2)$ state and the $ns^2S_{1/2}$. The error shown in parentheses in Table 3 is the standard deviation of the linear fit parameter for the slope of the line. For broadening, the linear form for fitting was y=mx+b but for the shift, the fit was made to y=mx.

To extract cross sections from the above data, we note that in general, $\gamma^{ph}=N\sigma_{Br}\bar{v}$ where σ_{Br} is the cross section for collision induced broadening, N is the perturber density and $\bar{v}$ is the relative velocity. At T=571°K, $N=1.69\times10^{16}cm^{-3}Torr^{-1}$. The relative velocity is given as $\bar{v}=(8k_BT/\pi\mu)^{1/2}$ where μ is the reduced mass. From section II, however, we see that the measured collision broadening rate is given by $\gamma_{13}^{ph} - (\frac{k_2}{k_1} - 1)\ \gamma_{12}^{ph} = \gamma_o^{ph}\ p$

where $\gamma_{13}^{ph} = N\sigma_{Br}^{13}\bar{v}$ and $\gamma_{12}^{ph} = N\sigma_{Br}^{12}\bar{v}$ and σ_{Br}^{ij} is the collisional broadening cross section for the ij superposition state. We are interested in σ_{Br}^{13} and hence must make the correction for the small contribution from σ_{Br}^{12}. Lewis[31] summarizes the values for σ_{Br}^{12} but the value $\sigma_{Br}^{12}\simeq127\text{Å}^2$ from McCartan and Farr[32] seems most appropriate. In principal a similar correction must be made to the line shift data. As described by Lewis, there is little agreement as to the value of the $3p^2P_{3/2}$ level shift. Fortunately the range of measurement shows that the cross section for the $3p^2P_{3/2}$ energy level shift is sufficiently small that the correction for the $ns^2S_{1/2}$ energy level shift is at the 0.1% level. Hence, no correction is necessary in the shift data to obtain the shift parameter. Table 3 shows the inferred cross section data for broadening of the $3s^2S_{1/2}$-$ns^2S_{1/2}$ superposition state.

Systematic errors in the measurement of γ_o/π and $\epsilon_o/2\pi$ can arise from uncertainties in frequency dispersion, pressure measurement, and temperature measurement. Frequency dispersion was determined using a 1 GHz FSR Fabry-Perot. The error is believed to be of the order of a few percent. The same frequency calibration was used to obtain the good agreement between our fine structure splitting and previous measurements discussed above. Pressure measurements were made using an MKS Baratron gauge and have an accuracy of better than 1%. Temperature measurements are accurate to within 1%.

A potentially more serious source of systematic error is higher order contributions to the nonlinear polarization. An example is that the fifth order term arising from a perturbation chain of the form $\rho_{11}\rightarrow\rho_{12}\rightarrow\rho_{22}\rightarrow\rho_{23}\rightarrow\rho_{22}\rightarrow\rho_{12}$ that leads to a resonant denominator with a pressure dependent linewidth determined by γ_{23}^{ph}; i.e., dephasing collisions of the superposition state between states 2 and 3. In the case of sodium this means the 3p-nd or 3p-ns superposition state. As indicated above, due to the physics of the collision process, this would not be expected to significantly alter the interpretation of the collision induced frequency shift measurements. However, it could cause some problem in interpreting the collisional broadening measurements. To avoid these difficulties, the power of the pump beam at 589 nm resonant on the 3s-3p transition was kept as low as possible, typically 200 μW corresponding to 1 mW/cm^2. This corresponds to an $I/I_{SAT}\simeq 0.1$ and in the absence of additional physics, ensures the

validity of assuming that only the third order polarization contributes to the signal.

Unfortunately, optical pumping can increase the significance of higher order terms by reducing the effective I_{SAT}. The intermediate coupling is through the $3p^2P_{3/2}(F=3)$ state from the $3s^2S_{1/2}(F=2)$ ground state and hence does not lead to an optical pumping induced depletion of the $3s^2S_{1/2}(F=2)$ groundstate. However, as we discussed elsewhere, state changing collisions of buffer gas atoms with the $3p^2P_{3/2}(F=3)$ state can lead to collision induced hyperfine structure optical pumping. Also, coupling from the $3p^2P_{3/2}(F=3)$ to ns or nd can lead to a variety of decay paths that lead to hyperfine structure optical pumping of the ground state. Both of these effects lead to a reduced I_{SAT} which increases the significants of higher order nonlinear polarizations. In a Doppler broadened medium hyperfine optical pumping leads to an increase in the "depth" of velocity hole burning. Hence to correctly calculate the significance of optical pumping, one must include velocity changing collisions which significantly lessen the effect of optical pumping. Such a global calculation is beyond the scope of this paper, but the physical picture described above indicates that further work may be necessary to evaluate the contribution of the dephasing of the 3p-nl superposition state to the measured linewidth. At this point however, we have not observed any measurable dependence of σ_{Br}^{13} on pump intensity.

4. Discussion of results

The objective of this work has been to demonstrate a new kind of frequency domain spectroscopy, to present frequency domain measurements of the collision induced broadening and shift as a function of principal quantum number in sodium, and to evaluate the success of the analytical description of the collision physics. Since a number of previous experimental studies of Rydberg collision physics have been described, it is useful, where possible, to compare our measurements with others in the literature.

Aside from the 3s-3p superposition state, the most extensively studied superposition state in sodium involves the 4d state. Table 4 summarizes the measurements of σ_{Br} for dephasing of the 4d state by helium, neon, and argon buffer gases. It is important to remember that because the cell temperature varies from one experiment to another, one must compare σ_{Br}, not γ_o. Recall $\gamma_o = N\sigma_{Br}\bar{v}/\pi$ (Hertz/Torr) where $\bar{v}$ is the temperature dependent average velocity and N is the temperature dependent number density at a pressure of 1 Torr. Our measurements are in reasonable agreement with the previous work demonstrating the reliability of FDTS. It is interesting to note, however, that there is a significant spread of cross section values in the literature. Moreover, it is unexpected that the measurement of the collisional dephasing of the 3p-4d superposition state, based on conventional linear spectroscopy, shows a σ_{Br} well within the spread of 3s-4d measurements. Intuitively, one might expect this cross section to be less than the dephasing cross section for the 3s-4d state since the larger overlap of the 3p and 4d

wavefunction compared to the overlap of the 3s and 4d wavefunctions should lead to smaller dephasing during a collision.

Comparison between FDTS and trilevel echo measurements of σ_{Br} for the 3s-nd superposition state shows the FTDS date to be 20%-40% lower than that of Flusberg[16] for helium and neon, but 20% higher for argon. For the 3s-ns superposition state, FDTS measurements of σ_{Br} are consistently 30% lower than those of Flusberg.

Figure 10 shows the measured value of the shift rate for the ns state as a function of principal quantum number as measured by FDTS. Figure 10 also shows the shift rate for the np state measured by Fuchtbauer[2] and the nd state measured by Krebs and Schearer[18]. The shift rate was inferred from their data for T=571°K. No correction for the quantum defect was made in this comparative plot of the data. The slight peak at n=9 was anticipated though not clearly demonstrated in the np shift measurements of Fuchtbauer. In comparing ϵ_o for intermediate values of n (<11), the measured shift of the nd states is less than the measured shift for np and ns showing the importance of angular momentum effects for intermediate values of n.

Physically, one expects the collision cross section to increase with increasing quantum number according to $\pi a_o^2 n^4$. Figure 10 shows such behavior between n=4 and n=8 for the ns state. However, as n increases, the coupling between the ionic core and the electron decreases, and the electron and core scatter the incoming perturber separately. Using this physical

picture, the analytical treatment of the asymptotic limit of the shift was first presented by Fermi[1] with more detailed calculations presented later by Alekseev and Sobelman[8]. Calculations by Ivanov[9] provided a series expansion in principal quantum number good for n>>1. There are two contributions to the shift. The largest contribution is due to the scattering of the electron by long range interaction of the incoming perturber. This part of the shift was calculated by Fermi to be $\epsilon = \pm(\hbar/m)(\pi\sigma_o)^{1/2}N$ where σ_o is the cross section for scattering of the electron by the perturber in the limit of very low velocities and N is perturber density (ϵ is in rad./sec). The electron scattering cross section is $4\pi^2L^2$ where L is the electron scattering length. In atomic units, L=1.1 for helium based on data of Fuchtbauer[9]. The shift is negative (red) if the perturber, such as argon, exhibits the Ramsauer-Townsend effect[34]. For helium, there is no Ramsauer-Townsend effect and the shift is positive. The second contribution is due to the polarization of the incoming perturber by the alkali atom. The polarization contribution is much smaller than the electron scattering contribution and is given, in the asympotic limit, by $-6.3\text{x}10^{-11}(\alpha^2 v)^{1/3}N$ where α is the polarizability of the perturber in atomic units and v is the perturber velocity in cm/sec. For helium, the reported value for α (in atomic units) is 1.31[9]. The series expansion including the polarization correction is given by[9]

$$\epsilon(n) = 3.8\text{x}10^{-8}L\left(1 + \frac{4}{3}\frac{\alpha}{n^2}\ln\frac{2.72}{n} + \frac{\gamma}{Ln^2}\right)N - 6.3\text{x}10^{-11}(\alpha^2\bar{v})^{1/3}N \quad (8)$$

where ϵ is in rad./sec, L and α are in atomic units, N is in cm^{-3}, and $\bar{v}$ is in cm/sec.. Figure 10 shows the calculated behavior assuming 1.69×10^{16} perturber density (atoms per cm^3 at 571°K at 1 Torr). Qualitative agreement is obtained using γ=10 (taken from Ivanov's fitting of Fuschtbauer) and the above values for L and α. Good quantitative agreement could easily be had by adjusting these parameters. For the above equation, the principal quantum number is the effective quantum number given by $n-\delta_l$ where δ_l is the quantum defect. For the above comparison, we have used the s-state value, δ_s=1.384, for the quantum defect[35].

The analytical treatment of the broadening cross section as a function of n has been presented by Omont[10]. The broadening is due to short range interactions. As above, the cross section is expected to increase as n^4. However, for n large, the dephasing resulting from the scattering of the electron becomes negligible, and the only remaining contribution is due to the polarization of the perturber by the alkali atom. This is different than for the shift described above and is the result of the short range type interaction characterizing dephasing. For the large n, the total cross section is given by the sum of the electron scattering term and the polarization term. In the limit appropriate for our work, Omont gives the total cross section as[10]

$$\sigma = 2\pi a_o^2 b_2 (2n^2 - b_1^2) + \pi a_o^2 b_1^2 \qquad (9)$$

where $b_1 = 6 \times 10^2 (\alpha/\bar{v})^{1/3}$

and $b_2 = 6.7 \times 10^{15} (L/n^3\bar{v})^2$.

The values for L and α are in atomic units and $\bar{v}$ is in cm/sec. Figure 11 shows a plot of the measured cross sections for dephasing of the 3s-ns superposition state and the theory of Omont. For this comparison, the parameters L and α were adjusted for a reasonable fit. For the curve shown, L=0.865 and α=0.75 (in atomic units). The value of L basicly determines the curve position for intermediate n, and the value for α determines the asymptotic limit. Note, that as n goes to infinity, $\sigma=\pi a_o^2 b_1^2$. It is interesting to note that the values of L a nd α used to fit the line broadening data do <u>not</u> give good agreement with the line shift data. It is certainly possible to determine a value of L to fit the line shift data for large n and a value for α to fit the line broadening data for large n. However, for intermediate values of n, the agreement is not good. The dashed lined in Fig. 11 shows the Omont theory for line broadening with the values for L and α used to fit Ivanov's theory to the shift data.

In summary, these experiments present measurements of line shift and line broadening of the 3s-ns superposition states using FDTS. Good qualitative agreement has been found between existing analytical treatments of both the broadening and the shift. However, the use of FDTS suggests that it should now be possible to work in a pressure range well within the limits of the impact approximation and obtain a precision not previously available. Improving the calibration of the system should enable reduction of the systematic error from 10% to less than 1%. Eliminating sources of systematic error will also necessitate a careful analysis of the differences between the FDTS technique and the trilevel echo. However, from the current work, and the work of Krebbs and Schearer[18], it is already clear that the

angular momentum of the orbiting electron must be included in calculating the shift. Furthermore, while it is possible to chose parameter α and L to fit the theory of Omont to the measured σ_{Br}, a different set of values must be used to fit the theory of Ivanov to the measured ϵ_o.

The authors would like to thank Dr. Juan Lam for helpful discussions on the theory of collisions and Dr. Steve Turley for help on the statistical error analysis. We would also like to thank John Shuler for his expert technical assistance.

This work was supported by Army Research Office Contract No. DAAG29-81-C-0008.

REFERENCES

1. Enrico Fermi, Nuovo Cimento, 11, 157 (1934).

2. Chr. Fuchtbauer, P. Schulz, and A.F. Brand, Z. Phys. 90, 403 (1935).

3. C. Fuchtbauer and F. Gossler, Z. Phys. 93, 648 (1935).

4. Chr. Fuchtbauer and P. Schulz, Z. Phys. 97, 699 (1935).

5. C. Fuchtbauer and W. von Hessen, Z. Phys. 113, 323 (1939).

6. M.A. Mazing and N.A. Vrublevskaya, JETP, 50,343 (1966).

7. V.A. Alekseev, M.A. Mazing, P.D. Serapinas, I.I. Sobel'man, and L.A. Vainshtein, Proceeding of the Vth ICPEAC, Leningrad, 1967, p.528.

8. V.A. Alekseev and I.I. Sobel'man, Zh. Eksp. Teor. Fis. 49, 1274 (1965) [Sov. Phys. JETP 22, 882 (1966)].

9. G.K. Ivanov, Opt. Spek. 40, 965 (1976) [Opt. Spectrosc., 40, 554, (1976)].

10. A. Omont, J. Phys. (Paris) 38, 1343 (1975).

11. F. Biraben, B. Cagnac, and G. Grynberg, J. Phys. Lett. (Paris) 36, L41 (1975).

12. F. Biraben, B. Cagnac. E. Giacobino and G. Grynberg, J. Phys. B: Atom. Molec. Phys., 10, 2369 (1977).

13. D.M. Bruce, M.Y. Mirza, and W.W. Duley, Optics Communications, 27, 76 (1978).

14. P.F. Liao, N.P. Economou, and R.R. Freeman, Phys. Rev. Lett., 39, 1473 (1977).

15. D.G. Steel. J.F. Lam, and R.A. McFarlane, Phys. Rev. A26, 1146 (1982).

16. A. Flusberg, R. Kachru, T. Mossberg, and S.R. Hartman, Phys. Rev. A19, 1607 (1979).

17. T.F. Gallagher, S.A. Edelstein, and R.M. Hill, Phys. Rev. Lett., 35, 644 (1975); Phys. Rev. A15, (1977).

18. D.J. Krebs and L.D. Schearer, Phys. Rev. A26, 1473 (1982).

19. Wan-U.L. Brillet and A. Gallagher, Phys. Rev. A22, 1012 (1980).

20. D.G. Steel and R.A. McFarlane, Phys. Rev. A27, 1217 (1983).

21. D.G. Steel and R.A. McFarlane, Phys. Rev. A27, 1687 (1983).

22. Michael M. Salour, Optics Communications, 18, 377 (1976).

23. K.W. Meisner and K.F. Luft, Ann. Phys. 29, 698 (1937).

24. D. Pritchard, J. Apt, and T.W. Ducas, Phys. Rev. Lett., 32, 641 (1974).

25. T.W. Hansch, K.C. Harvey, G. Melsel, and A.L. Shawlow, Opt. Comm. 11, 50 (1974).

26. J.N. Echstein, A.I. Ferguson, and T.W. Hansch, Phys. Rev. Lett., 40, 847 (1978).

27. S. Haroche, M.Gross, and M.P. Silverman, Phys. Rev. Lett. 33, 1063, (1974).

28. C.Fabre, M. Gross and S. Haroche, Optics Communications, 13, 393, (1975).

29. E. Luc-Koenig, Phys. Rev. A13, 2114 (1976).

30. I.I. Sobel'man, Introduction to the Theory of Atomic Spectra, Pergamon Press, 1972.

31. E.L. Lewis, Phys. Rep., 58, 1 (1980).

32. D.G. McCartan and J.M. Farr, J. Phys. B.:Atom. Molec. Phys. 9, 985 (1976).

33. J.F. Kielkopf and R.B. Knollenberg, Phys. Rev. A12, 559 (1975).

34. H.S.W. Massey and E.H.S. Burhop, Electronic and Ionic Impact Phenomena, Vol. 1, Oxford at the clarendon Press, 1969.

35. Claue. Fabre, "ETUDE THEORIQUE ET EXPERIMENTALE DE L'INTERACTION D'UN ATOME TRES EXCITE AVEC LE RAYONNEMENT. APPLICATION A LA SPECTROSCOPIE DES ETATS DE RYDBERG DU SODIUM". These de Doctorat D'Etat, l'Universite' Pierre et Marie Curie, Paris, 1980.

TABLE 1. Fine structure splitting of the sodium nd state.

	$\nu(J=5/2) - \nu(J=3/2)$		
n	FDTS Exp. (MHz)	Exp. (MHz)	Theory[g] (MHz)
4	-1033(10)	-1038(50)[a] -1025(6)[b] -1035(10)[c] -1028.4(0.4)[d]	-915
8	-178.5(4)	-173(10)[e]	-157
9	-127.8(2.6)	-124.5(1.5)[f]	-113
10	-91.3(2)	-91.5(1)[f]	-85
11	-68.4(1.5)	-70.0(0.7)[f]	-63
12	-47.6(1)	-54.0(0.5)[f]	-49

a) Ref. 23
b) Ref. 24
c) Ref. 25
d) Ref. 26
e) Ref. 22
f) Ref. 27, 28
g) Ref. 29

TABLE 2. Buffer gas broadening rate measured by FDTS for the stated superposition state.

	BUFFER GAS BROADENING RATE, γ_o/π (MHz/Torr)		
Superposition State	Helium	Neon	Argon
$3s^2S_{1/2}(F=2)-4d^2D_{5/2}$	31.5	16.5	40.7
$3s^2S_{1/2}(f=2)-8d^2D_{5/2}$	71.9	23.1	224
$3s^2S_{1/2}(F=2)-9d^2D_{5/2}$	64.1	24.2	282
$3s^2S_{1/2}(F=2)-10d^2D_{5/2}$	76.9	24.1	266
$3s^2S_{1/2}(F=2)-11d^2D_{5/2}$	76.3	24.2	263

TABLE 3. Buffer gas broadening rate and shift parameter measured by FDTS on the stated superposition state. The buffer gas is helium. The cross section for broadening is also given. See text for explanation of cross section derivation.

Superposition State	ν_o/π (MHz/Torr)	$\sigma_{Br}(A^2)$	$\epsilon_o/2\pi$ (MHz/Torr)
$3s^2S_{1/2}(F=2)$-$8s^2S_{1/2}$	35(0.7)	309(6)	104(0.8)
$3s^2S_{1/2}(F=2)$-$9s^2S_{1/2}$	25.7(0.9)	212(7)	110(2.8)
$3s^2S_{1/2}(F=2)$-$10s^2S_{1/2}$	19.9(0.4)	151(3)	112(1.3)
$3s^2S_{1/2}(F=2)$-$11s^2S_{1/2}$	18.0(0.6)	130(4)	106(1.6)
$3s^2S_{1/2}(F=2)$-$12s^2S_{1/2}$	16.7(1.4)	116(10)	103(2.2)
$3s^2S_{1/2}(F=2)$-$13s^2S_{1/2}$	---------	-------	104(2.1)
$3s^2S_{1/2}(F=2)$-$14s^2S_{1/2}$	---------	-------	102(2.4)

TABLE 4. Comparison of different measurements for buffer gas broadening cross sections.

Method	Superposition State	Helium	Neon	Argon
FDTS ($571^{\circ}K$, 3Torr)	$3s^2S_{1/2}(F=2)-4d^2D_{5/2}$	307(8)	285(9)	826(26)
Trilevel Echo[16] ($400^{\circ}K$, 0.1Torr)	$3s^2S_{1/}2-4d^2D_{3/2}$	391(16)	382(13)	1045(174)
DFWM[14] ($673^{\circ}K$, 10Torr)	$3s^2S_{1/2}-4d^2D$	386(32)	305(57)	1041(66)
Two-Photon Abs.[11] ($413^{\circ}K$, 5Torr)	$3s^2S_{1/2}-4d^2D_{5/2}$		239(37)	
Two-Photon Abs.[12] ($563^{\circ}K$, 3Torr)	$3s^2S_{1/2}-4d^2D_{5/2}$	408(48)	400(28)	1049(109)
Two-Photon Abs.[13] ($600^{\circ}K$, 2000Torr)	$3s^2S_{1/2}-4d^2D_{5/2,3/2}$	223(44)		918(168)
Discharge Lamp[33] and Linear Spectroscopy ($500^{\circ}K$, 100Torr)	$3p^2P_{1/2}-4d^2D_{3/2}$	386(21)	361(38)	954(67)

AD-A146 827 NONLINEAR OPTICAL STUDIES OF RYDBERG ATOMS USING DEGENERATE FOUR-WAVE MIXING(U) HUGHES RESEARCH LABS MALIBU CA J F LAM ET AL. AUG 84 ARO-17432.13-PH 2/2

UNCLASSIFIED DAAG29-81-C-0008 F/G 20/6 NL

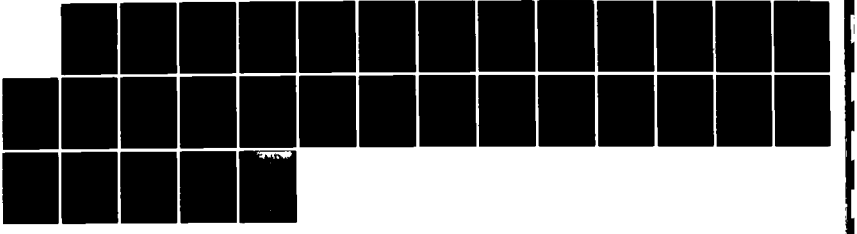

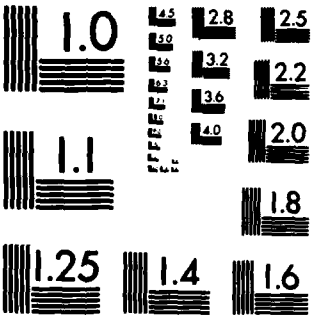

FIGURE CAPTIONS

Figure 1. Four-wave mixing geometry for FDTS. Two counterpropagating plane waves E_1 and E_2 interact with a three state resonant system. A third plane, E_2' is nearly collinear with E_2.

Figure 2. Cascade up three level system for calculating the FDTS nonlinear response. γ_{ij}^{sp} is the spontaneous emissions coefficient and γ_j is the decay to the reservoir, either by radiative decay or inelastic collisions.

Figure 3. Perturbation sequence for solving the density matrix quantum mechanical transport equation. Purturbation order is determined by the applied electromagnetic fields.

Figure 4. Simplified energy level diagram for atomic sodium. FDTS results in a coupling from the 3s ground state to the ns or nd Rydberg state by resonant coupling through the intermediate 3p state.

Figure 5. Experimental configuration for FDTS. Frequencies ω_1 and ω_2 are generated by two Coherent Radadiation stabilized ring dye lasers. The three beams intersect in the sodium cell.

Figure 6. FDTS spectra of the 8d state obtained by holding ω_1 fixed and scanning ω_2 over the upper level resonances. The fine structure splitting is clearly resolved. The small

secondary resonance are due to weak coupling through $3p^2P_{3/2}(F=2)$ intermediate state. The spacing is explained in the text.

Figure 7. Example of pressure broadening of the FDTS signal. The smooth curve in 7b is the result of a least square fit of a Lorentzian profile.

Figure 8. Example of the pressure induced resonance shift with 1.825 torr of Helium. The transition is between the 3s state and the 9s state.

Figure 9. Demonstration of the linear dependence of the line width and frequency shift on buffer gas pressure. The error bars represent the statistical error of the least square fit for that data point, and do not include systematic errors.

Figure 10. The collision induced frequency shift as a function of principal quantum number for helium buffer gas. Curve 1 is the ns state (this work), curve 2 is the np state (Fuchtbauer[2]), curve 3 is the nd state (Krebs and Schearer[18]), and curve 4 is the theory of Ivanov[9] with the electron scattering length L=1.1, α=1.31, and γ=10 (atomic units). The s-value for the quantum defect was used in the theoretical curve. No adjustment for differing quantum defects was made in plotting the np or nd data. The data point at n=5 (curve 1) is from reference 12.

Figure 11. Collisional broadening cross section as a function of principal quantum number for helium buffer gas. The smooth curve is the theory of Omont with L=0.863 and α=0.75. The dashed line represents Omont's theory with L and α values used in Ivanov's theory.

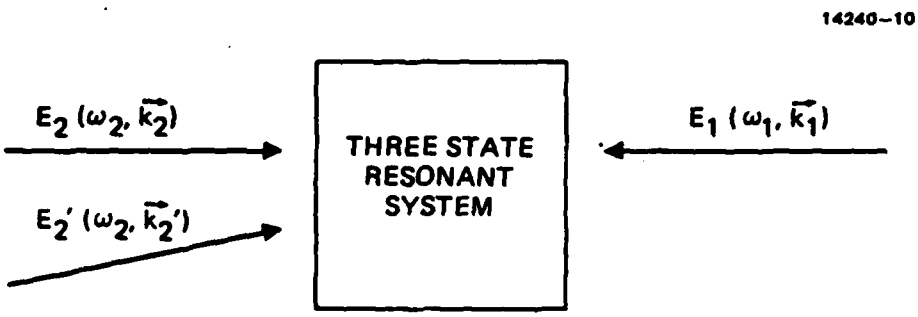
14240–10
$E_2(\omega_2, \vec{k_2})$
$E_2'(\omega_2, \vec{k_2}')$
THREE STATE RESONANT SYSTEM
$E_1(\omega_1, \vec{k_1})$

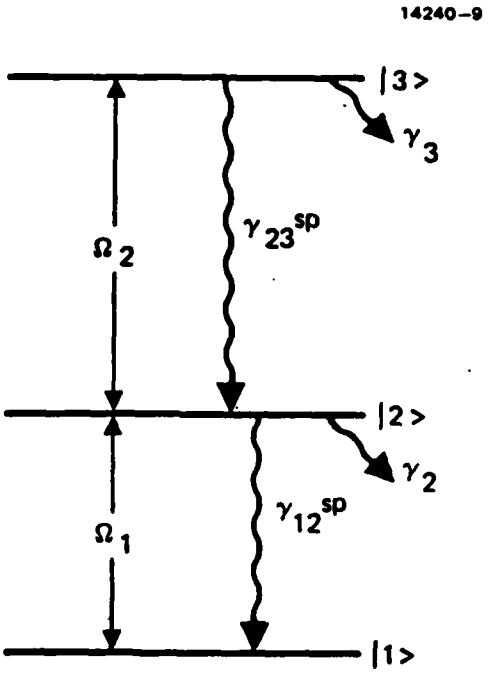
14240-9
|3>
γ_3
Ω_2
γ_{23}^{sp}
|2>
γ_2
γ_{12}^{sp}
Ω_1
|1>

14240-1

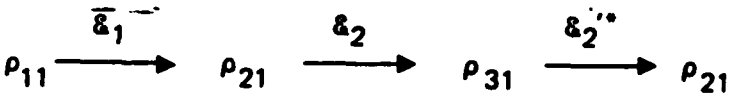

3

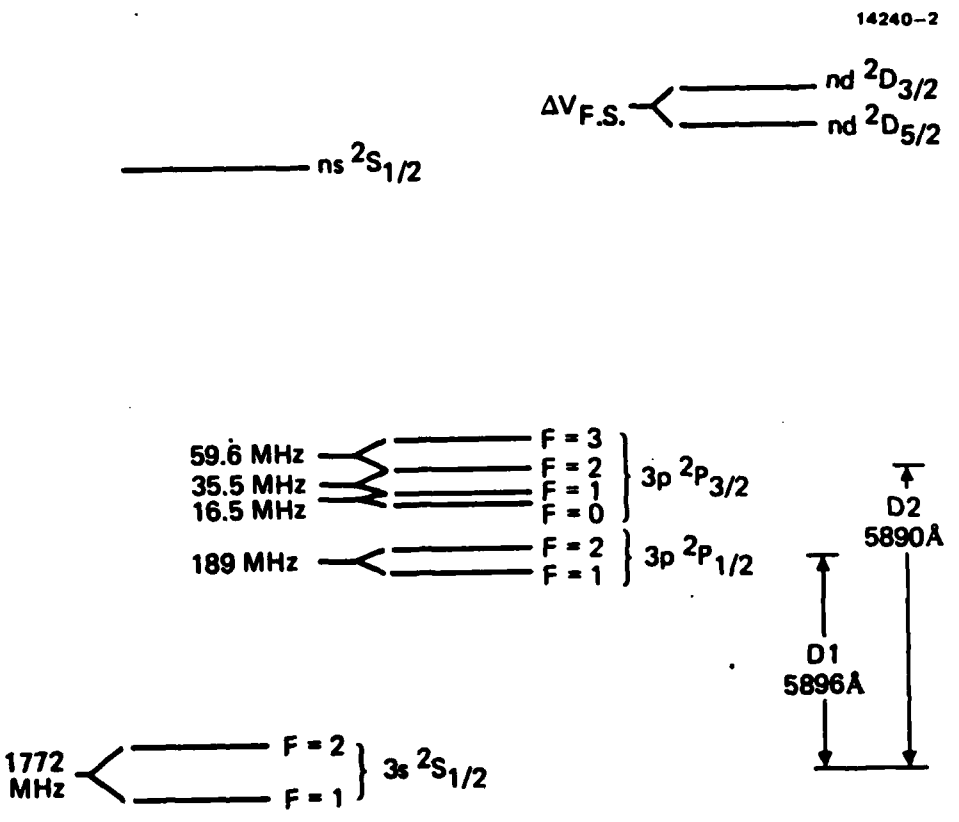
14240-2
$\Delta V_{F.S.}$
nd $^2D_{3/2}$
nd $^2D_{5/2}$
ns $^2S_{1/2}$
59.6 MHz
35.5 MHz
16.5 MHz
F = 3
F = 2
F = 1
F = 0
3p $^2P_{3/2}$
189 MHz
F = 2
F = 1
3p $^2P_{1/2}$
D2
5890Å
D1
5896Å
1772 MHz
F = 2
F = 1
3s $^2S_{1/2}$

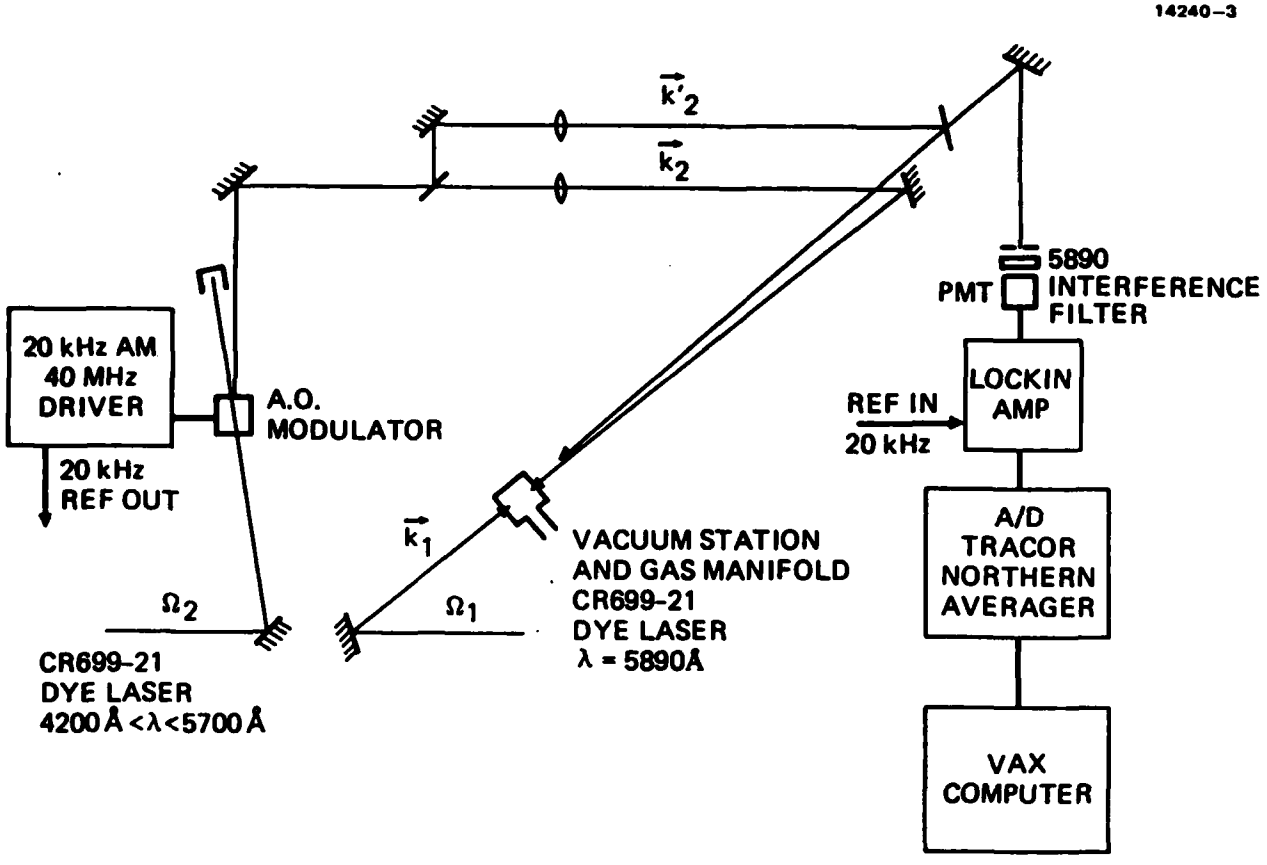
14240-3
$\vec{k}'_2$
$\vec{k}_2$
5890
PMT
INTERFERENCE
FILTER
20 kHz AM
40 MHz
DRIVER
A.O.
MODULATOR
LOCKIN
AMP
REF IN
20 kHz
20 kHz
REF OUT
$\vec{k}_1$
VACUUM STATION
AND GAS MANIFOLD
CR699-21
DYE LASER
λ = 5890Å
A/D
TRACOR
NORTHERN
AVERAGER
Ω_2
Ω_1
CR699-21
DYE LASER
4200 Å < λ < 5700 Å
VAX
COMPUTER

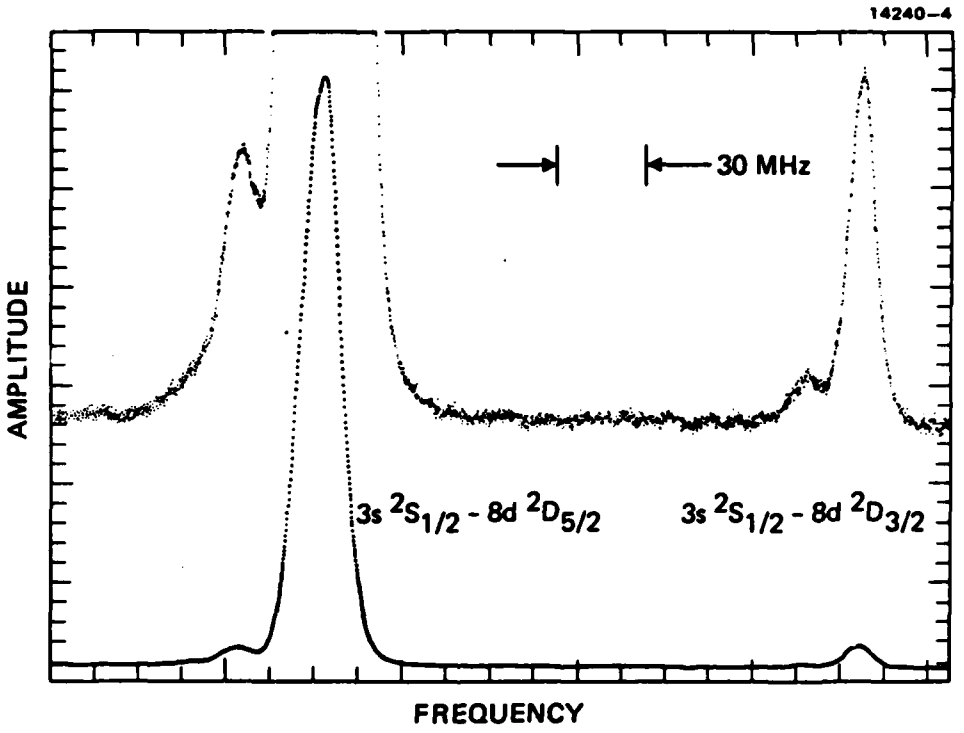
14240-4
30 MHz
AMPLITUDE
3s $^2S_{1/2}$ - 8d $^2D_{5/2}$
3s $^2S_{1/2}$ - 8d $^2D_{3/2}$
FREQUENCY

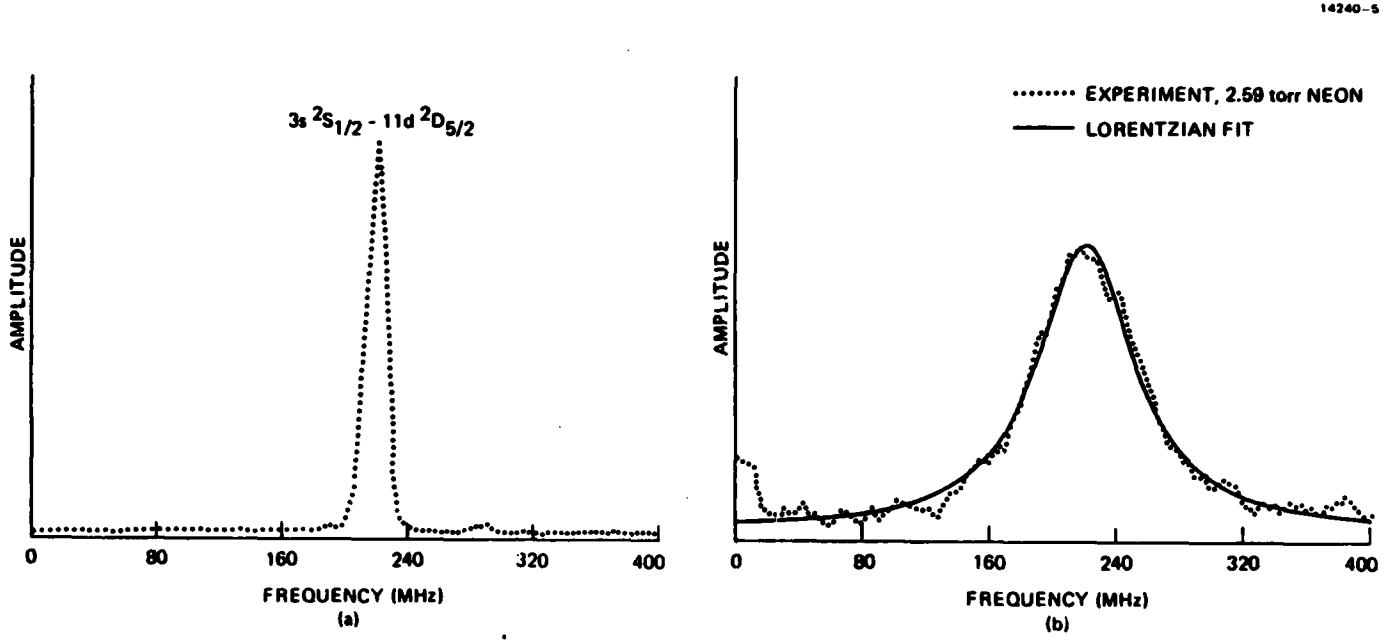
14240-5
3s $^2S_{1/2}$ - 11d $^2D_{5/2}$
AMPLITUDE
0
80
160
240
320
400
FREQUENCY (MHz)
(a)
EXPERIMENT, 2.59 torr NEON
LORENTZIAN FIT
AMPLITUDE
0
80
160
240
320
400
FREQUENCY (MHz)
(b)

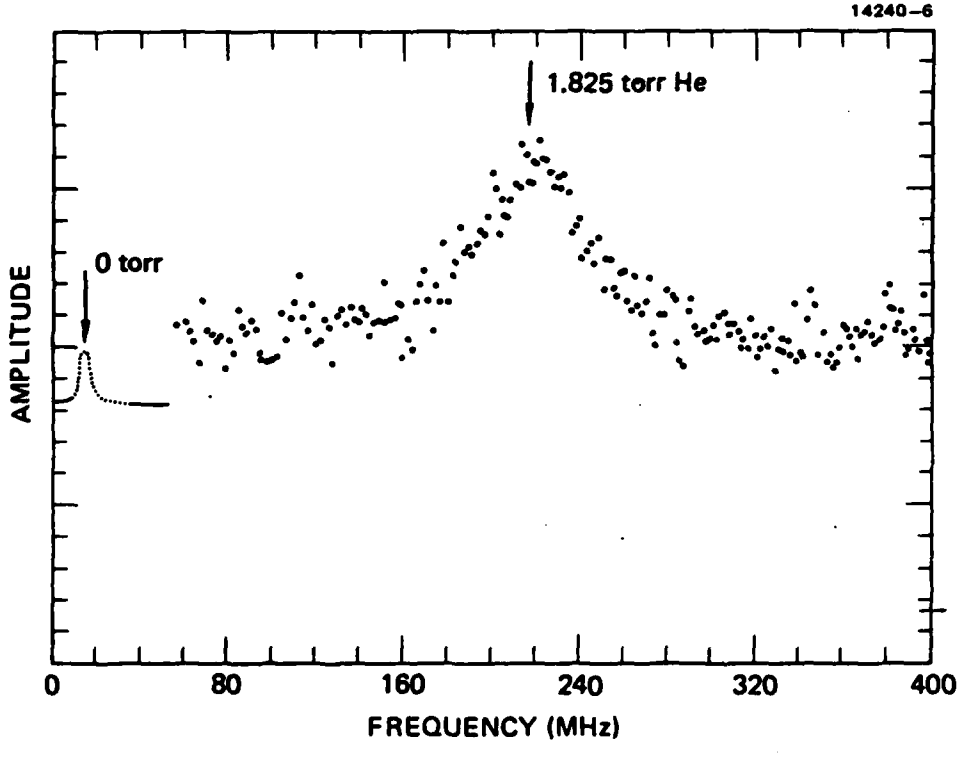
14240–6
1.825 torr He
0 torr
AMPLITUDE
0
80
160
240
320
400
FREQUENCY (MHz)

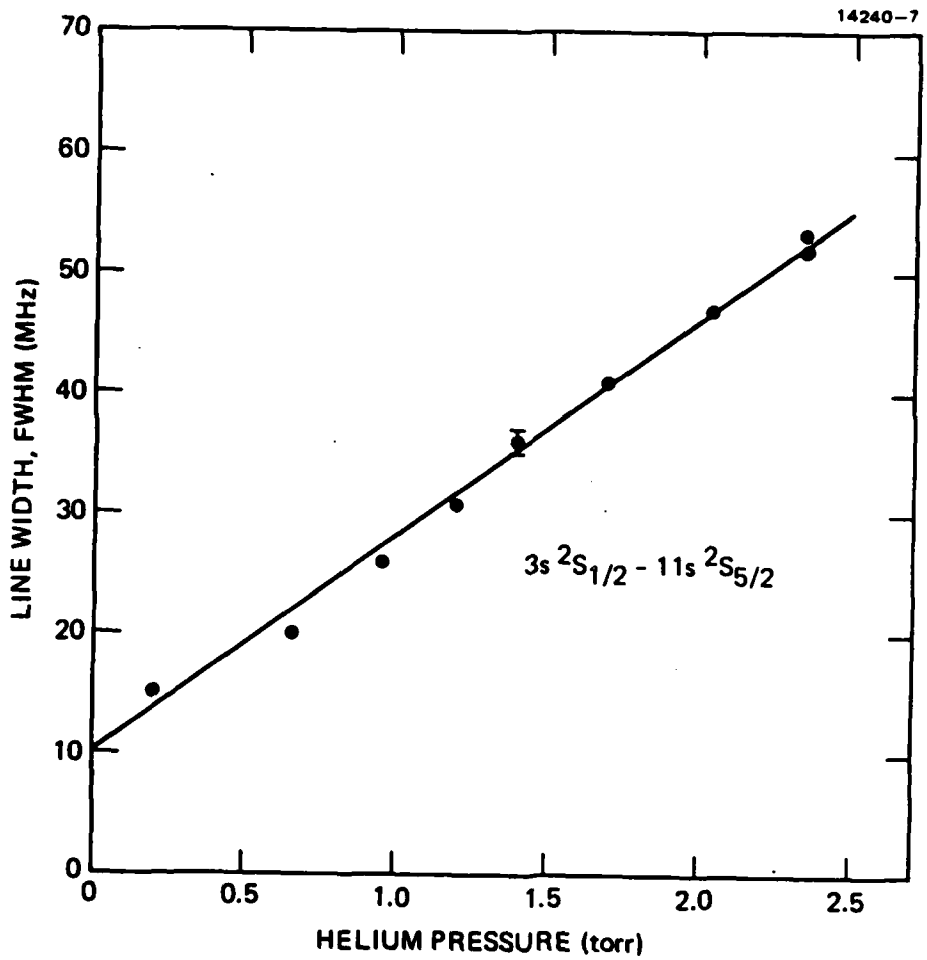
14240-7
70
60
50
40
30
20
10
0
0
0.5
1.0
1.5
2.0
2.5
LINE WIDTH, FWHM (MHz)
HELIUM PRESSURE (torr)
3s $^2S_{1/2}$ - 11s $^2S_{5/2}$

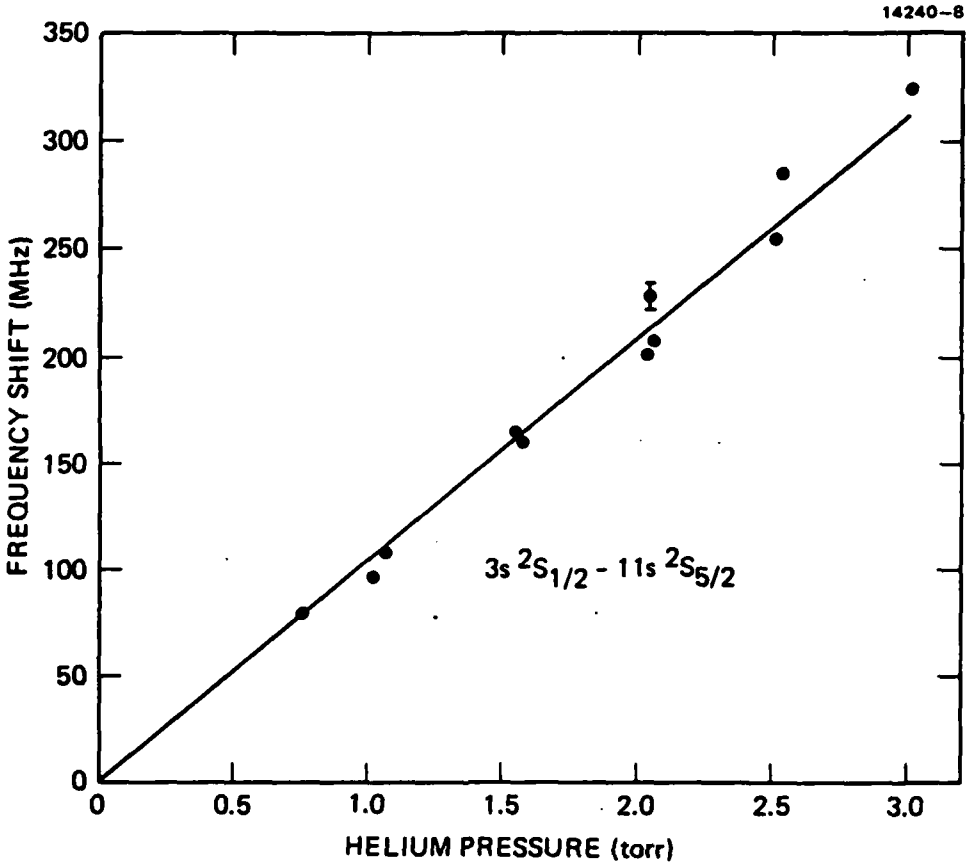
14240-8
350
300
250
200
150
100
50
0
FREQUENCY SHIFT (MHz)
0
0.5
1.0
1.5
2.0
2.5
3.0
HELIUM PRESSURE (torr)
3s $^2S_{1/2}$ - 11s $^2S_{5/2}$

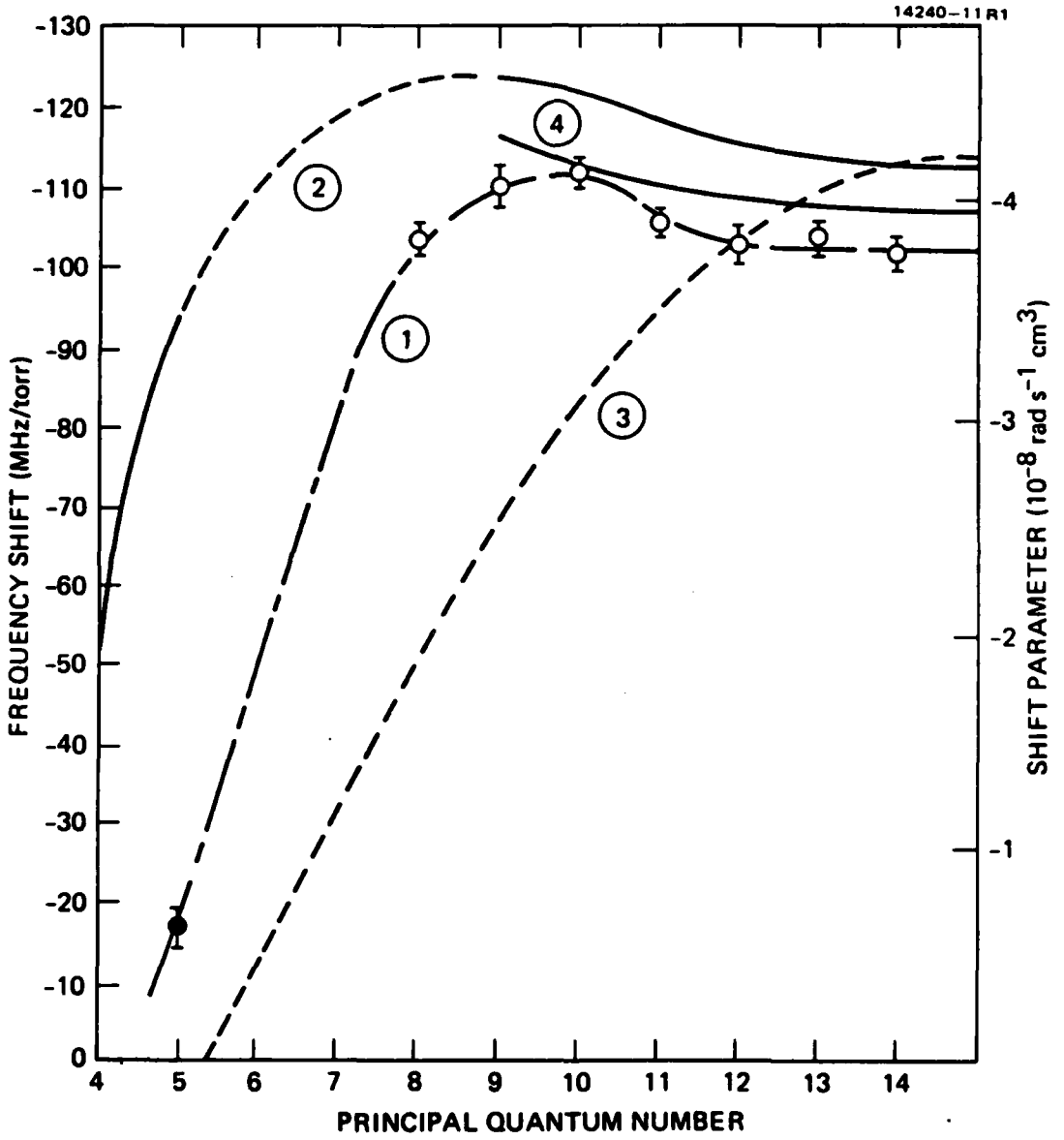
14240-11R1
-130
-120
-110
-100
-90
-80
-70
-60
-50
-40
-30
-20
-10
0
FREQUENCY SHIFT (MHz/torr)
-4
-3
-2
-1
SHIFT PARAMETER (10^{-8} rad s^{-1} cm^3)
4
5
6
7
8
9
10
11
12
13
14
PRINCIPAL QUANTUM NUMBER
1
2
3
4

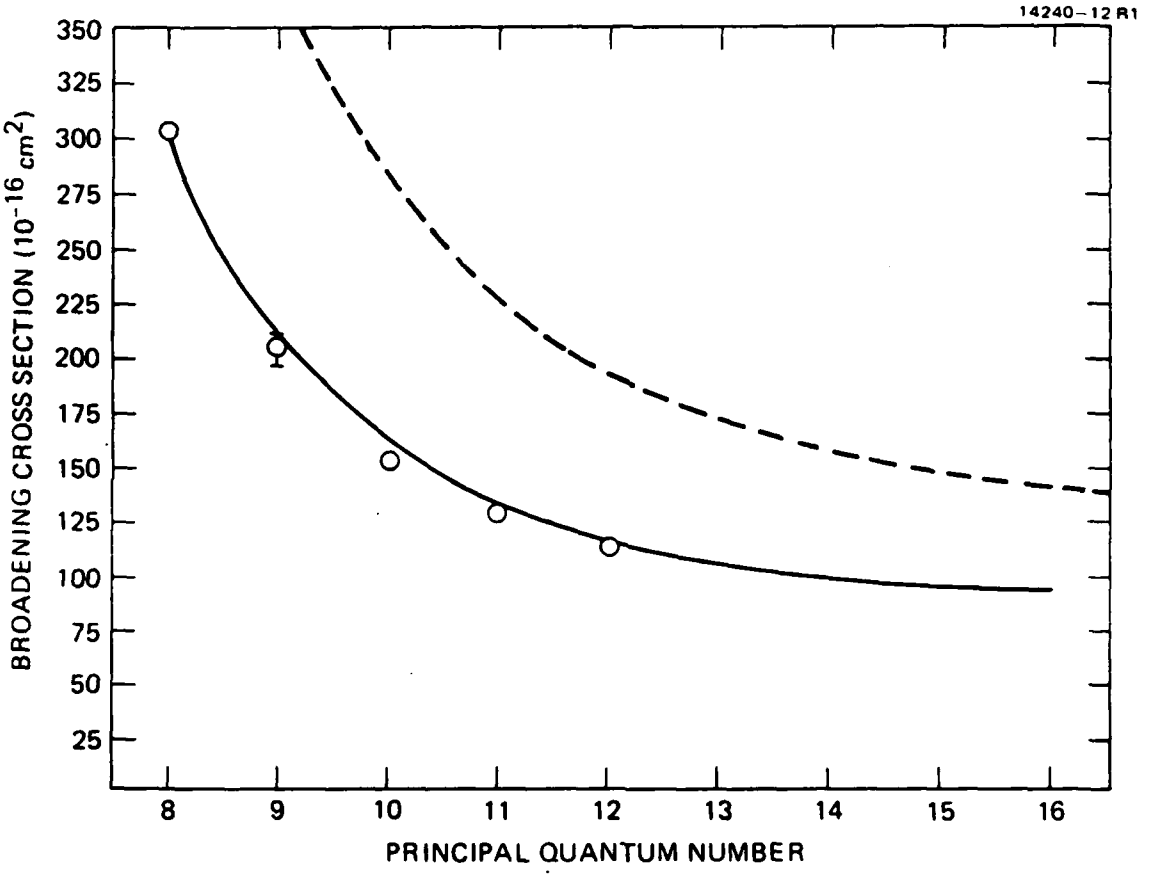
14240-12 R1
BROADENING CROSS SECTION (10^{-16} cm^2)
350
325
300
275
250
225
200
175
150
125
100
75
50
25
8
9
10
11
12
13
14
15
16
PRINCIPAL QUANTUM NUMBER

INTERPRETATION OF PUMP-PROBE AND 4-WAVE MIXING LINE SHAPES

Paul R. Berman, Galina Khitrova

Physics Department, New York University
New York, New York 10003 USA

Juan F. Lam

Hughes Research Laboratories
Malibu, California 90265 USA

There has been considerable interest in providing a simple interpretation of the structure observed in both pump-probe (1) and 4-wave mixing (2) spectroscopic line shapes. In pump-probe spectroscopy, one measures the absorption profile of a weak probe field in the vicinity of an atomic transition that is driven by an arbitrarily strong pump field. In a 4-wave mixing experiment, one can use three fields having frequencies Ω, Ω, and $(\Omega + \delta)$ to generate a phase conjugate signal at frequency $(\Omega - \delta)$; the intensity of the phase-conjugate signal as a function of δ is monitored.

Using an amplitude rather than a density matrix approach, we present a new method for explaining both the collision-free and collision-"induced" features of the line shapes. Collisions are simulated by allowing the ground state of the atoms to have a finite width (3). For the case of pump-probe spectroscopy with a pump field of amplitude E, a detuning Δ between the pump field and the atomic transition frequency, and a frequency offset of δ between the probe and pump fields, we are able to explain the following known features found in homogeneously broadened systems (characteristic line width $=\gamma$): (a) For closed systems (i.e. - no collisions and no decay to an external resevoir) with $|\Delta| >> \gamma$, there is an absorption

component at $\delta = -\Delta$ of order E^0, a dispersion-like component at $\delta = 0$ of order E^4 and an emission component at $\delta = +\Delta$ of order E^4; (b) With collisions present, the dispersion-like component at $\delta = 0$ is of order E^2 and it is possible to have gain in this part of the profile; (c) For $|\Delta| < \gamma$, a narrow dip of order E^2 can appear inside the homogeneous absorption width when collisions are present. Collision-induced features of 4-wave mixing lineshapes can also be explained.

In using the amplitude approach, one must sum the absolute squares of the sum of amplitudes corresponding to the same final state. Amplitudes corresponding to different final states (e.g., states for which different numbers of pump photons are absorbed) cannot interfere. The pump-probe dispersion like structure near $\delta = 0$ is seen to arise from final states in which the atom is left in its ground state, while the 4-wave mixing resonances arise from amplitudes in which two pump photons are absorbed and a probe and signal photon are emitted. The disappearance of the $\delta = 0$ resonance structure for closed systems is seen to be linked to conservation of energy.

This research is supported by the U.S. Office of Naval Research, and the work of J.F. Lam is supported by Army Research Office under contract No. DAAG29-81-C-0008.

References

1. See, for example: G. Nienhuis, J. Phys. B14, 1693 (1981), and references to earlier work contained therein; M. Sargent, Phys. Rep. 43, 223 (1978); R.W. Boyd and S. Mukamel, Phys. Rev. A, to appear.
2. See, for example: L.J. Rothberg and N. Bloembergen, in Laser Spectroscopy VI, edited by H.P. Weber and W. Luthy (Springer-Verlag, Berlin, 1983) pp. 178-182, and references to earlier work contained therein.
3. P.R. Berman, Phys. Rev. A13, 2191 (1976); Phys. Rep. 43, 101 (1978).

Observation of Collision-induced Subnatural Zeeman Coherence Linewidths in the Doppler Limit

J.F. Lam, D.G. Steel and R.A. McFarlane
Hughes Research Laboratories
3011 Malibu Canyon Road
Malibu, California 90265
(213) 456-6411

Abstract

We report the observation of the subnatural linewidth of Zeeman coherences in the presence of buffer gases using polarization nearly degenerate four-wave mixing. The origin of the ultranarrow linewidth is attributed to the physics of the evolution from closed to open quantum systems.

Investigations of four-wave mixing processes in gaseous media have provided a rich variety of new spectroscopic results, especially in the presence of buffer gases. Examples are the experimental verification of pressure-induced extra resonances (PIER),[1,2] observation of collisional narrowing of spectral line features associated with the population relaxation rate[3] and the appearance of a coherent dip in homogeneously broadened transitions.[4,5] These features can be interpreted as arising from the non-cancellation of quantum mechanical amplitudes mediated by collisions with ground state perturbers.[1,6,7]

We report the first observation of an optical resonance having a subnatural linewidth generated by the nonlinear excitation of ground state Zeeman coherence through the process of polarization nearly degenerate four-wave mixing (PNDFWM). Our results are explained by a simple physical model and analyzed using a statistical tensor formalism. We show that an upper bound of 10^{-18} cm^2 exists for the spin depolarization cross section of $Na(3S_{1/2}[F=2])$ in the presence of Ne buffer gas as inferred from the observed pressure dependence of the linewidth.

The technique of PNDFWM spectroscopy involves the nonlinear interaction of three input fields denoted $\vec{E}_f$, $\vec{E}_b$ and $\vec{E}_p$ oscillating at frequencies ω, ω and $\omega+\delta$ respectively, with a set of moving 2-level atoms having transition frequency ω_o. $\vec{E}_f$ and $\vec{E}_b$ are

counterpropagating pump fields and $\vec{E}_p$ is the probe field which is nearly collinear with $\vec{E}_f$. We shall assume that the polarization states of $\vec{E}_f$, $\vec{E}_b$ and $\vec{E}_p$ are $\hat{x}$, $\hat{x}$ and $\hat{y}$; respectively. Using the x direction as the quantization axis, $\vec{E}_f$ and $\vec{E}_b$ can induce electric dipole allowed π transitions while $\vec{E}_p$ induces σ transitions. Each energy level of the resonant atom is described by a principal quantum number α and a total angular momentum J_α. The physical process giving rise to a four-wave mixing signal in such a system can be described as follows. The interference between $\vec{E}_f$ and $\vec{E}_p$ generates Zeeman coherences or electric quadrupoles in both the ground and excited levels. Due to the frequency difference between $\vec{E}_f$ and $\vec{E}_p$, the Zeeman coherence corresponds to a moving grating from which the field $\vec{E}_b$ scatters, thus generating a signal field $\vec{E}_s$ propagating in the opposite direction to $\vec{E}_p$. Conservation of energy imposes the condition that the frequency of the signal field is given by $\omega-\delta$. As a result of the motion of the atoms, two resonances are observed. The first occurs at $\delta=0$ when $\vec{E}_f$ and $\vec{E}_p$ are resonant with a specific velocity group and leads to the generation of a Zeeman coherence signal. The width of this resonance is determined by the electric quadrupole dephasing time. The second resonance occurs at $\delta=-2(\omega_o-\omega)$ when $\vec{E}_f$ and $\vec{E}_s$ are resonant with the same velocity group and its width is determined by the electric dipole dephasing time. Due to the distinct nature of collisional processes operative on electric dipoles and on quadrupoles, PNDFWM, in principle, permits a simultaneous and independent measurement of phase-interrupting and spin depolarization collisional cross sections.

In the absence of foreign perturbers, the ground and excited levels are coupled together by the vacuum radiation field. The spontaneous decay rate γ is a measure of the strength of this coupling. Because of it, both quantum levels evolve as a single entity even in the presence of applied radiation fields, and this entity has a unique spectral response, i.e., the bandwidth is determined by γ. In the presence of foreign perturbers, the ground and excited levels experience different collisional interactions which effectively decouples them even in the presence of the vacuum radiation field. In this case, the responses of the ground and excited levels to applied radiation fields reflect their evolution as distinct entities. Hence, the PNDFWM signal has contributions arising from both the ground and excited states separately. The spectral response of the individual contributions are characterized by their respective collisional cross sections. For the signal arising from the ground level, $|J_1\rangle$, the bandwidth is determined by $\gamma_\tau + \Gamma_1$ while that of the excited level, $|J_2\rangle$, is determined by $\gamma + \gamma_\tau + \Gamma_2$. Here Γ_α is the effective collisional depolarization rate for level α and γ_τ is the reciprocal of the transit time for an atom through the laser beam. For low pressures, one notes that $(\gamma_\tau + \Gamma_1) << (\gamma + \gamma_\tau + \Gamma_2)$. Hence, the contribution to the signal from the ground level will dominate over that from the excited level. The bandwidth is determined by $\gamma_\tau + \Gamma_1$ and is much narrower than the bandwidth associated with the rate γ. A measurement of the bandwidth at the resonance line δ=0 will provide a direct measurement of the ground level depolarization rate Γ_1 provided that the transit time $(1/\gamma_\tau)$ is known accurately.

The phenomenon of collisional induced decoupling of the ground and excited levels appears to have a broad application[3,5], regardless of the ratio of laser detuning (and pressure broadened linewidth) to the Doppler width. It is a unique example of the evolution from a closed quantum system to an open quantum system initiated by the presence of an additional randomizing state-selective reservoir, i.e., the buffer gas.

A theoretical description of this physical phenomenon is accomplished by solving the density matrix equation in the statistical tensor formulation.[8] This procedure is required to account for the degeneracy of the energy levels. The collisional rates are denoted by $\Gamma^{(k)}_{\alpha\beta}$, where k denotes either population (k=0), orientation (k=1) or alignment (k=2). $\alpha\beta$ refers to the ground and/or excited levels. In writing such a decay rate, we assume that there is no coupling between distinct multipoles. The solution of the set of statistical tensor equations in third order perturbation theory is given by

$$\vec{P}^{(3)}(\vec{r},t) = \sum_{\alpha=1,2} \sum_{\tilde{q}=0,\pm1} \sum_{k} \sum_{-k<q<k} \sum_{\substack{Q \\ =0,\pm1}} \sum_{\lambda\,\lambda''} \frac{|\langle J_1||\mu||J_2\rangle|^4}{(ih)^3}$$

$$\times \quad \begin{Bmatrix} 0 & 1 & 1 \\ J_2 & J_1 & J_1 \end{Bmatrix} \langle T(J_1J_1)_{00}^{+} \rangle \hat{\epsilon}^{*}_{-q}$$

$$\times E_b^{(\lambda'')} \; E_f^{(\lambda)} \; E_p^{(Q)*} \quad e^{i(\vec{k}_f-\vec{k}_b-\vec{k}_p)\cdot\vec{r} \; - i \; (\omega_f+\omega_b-\omega_p)t}$$

$$\times (-1)^{\alpha+1} \; M^{k11}_{\substack{\sim \\ qq\lambda''}}(\alpha) \; M^{k11}_{qQ\lambda}(\alpha) \quad \times \int_{-\infty}^{\infty} \vec{dv} \; W(\vec{v}) \qquad (1)$$

$$\times L_{12}^{(1)}(\omega_f-\omega_b-\omega_p) \quad [L_{12}^{(1)}(\omega_p) + L_{12}^{(1)}(\tilde{\omega}_f)] \quad L_{\alpha}^{(k)}(\omega_f-\omega_p) \quad [B_{qQ\lambda}^{k11}(\omega_f-\omega_p)]^{\beta}$$

where $\beta = (1 + (-1)^{\alpha+1})/2$ and

$$B_{qQ\lambda}^{k11}(\omega_f-\omega_p) = (-1)^k \tilde{\gamma}^{(k)} \frac{M_{qQ\lambda}^{k11}(2)}{M_{qQ\lambda}^{k11}(1)} L_2^{(k)}(\omega_f-\omega_p) - 1 \qquad (2)$$

represents the contribution due to spontaneous emission. $\tilde{\gamma}^{(k)}$ is the spontaneous emission rate of the kth pole. $M_{qQ\lambda}^{k11}$ are just geometrical factors, given in terms of the Wigner's 3j and 6j symbols. $\langle T(J_1J_1)_{00}^{+} \rangle$ is proportional to the initial population of the ground level. The complex Lorentzians are defined by

$$L_{12}^{(1)}(\omega_n) = [\Gamma_{12}^{(1)} + i(\omega_n-\omega_o - \vec{k}_n \cdot \vec{v})]^{-1} \qquad (3a)$$

$$L_{\alpha}^{(k)}(\omega_f-\omega_p) = [\Gamma_{\alpha}^{(k)} + \left(\frac{1+(-1)^{\alpha}}{2}\right)\gamma^{(k)} + i(\omega_f-\omega_p) - i(\vec{k}_f-\vec{k}_p)\cdot\vec{v})]^{-1} \qquad (3b)$$

and the integration is performed for a Maxwellian distribution $W(\vec{v})$. Expressions (1) through (3) are the main theoretical results of this paper and account for the arbitrary polarization state of the radiation fields. The integration has been carried out and the spectral response is plotted in the left hand column of Figures 1 and 2 for distinct values of neon buffer gas pressure. Fig 1 corresponds to the case where the polarization states of the pump fields are linear and 90° cross polarized to that of the probe

field. Fig 2 corresponds to the case where all input fields are linearly co-polarized. The data, in both figures, correspond to the case where the counterpropagating pump waves are on resonance with the 2-level system, i.e. $\omega=\omega_o$. In this case, the two resonances overlap and in the absence of buffer gas their linewidths are determined by the spontaneous decay rate of the 2-level system.

The experimental study of PNDFWM was made using the $3s^2S_{1/2}(F=2)$-$3p^2P_{3/2}(F=3)$ transition on the D_2 line of atomic sodium. This transition is not subject to ordinary hyperfine structure optical pumping. The experimental setup was similar to that described earlier[3] where one frequency stabilized tunable cw dye laser supplied the pump beams and the probe beam was supplied by a second cw frequency stabilized laser. In the first set of experiments, the two pump beams were linearly s-polarized and the probe was linearly p-polarized. As studied earlier, the resultant signal is linearly p-polarized and was detected with a PMT and a p-oriented polarization analyzer while in the second set of experiments all beams were set to be s-polarized. To avoid contributions from nonlinear Hanle effects, the earth's magnetic field was cancelled using three orthogonal pairs of Helmholtz coils. The pump frequency was adjusted to be on or near the atomic resonance, and the signal was observed as a function of the probe frequency. The relative laser jitter was of the order of one megahertz. The angle between the propagation directions of $\vec{E}_f$ and $\vec{E}_p$ was maintained at <0.5°. This geometry gives a residual Doppler

width of the order of 3 megahertz. In the absence of collisions, the measured linewidth of 25 Mhz is given by the sum of the spontaneous emission rate, residual Doppler width and laser jitter. The results of the experiment are illustrated on the right hand column of Figs 1 and 2, and show excellent agreement with the theoretical results.

The distinct behavior of the two data sets can be traced to the origin of the collisional interaction for the population and electric quadrupole. In the presence of buffer gases,population relaxes according to velocity changing collisions. The cross section for such a collisional interaction is approximately $10^{-15}cm^2$ for the ground state of sodium atoms.[9] However, the ground state electric quadrupole experiences spin depolarizing collisions which have a cross section in the range of 10^{-19} - $10^{-26}cm^2$ for the case of sodium vapor.[10] Since the collisional decay rate is defined as $\Gamma=n\langle\sigma v\rangle$, one expects that the decay rate for the population is significantly larger than the one for the electric quadrupole, for the same pressure range. This physical argument explains the behavior of the linewidth as a function of buffer gas pressure in Figures 1 and 2. The results in Fig 1 shows that the subnatural linewidth, arising from the ground state electric quadrupole, undergoes no additional changes when the buffer gas pressure increases from 25 to 250 torr. On the contrary, the results in Fig 2 shows that the subnatural linewidth, due to the ground state population, at 25 torr experiences

significant broadening when the buffer gas pressure is raised to 250 torr. Furthermore, the data in Figure 1 allows a direct estimate of the magnitude of the spin depolarizing cross section for the ground state of sodium. Using the measured value of the linewidth at 250 torr and the average value of the relative velocity of the perturbers with respect to the sodium atoms at 300°c, the cross section for the spin depolarizing collsion is estimated to have an upper bound of $10^{-18}cm^2$. This estimate is limited by the minimum linewidth capability of the laser system.

In conclusion, we used the technique of PNDFWM to study the effect of collisions on the population and electric quadrupole of the ground state of sodium vapor. Furthermore, we have elucidated the physical origin of the subnatural linewidth in the presence of buffer gases and attribute it to the fundamental concept of evolution from closed to open quantum systems.

This work is supported in parts by the Army Research Office under contract # DAAG29-81-C-0008.

REFERENCES

1. N. Bloembergen, Laser Spectroscopy IV, ed. by H. Walther and K.W. Rothe (Springer Verlag 1979) p. 340.

2. Y. Prior, A.R. Boydan, M. Dagenais and N. Bloembergen, Phys. Rev. Lett. 46, 111 (1981).

3. J.F. Lam, D.G. Steel and R.A. McFarlane, Phys. Rev. Lett. 49, 1628 (1982).

4. M. Sargent, Phys. Rep. 43, 225 (1978).

5. L.J. Rothberg and N. Bloembergen, Laser Spectroscopy VI, ed. by H.P. Weber and W. Luthy. (Springer Verlag 1983) p. 178.

6. G. Grynberg, J. Phys. B: Atom. Mol. Phys. 14, 2089 (1981).

7. P.R. Berman, G. Khitrova and J.F. Lam, Proc. International Conference Spectral LineShapes, Aussois, France (1984).

8. K. Blum, Density Matrix Theory and Applications, Plenum Press 1981, New York, Chapter 4.

9. P.F. Liao, J.E. Bjorkholm and P.R. Berman, Phys. Rev. A 21, 1927 (1980)

10. W. Happer, Rev. Mod. Phys. 44, 169 (1972)

FIGURE CAPTIONS

Figure 1. PNDFWM spectral response as a function of neon gas pressure. The polarization states of $\vec{E}_f$, $\vec{E}_b$ and $\vec{E}_p$ are s, s, p; respectively. Left-hand column corresponds to theory while right-hand column describes experiments.

Figure 2. NDFWM spectral response as a function of neon gas pressure. All radiation fields are linearly co-polarized. Left-hand column coresponds to theory while right-hand column describes experiments.

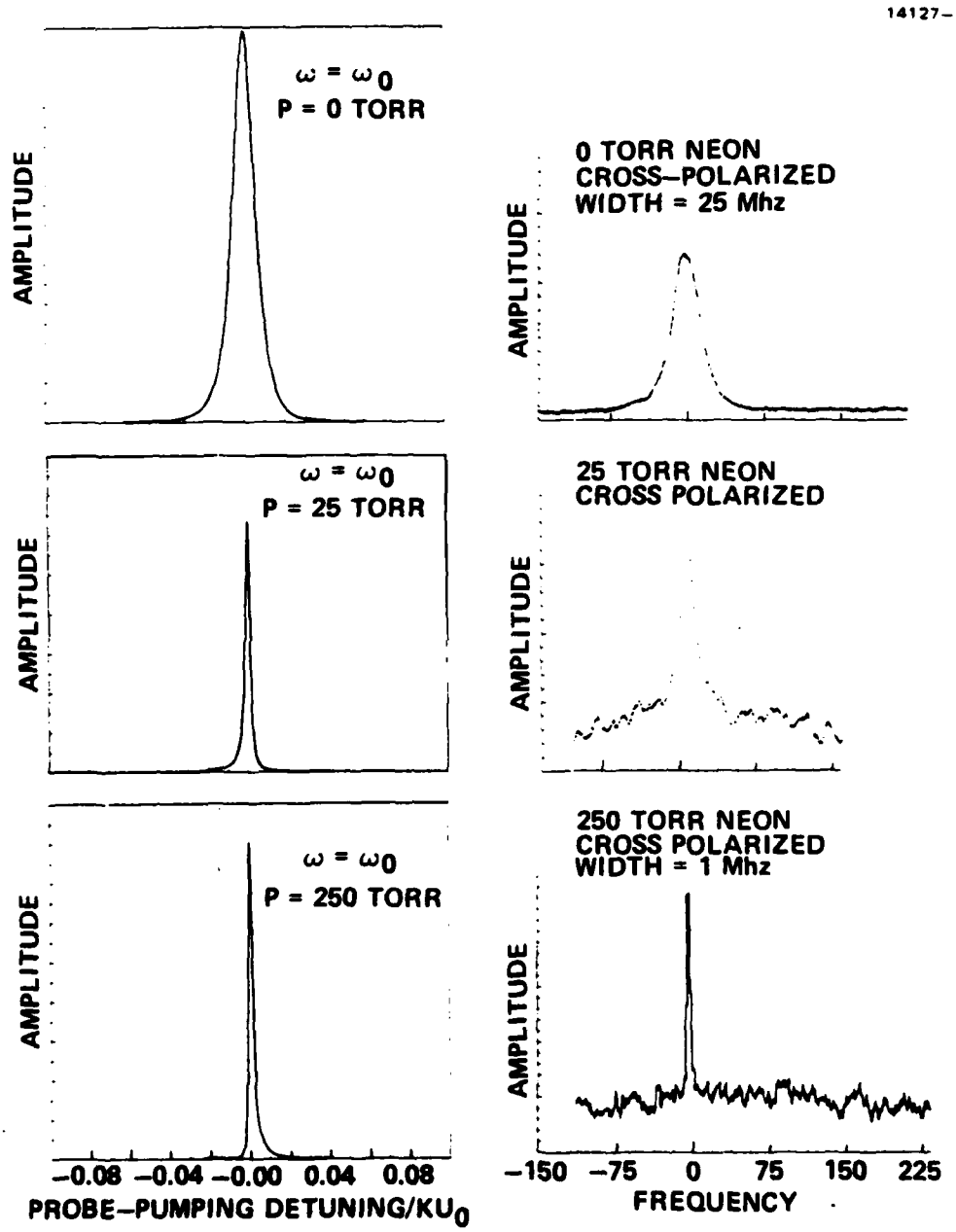
14127-10
ω = ω0
P = 0 TORR
AMPLITUDE
0 TORR NEON
CROSS-POLARIZED
WIDTH = 25 Mhz
AMPLITUDE
ω = ω0
P = 25 TORR
AMPLITUDE
25 TORR NEON
CROSS POLARIZED
AMPLITUDE
ω = ω0
P = 250 TORR
AMPLITUDE
250 TORR NEON
CROSS POLARIZED
WIDTH = 1 Mhz
AMPLITUDE
-0.08 -0.04 -0.00 0.04 0.08
PROBE-PUMPING DETUNING/KU0
-150 -75 0 75 150 225
FREQUENCY

14127-11

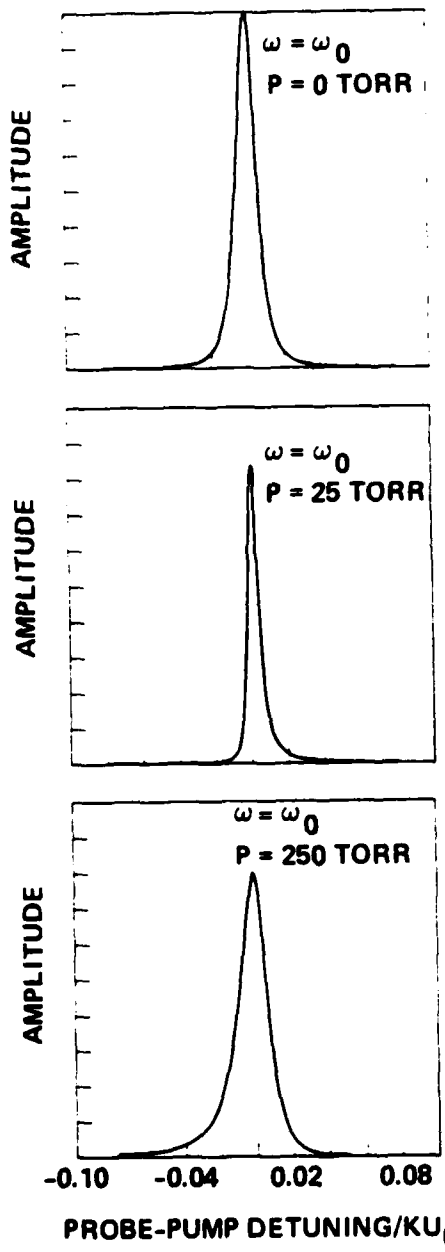
ω = ω0
P = 0 TORR
AMPLITUDE
ω = ω0
P = 25 TORR
AMPLITUDE
ω = ω0
P = 250 TORR
AMPLITUDE
-0.10
-0.04
0.02
0.08
PROBE-PUMP DETUNING/KU0

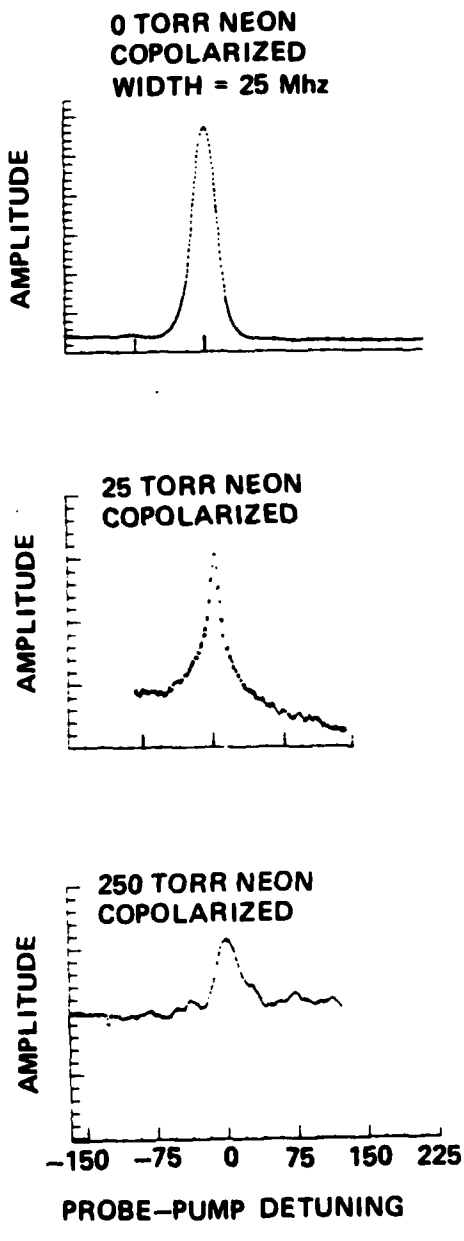
0 TORR NEON
COPOLARIZED
WIDTH = 25 Mhz
AMPLITUDE
25 TORR NEON
COPOLARIZED
AMPLITUDE
250 TORR NEON
COPOLARIZED
AMPLITUDE
-150
-75
0
75
150
225
PROBE-PUMP DETUNING

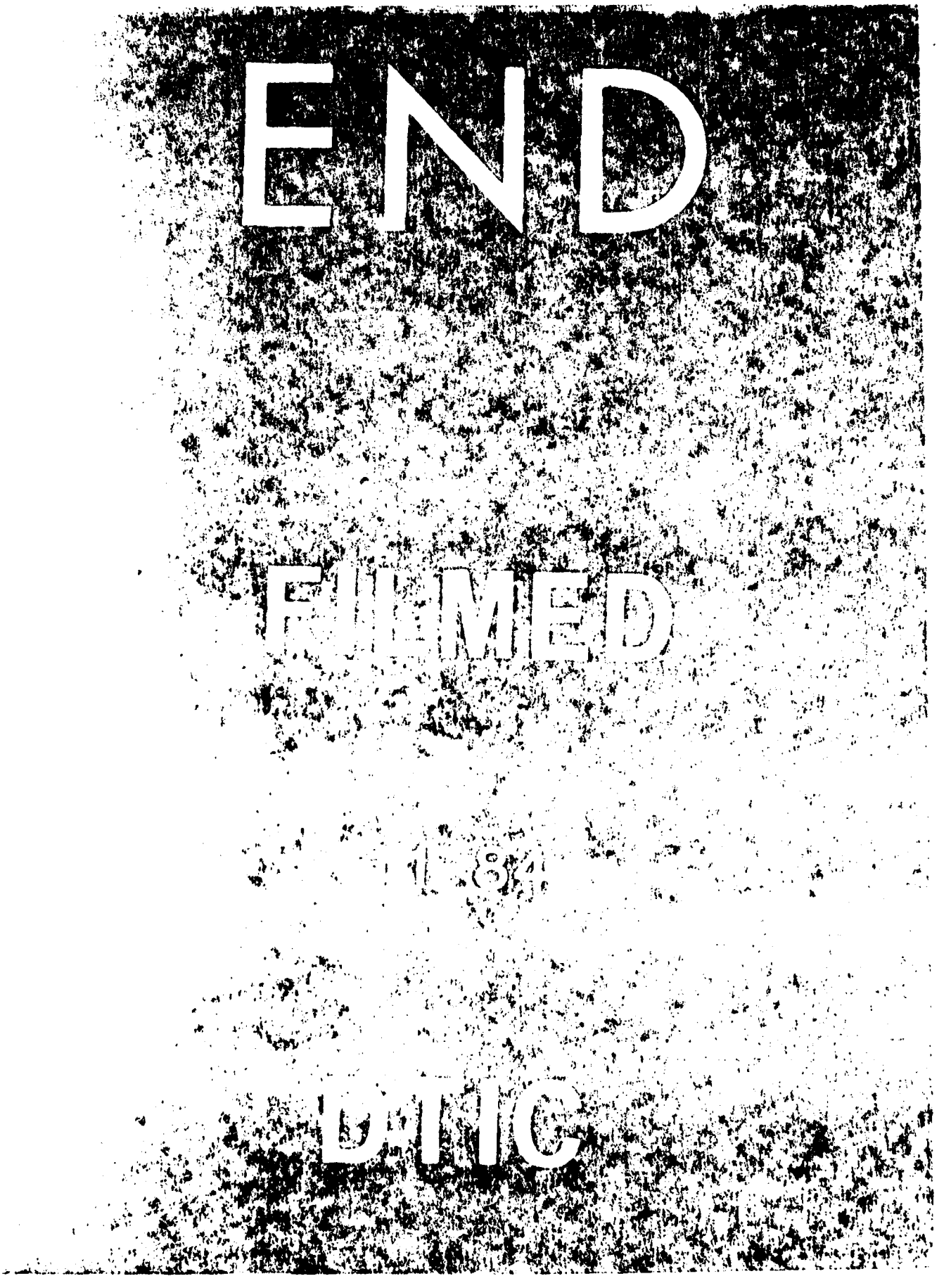
END
FILMED
DTIC